Copyright Warning & Restrictions

The copyright law of the United States (Title 17, United States Code) governs the making of photocopies or other reproductions of copyrighted material.

Under certain conditions specified in the law, libraries and archives are authorized to furnish a photocopy or other reproduction. One of these specified conditions is that the photocopy or reproduction is not to be "used for any purpose other than private study, scholarship, or research." If a, user makes a request for, or later uses, a photocopy or reproduction for purposes in excess of "fair use" that user may be liable for copyright infringement,

This institution reserves the right to refuse to accept a copying order if, in its judgment, fulfillment of the order would involve violation of copyright law.

Please Note: The author retains the copyright while the New Jersey Institute of Technology reserves the right to distribute this thesis or dissertation

Printing note: If you do not wish to print this page, then select "Pages from: first page # to: last page #" on the print dialog screen

ABSTRACT

THE IMPACT OF MATERIAL AND ENVIRONMENTAL PROPERTIES ON THE ETTRINGITE – METAETTRINGITE THERMOCHEMICAL REACTION

by
Aaron Strand

The use of energy is an essential need for people, with demand constantly increasing due to an increasing population and an increase in living and comfort standards. Since 1965, world energy consumption has quadrupled. During peak utilization, the strain on the grid infrastructure can be immense. As energy demand fluctuates during different times of the day and year, the energy production needs to scale accordingly This creates inefficiencies within the system such as over building generation capacity or losses from start up or ramping up production. This can be alleviated through load leveling where excess energy generated during low demand periods can be stored and used during higher demand periods. Also, storage systems are needed with the increasing use of renewables in energy generation.

Long-term energy storage through reversible thermochemical energy processes is being increasingly examined due to their capability of high energy densities. One possible form of this storage is with the ettringite-metaettringite conversion process. The thermochemical reaction using ettringite is focused on the hysteresis in the dehydration and rehydration between the two states, where decomposition of the crystal will result in energy being unrecoverable. The ettringite crystal is rarely found in nature, but it is commonly found as a product from the hydration of hydraulic cements. Specialty types of cement binders such as calcium sulfoaluminate (C$A) cement; the binary systems of calcium aluminate cement (CAC) with calcium sulfate (C$); and the ternary systems of

ordinary portland cement (OPC) with CAC and C$ can be used in which ettringite can be found as a primary hydration product. The primary concerns related to these systems are the stability of the ettringite-metaettringite reaction and the efficiency of energy storage.

The effect of the cement type and dehydration temperature is studied for the macrostability of the specimens by measuring the number of cycles that could be completed before failure of the specimens. The compressive strength of the pastes is used to investigate the stability of the systems during the dehydration and rehydration cycle before failure. The microstructural properties of the cement pastes are investigated through the use of X-ray diffraction (XRD) and scanning electron microscopy (SEM) with energy dispersive spectroscopy (EDS). This work shows that the type of cement and dehydration temperature does impact the stability and microstructure of the systems. The stability of long-term storage of specimens is also investigated for the C$A cement. Storage of the C$A paste system is possible when the relative humidity (RH) is kept below 45%.

The energy released on rehydration of the paste systems is studied for the three cements at five different dehydration temperatures. Presented in this dissertation are the heat flow and cumulative heat for these systems during the first 24 hours of rehydration. Results indicate that the type of cement and dehydration temperature do impact the amount of energy released during rehydration. Coupled with the results on stability, the OPC-CAC-C$ cement, which performed the best for stability, performed the worst of the three for energy recovery. The C$A system is also studied at three dehydration temperatures for the heat released when subjected to multiple cycles. The results indicate that there is a decreasing trend of energy release as cycle count is increased for two of the three temperatures.

THE IMPACT OF MATERIAL AND ENVIRONMENTAL PROPERTIES ON THE ETTRINGITE – METAETTRINGITE THERMOCHEMICAL REACTION

by
Aaron Strand

A Dissertation
Submitted to the Faculty of
New Jersey Institute of Technology
in Partial Fulfillment of the Requirements for the Degree of
Doctor of Philosophy in Civil Engineering

John A. Reif, Jr. Department of Civil and Environmental Engineering

May 2022

.

APPROVAL PAGE

THE IMPACT OF MATERIAL AND ENVIRONMENTAL PROPERTIES ON THE ETTRINGITE – METAETTRINGITE THERMOCHEMICAL REACTION

Aaron Strand

Dr. Matthew P. Adams, Dissertation Advisor Assistant Professor of Civil and Environmental Engineering, NJIT	Date
Dr. Methi Wecharatana, Committee Member Professor of Civil and Environmental Engineering, NJIT	Date
Dr. Matthew J. Bandelt, Committee Member Assistant Professor of Civil and Environmental Engineering, NJIT	Date
Dr. Rayan H. Assaad, Committee Member Assistant Professor of Civil and Environmental Engineering, NJIT	Date
Dr. Siva P.V. Nadimpalli, Committee Member Associate Professor of Mechanical Engineering, Michigan State University	Date

BIOGRAPHICAL SKETCH

Author: Aaron Strand

Degree: Doctor of Philosophy

Date: May 2022

Undergraduate and Graduate Education:

- Doctor of Philosophy in Civil Engineering,
  New Jersey Institute of Technology, Newark, NJ, 2022

- Bachelor of Science in Civil Engineering,
  Oregon State University, Corvallis, OR, 2015

Major: Civil Engineering

Presentations:

Strand, AJ, Adams, MP. "Use of High Ettringite Producing Calcium Aluminate Cement Blend Systems for Thermochemical Energy Storage." 5th International Conference on Calcium Aluminates. Cambridge, UK. July 2022.

Strand, AJ, Adams, MP. "Use of C$A Based Ettringite Cement Systems for Long Term Energy Storage Through Thermochemical Reactions." 9th Advances in Cement-Based Materials (Cements 2018). Pennsylvania State University, State College, PA. 12 June 2018.

To my parents, Gregg and Jenny
My sister, Jolene
And those who have helped me get to here.

ACKNOWLEDGMENT

I would like to sincerely thank to all those who assisted and contributed so that this work was able to be accomplished. Without the assistance of my advisor, committee members, colleagues, family, and friends this work would not have been completed.

To my advisor Dr. Matthew P. Adams, I would like to express my sincere gratitude for the opportunity you provided to continue to pursue the passion I have for research after my assistance as an undergraduate researcher at Oregon State University. Without you, I would not be where I am today. I am forever grateful to your guidance and your patience as I worked through the many difficulties of this project. Especially, as I worked to get things up and running in the lab. Dr. Adams has continued to push me to do my best throughout my time working for him and I am very grateful to have him as my advisor.

I would like to express my sincere gratitude for my committee members for serving on this project. To Dr. Matthew J. Bandelt who has assisted greatly in making sure that things are running smoothly on all the projects I have assisted with. I would like to thank my Committee members Dr. Methi Wecharatana, Dr. Rayan H. Assaad, Dr. Siva P.V. Nadimpalli, and the late Dr. Bruno Gonçalves da Silva for their comments and feedback on this project.

I would like to thank the Department of Civil and Environmental Engineering Department that assisted with funding through both teaching and research assistantships. Funding from the Federal Highway Administration through Task Order No. 693JJ318F000303 (subcontract through Center for Advanced Infrastructure and Transportation) is greatly appreciated. Through this funding I was able to branch out and study different topics such as corrosion on separate projects.

I would like to thank all my colleagues; Marwa Korayem, Jin Fan, Noah Thibodeaux, Masoud Shrkhorshidi, Mandeep Pokhrel, and Anuruddha Jayasuriya for their assistance throughout this process. I would like to also acknowledge the assistance of Steve George for his help in the lab making sure that I could complete the work that I needed to!

Finally, I would like to acknowledge the unconditional support and love of my family. They were my source of strength and reassurance when thanks were hard and my biggest cheerleaders for this journey.

TABLE OF CONTENTS

TABLE OF CONTENTS
(CONTINUED)

Chapter **Page**

TABLE OF CONTENTS
(CONTINUED)

Chapter **Page**

TABLE OF CONTENTS
(CONTINUED)

Chapter **Page**

TABLE OF CONTENT
(CONTINUED)

Chapter **Page**

LIST OF TABLES

LIST OF FIGURES

LIST OF FIGURES
(CONTINUED)

Figure **Page**

LIST OF FIGURES
(CONTINUED)

Figure **Page**

LIST OF FIGURES
(CONTINUED)

Figure **Page**

LIST OF SYMBOLS

OPC	ordinary portland cement
CAC	calcium aluminate cement
OPC-CAC-C$	ternary blend of OPC, CAC and C$
C$A	calcium sulfoaluminate cement
$C\$H_x$ or C$	calcium sulfate
$C_4A_3\$$	ye'elimite (Klein's compound)
$3C_3A\$H_{32}$	ettringite ($3CaO{\cdot}Al_2O_3{\cdot}3CaSO_4{\cdot}32H_2O$)
C_3A	tri-calcium aluminate ($3CaO.Al_2O_3$)
C_3S	tri-calcium silicate ($3CaO.SiO_2$), "alite"
C_2S	di-calcium silicate ($2CaO.SiO_2$), "belite"
C_4AF	tetra-calcium aluminate ferrite (4CaO.Al2O3.Fe2O3)
CA	calcium mono-aluminate ($CaO.Al_2O_3$)
CH	calcium hydroxide (mineral name portlandite)
SEM	scanning electron microscope
EDS or EDX	energy dispersive (X-ray) spectroscopy
BSE	backscattered electron
XRD	x-ray diffraction
TCES	thermochemical energy storage
RH	relative humidity

CHAPTER 1

INTRODUCTION AND LITERATURE REVIEW

1.1 Scope and Layout

This dissertation contains an examination of three high ettringite cements for their use in thermochemical energy storage (TCES). These cements were chosen for their high ettringite content on hydration compared to traditional OPC systems. The work presented was undertaken to develop an understanding of the stability and energy of the high ettringite cements during the dehydration and rehydration of the system. The research is presented through a literature review, experimental methods, two manuscripts, and an overarching conclusion to the work. The dissertation is outlined as follows:

Chapter 1: Introduction and Literature Review – This chapter provides an introduction to the work presented in this dissertation as well as the motivation and scope of the work. This chapter also includes a review of the literature related to the types of cement use including their history, composition, hydration, and stability. Literature examining the crystal of interest of this study, ettringite, is presented related to its structure, dehydration, impact of dehydration, and stability. Additionally, an overview of energy and energy storage is presented with a focus on the process of TCES.

Chapter 2: Experimental Methods – This chapter provides an overview of the experimental methods used for the work presented in this dissertation. Each procedure and testing method is described, and images of the equipment used are also included.

Chapter 3: "Energy Output of High Ettringite Producing Cements for use in Thermochemical Energy Storage" – This chapter examines the energy output during rehydration of the cements when dehydrated at different temperatures. The peak heat flow and cumulative heat were analyzed to determine the amount of heat that was able to be recovered from the systems. Energy results were also collected for C$A paste over multiple rehydration cycles for the dehydration temperatures of 60ºC, 75ºC, and 90ºC. The microstructural changes were also analyzed to assist with the understanding of the energy observations.

Chapter 4: "Stability of High Ettringite Producing Cements for use in Thermochemical Energy Storage" – This chapter examines the stability of the cement paste systems as they underwent dehydration and rehydration cycling. The compressive strength was also measured for each system in three different states; at 28 days of hydration, 28 days of hydration plus three days of dehydration, and 28 days of hydration plus one dehydration and rehydration cycle. The mass of dehydrated C$A systems stored at different RH was measured to determine the ability of the systems to be stored for extended periods of time. The microstructural changes were also analyzed to assist with the understanding of the macro-structural observations.

Chapter 5: General Conclusions – This chapter summarizes the goals and findings of the research included in this dissertation. The conclusions from the manuscripts are unified and future research work is presented.

1.2 Introduction

Energy systems have to be designed to consistently meet peak energy demand situations, resulting in costly, inefficient systems that waste energy during low demand periods. In order to create a more efficient, economical, and sustainable system, energy storage solutions that can store energy over long time periods with minimal loss are needed. To date, much of the research has focused on battery energy storage solutions, however the U.S. Department of Energy (USDOE) has noted the need for more revolutionary materials and solutions [1]. Ettringite based cement systems offer a potential solution to this issue using raw materials that are inexpensive and abundant. Ettringite based cements are a special type of hydraulic binder that, when mixed with water, result in the hydration product known as ettringite ($C_6A\$_3H_{32}$). Ettringite crystals can undergo a reversible, stable, thermochemical conversion that may be a viable tool for energy storage. The understanding of the applicable use of these systems is limited for the following main reasons:

1. Ettringite is not commonly found in nature so synthetic or other chemical reactions are needed for its creation, where there is limited information for this use.
2. There is insufficient data on the conditions at what this reaction is stable in, especially in heterogeneous systems.
3. For viable use in energy storage, the amount of energy recovered.
4. There is limited data on the reaction over multiple cycles.

This dissertation presents work that addresses these items. This work examined the influence of three different types high ettringite cements and five different temperatures on the stability of the system (addresses challenge 1, 2, and 4). Additional work was completed to study the compressive strength and the long-term storage of the systems (addresses challenge 2). Finally, the examination of the heat during rehydration was studied for the

following influence factors, cement type, dehydration temperature, and number of cycles (addresses challenges 2 and 4).

1.3 Literature Review

1.3.1 Energy Use

The use of energy has been an essential need for people. The demand is constantly increasing due to an increasing population and an increase in living and comfort standards. Figure 1.1 shows this increase of world energy consumption since 1965, with a quadrupling of the consumption during this period. More than half of the energy used in residential buildings is used for heating and cooling needs [2]. For heating, many different energy sources can be utilized, though for cooling electricity is the primary source [2]. During peak utilization of, especially, cooling systems, the strain on the grid infrastructure can be immense [2]. This is highlighted through the analysis of the energy loads for a typical office building. Figure 1.2 shows the energy load of the typical office building during a day. At peak load, the cooling is responsible for approximately 40% of the total energy loads of the building [2]. This is only expected to increase as air conditioner use in the United States is expected to grow 8 to 13 percent over the next decade and this use could exceed the electric generation capacity [3]. High temperatures causing rolling blackouts have been seen in California in 2020 where the system was expected to be short 4,400 megawatts of power in the late afternoon [4].

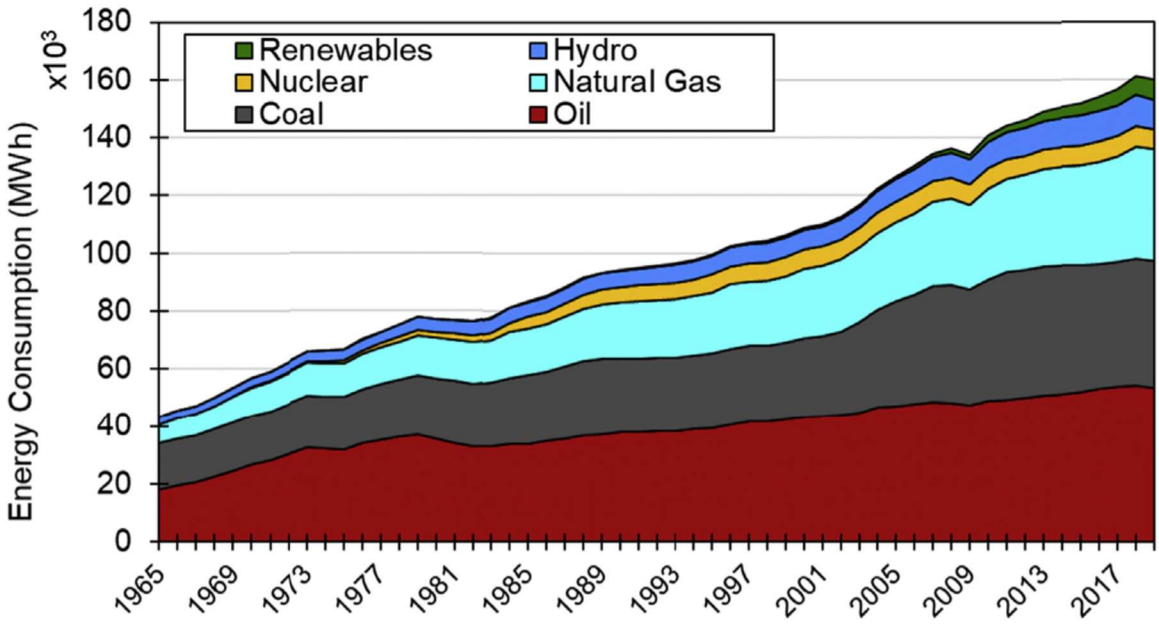

Figure 1.1 World total energy consumption since 1965.
Source: [2].

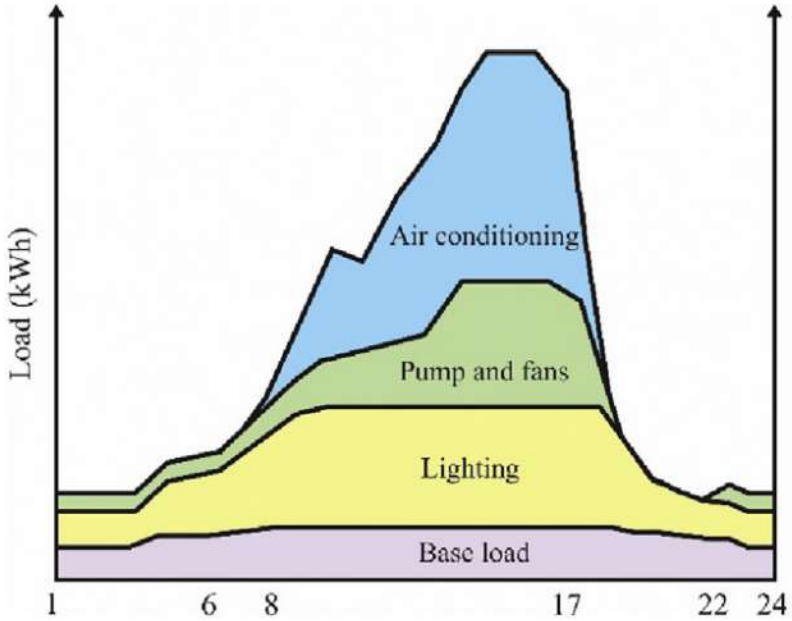

Figure 1.2 Energy loads during the day for a typical office building.
Source: [2].

The interest in the use of renewables has increased over the past decade, especially related to concerns of energy security and sustainability [2]. A current limitation for use is the discontinuous nature in generation of renewable energy. This results in the energy needing to be stored for periods of time to meet demand when generation is low. Another issue that is found in current widely used generation methods is the fluctuation in load due to variabilities in energy consumption. This issue is discussed further in the next section.

1.3.2 Load Leveling

As energy demand fluctuates during different times of the day and year, the energy production needs to scale accordingly. The fluctuations result in inefficiencies within the system such as over building generation capacity or loss from start up or ramping up production. Energy such as electricity can fluctuate on a daily, weekly, and yearly periods. These fluctuations are shown in Figure 1.3 for data collected from the United Kingdom. Based on data from the United Kingdom, electrical usage during low demand periods can be 80% less than found at peak load and on average is 30% less than peak load [2]. These daily trends (Figure 1.3a) are also observed on the weekly (Figure 1.3b) and yearly (Figure 1.3c) time scales.

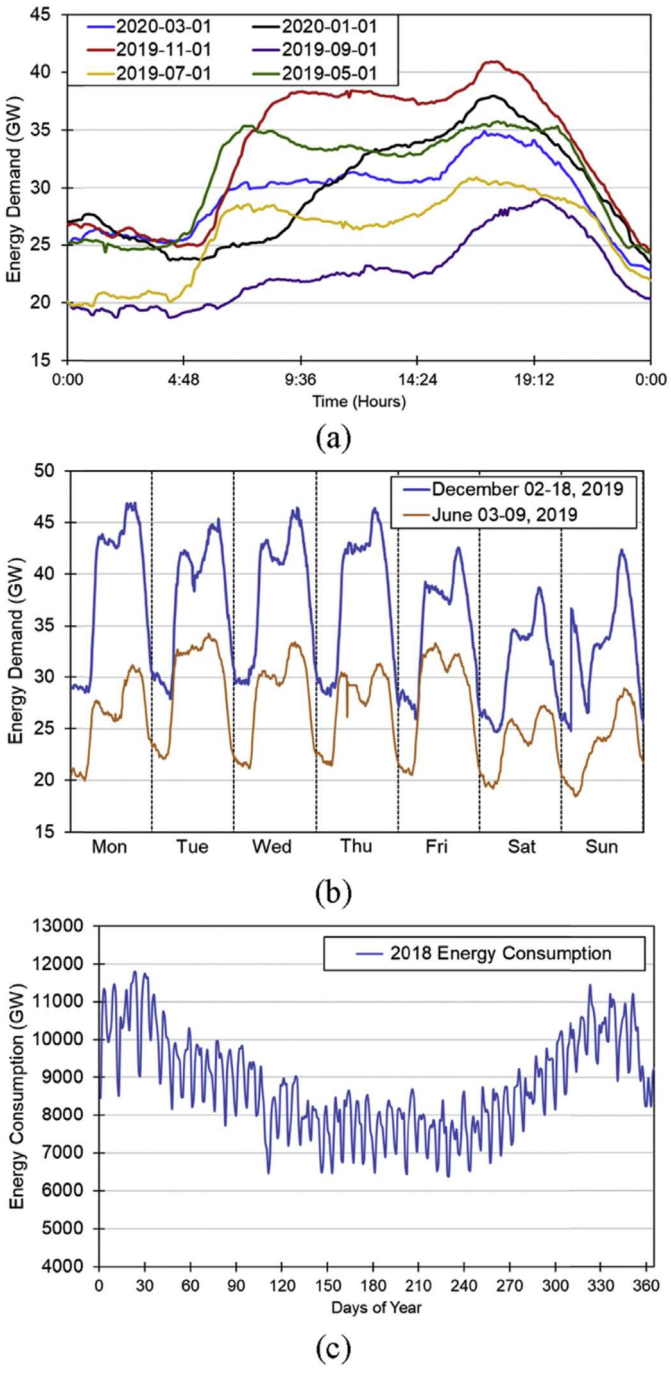

Figure 1.3 Energy consumption in the United Kingdom (a) daily, (b) weekly, and (c) yearly.
Source: [2].

To ensure constant supply of energy, generation capabilities must be designed to meet the maximum output, this results in inefficiencies where extra power plants are needed to be built and only used during these short maximum output periods, else, energy

may need to be imported at high costs [2]. Energy storage in the grid allows for leveling of production and a more optimized use of resources and facilities. A pictorial example of how load leveling works is shown in Figure 1.4 [5]. The goal is to balance the areas of the curve which represent addition to and subtraction from storage, this results in a consistent power generation and better utilization of generation facilities.

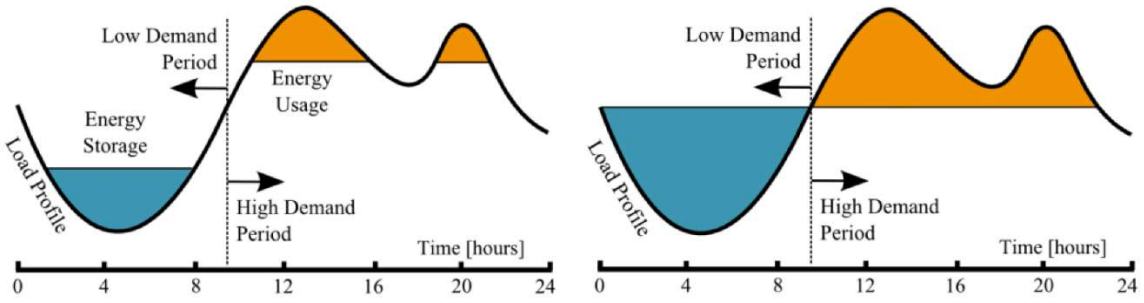

Figure 1.4 Example of load leveling.
Source: [5].

1.3.3 Energy Storage Methods

Practical applications of energy storage can be broken into six different branches, with each branch having many different sub-applications; chemical, thermal, mechanical, electrochemical, biological, and magnetic and electromagnetic energy storage. Each method has advantages and disadvantages depending on usage with many different techniques being studied and improved upon [2]. A breakdown of the classification of energy storage methods is presented in Figure 1.5

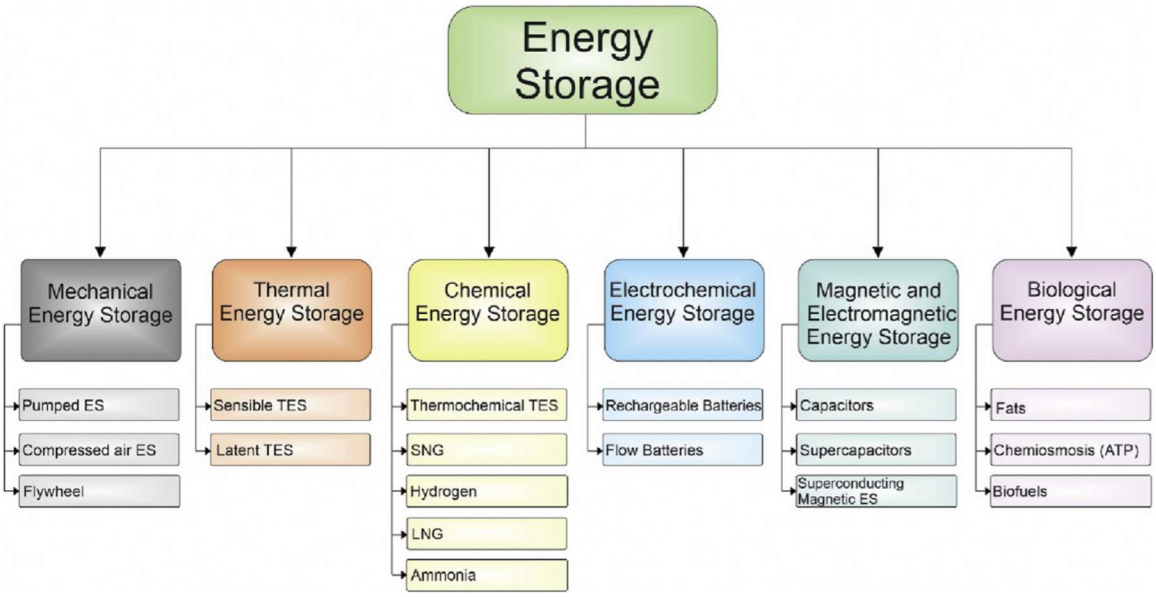

Figure 1.5 Breakdown of different types of energy storage methods with examples of for each type of storage method.
Source: [2].

A 2013 report by the United States Department of Energy (USDOE) focused on how energy storage will play a role in the modernization of the energy grid in order to meet projected energy needs [1]. The primary current concerns outlined in the report are that at present, the United States has 24.6 GW of energy storage, which approximates 2.3% of electric production capacity [1, 6]. A percentage that lags behind other developed countries and regions such as Japan and Europe [1, 6]. As of June 2018, the storage capacity had been marginally increased to 25.2 GW of energy [7, 8]. At the average national rate of 867 kWh per month, this storage capacity represents power for one month for approximately 29,000 households [9]. To compound this problem, 95% of current storage is from the singular method of pumped hydro storage, a form of mechanical energy storage [1, 6]. In pumped hydro storage water is pumped to a higher elevation during lower demand periods to be used for generation during peak time. As this method requires great elevation changes

and ample water supplies, it in unsuitable in flat landed and arid regions. Thus, the USDOE recommends that a diverse portfolio of storage methods should be deployed.

Technology methods outlined in the report and discussed by other entities are fly wheels, advanced batteries (lead-acid batteries, sodium sulfur, lead carbon, lithium-ion), flow batteries, electrochemical capacitors, and thermochemical energy storage. Thermochemical energy storage, which the reaction of the ettringite system falls under, is of interest as an emerging technology that's primary benefit over other methods is its very high energy density, 5 to 20 times conventional storage [1]. No thermochemical storage options were given in the Department of Energy report, but some options such as silica gel, two phase solid-gas salt hydrate, and three phase solid-liquid-gas salt hydrate systems were discussed in an article by Ding and Riffat [10]. The applications of thermochemical energy storage are for load leveling, regulation, and grid stabilization. Though, as an emerging method its use cases are limited and cost prohibitive. The proposed work will focus on furthering the understanding the impacts and governing factors of the ettringite-metaettringite thermochemical reaction in terms of its use as an energy storage medium.

1.3.4 Thermochemical Energy Storage

Storing energy through heat (thermal) processes has a wide range of applications. The study of these systems is important and promising due to the fact that most irreversible losses within systems is in the form of heat and more than half of energy generated and consumed in the world occurs through thermal processes [11]. The three methods of thermal energy storage are, sensible heat, latent heat, and thermochemical. A breakdown of the classification of thermal energy storage mechanisms is presented in Figure 1.6. Most commonly used and best understood are sensible and latent heat which are used for heating,

cooling, and air-conditioning applications [11]. A change of heat in an object without changing the phase is sensible heat where latent heat relates to the heat during the phase change the material [11].

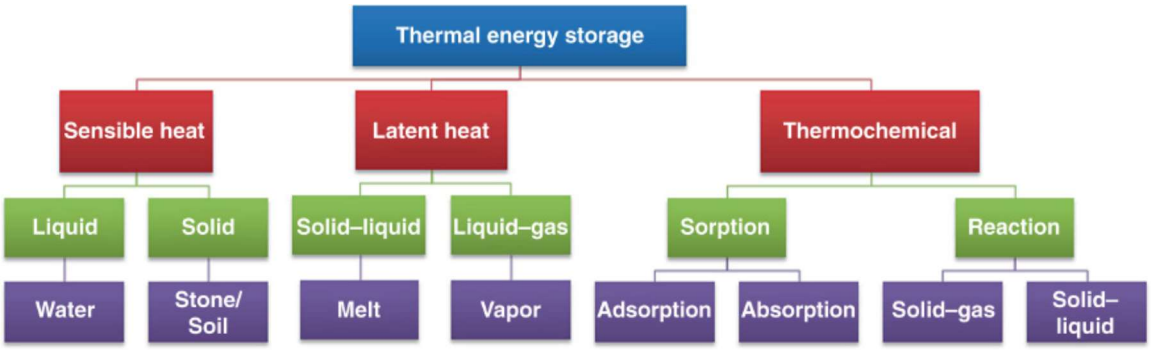

Figure 1.6 Breakdown of different types of thermochemical energy storage methods [12].
Source: [12].

Thermochemical energy storage is the process of using heat in a reversible chemical reaction. In this chemical reaction the chemical compound of generic type A-B can be split into its separate components A and B through the application of heat. After the application of heat, if the components A and B can be kept from recombining then the energy can be stored in the chemical bonds of the system for any period of time [2]. The key component of this reaction is that the energy is stored in the chemical bonds and will remain stored without loss for any length of time as long as the system remains stable. The basic process of TCES has three stages as follows:

- Charging Period: Heat is applied to the system to create an endothermic chemical reaction. This reaction can be conducted as a primary means of charging, typically from a renewable energy source, or during a low energy demand period as part of load-leveling initiates.

- Storing Period: The TCES system is kept in a storage state that will keep the system in a steady condition by preventing the chemical reaction from reversing through uncontrolled means.

- Discharging Period: The TCES will be discharged through the allowing of the exothermic reaction of the stored system to proceed. The heat released from the exothermic reaction can then be used.

An example of TCES is found in the dehydration of salt hydrates. For magnesium hydroxide, the application of heat results in the removal of water from the salt forming magnesium oxide. Stability of the charged system is maintained through the avoidance of water to the system. Once water is introduced magnesium hydroxide will reform with a corresponding release of heat energy. This reversible reaction is shown by Equation (1.1) [12].

$$MgO + H_2O \leftrightarrow Mg(OH)_2 + \Delta_R H \tag{1.1}$$

To function as a storage method, the thermal process for the storage in the medium must be able to be cycled. Thus, the primary disadvantage of TCES is developing a system that is able to keep the unstable system in a state where discharging is not possible [2]. The benefit of this method of storage of energy is that it is able to result in higher energy storage densities than is found in more traditional storage mediums [2]. TCES systems also have the capability of storage of renewables [2]. The method of storage is through energy states of the medium and thus the safety of the system is based on the material that is used for storage and the process to convert the medium between the energy states. The medium used for storage can be of any physical state; liquid, solid, or gas. When compared to other heat energy storage methods such as sensible heat and latent heat storage systems, TCES systems result in a high heat storage capacity without any losses during storage if properly stored.

1.3.5 Thermochemical Storage Concepts

For practical use as a storage medium, methods are needed to operate and regulate the thermochemical systems. The operation of the systems can be divided into two different types, open- and closed-systems. In an open system the reaction is performed at atmospheric temperature and is in contact with the surrounding environment. In a closed-system the reactor is isolated from the environment with the water or water vapor used cycled in is closed loop, typically under negative pressure [12]. Additional systems to evaporate/condense the water as well as extra water reservoir space is necessary in a closed-system. Due to this, the design of an open system is simpler and requires a lower technical effort to use. A comparison of the two types of systems is presented in Figure 1.7.

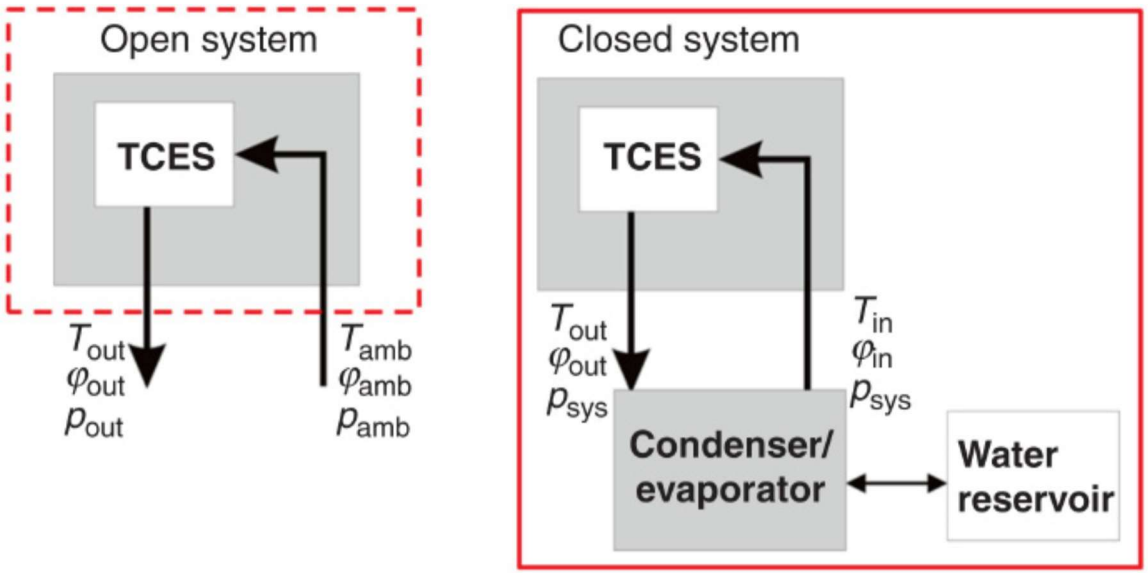

Figure 1.7 Comparison of working process for an open system reactor and a closed system reactor.
Source: [12].

1.3.6 Thermochemical Dehydration-Rehydration of Ettringite

In the cement based systems the thermochemical reaction occurs through the chemical binding and unbinding of water within the ettringite crystal. The low water content state of the ettringite crystal has been termed metaettringite [13]. The phases of the idealized reaction are as follows:

- Charging Period: Heat is applied to the cement paste system to create an endothermic chemical reaction. The application of heat results in the removal of water from the ettringite crystal, turning it to the metaettringite state. This reaction has been found to be stable at dehydration temperatures in the range of 60 to 120°C [14, 15].

- Storing Period: The cement paste system is stored in an environment free from moisture, preventing the chemical reaction from reversing.

- Discharging Period: Water is reintroduced to the system resulting in heat being discharged through the exothermic reaction of the water chemically binding to the met-ettringite to reform the ettringite state. The heat released from the exothermic reaction can then be used.

The process can then be repeated with the cyclic reaction proceeding according to Figure 1.8 as long as the ettringite crystal and the system maintain stability. The reaction of the cyclic reaction proceeds according to Equation (1.2) where x is the amount of water that remains in the metaettringite crystal.

Figure 1.8 Simplified diagram of the cyclic conversion process of the ettringite-metaettringite thermochemical reaction.

$$C_6A\$_3H_x + (32 - x)H \leftrightarrow C_6A\$_3H_{32} + \Delta_R H \quad (1.2)$$

1.3.7 Cement Basics

Hydraulic cements are a class of finely ground materials that form hydrates when exposed to water. Hydraulic cements, such as ordinary portland cement (OPC), the most common hydraulic cement, are a primary constituent of cement paste, mortar, and concrete. Cement pastes are formed from just the hydration of the cement, while mortar and concrete consist of aggregates mixed with the hydrated cement [16]. Cement is manufactured by heating a mixture of several compounds to a high temperature where reactions between calcium oxide and silica, alumina, and iron oxide occur to form large granules called clinker. The clinker is then finely ground to produce the anhydrous cement. The principal anhydrous compounds formed and make up OPC are C_3S (45-60%), C_2S (15-30%), C_3A (6-12%), and C_4AF (6-8%)[16]. Recently, other types of hydraulic cements have been developed to meet different needs. The research outlined in this dissertation will look at the hydraulic cements known as calcium sulfoaluminate (C$A) cement and associated high ettringite producing blended calcium aluminate cement (CAC) systems for their use in storage of thermal energy.

In C$A cements, the main compound is $C_4A_3\$$ which represents between 50 and 90% by weight of the clinker [17]. The compound $C_4A_3\$$ is also referred to as tetracalcium trialuminate sulfate, Klein's salt, and ye'elimite [18]. The compounds, and their amounts, will influence the hydrates that form upon mixture with water.

Calcium trisulfoaluminate hydrate or ettringite is a common hydration product found in OPC and other alternative hydrated hydraulic cements. The ettringite crystals that

form during hydration are typically long needle like crystals, however, when formed after hardening, can cause expansion and cracking of the macro-system. This is typically only seen in mass concrete where the heat generation during hydration results in the ettringite going into solution and reforming at later ages when the temperature drops. The chemistry of these systems has been well defined by past researchers and is not a part of the work in this dissertation. The goal of this work is focused on a new beneficial use of the alternative cement systems related to the use of the ettringite hydrate in energy storage.

1.3.8 Ettringite in Hydrated Cements

Calcium trisulfoaluminate hydrate or ettringite is a mineral that while found rarely in nature, is a common hydration product found in hydrated portland cements and other hydrated hydraulic cements. In portland cement based systems, ettringite is formed during the early stages of hydration and at later ages (>1 day) converts to monosulfate hydrate. In OPC based systems ettringite and monosulfate hydrates occupy 15 to 20 % of the hardened cement paste volume [16, 19, 20], with ettringite occupying ten percent of the paste volume [14]. In other binders, such as C$A, ettringite content can be >80% of the hardened paste by mass [21–23].

The ettringite crystals that form during hydration are typically long needle like crystals. Ettringites can come in different forms and are based on their solid forms. The form of ettringite, calcium trisulfoaluminate hydrate, is known as sulfate ettringite. The sulfate ettringite is formed when calcium sulfate reacts with tricalcium aluminate (C_3A) at room temperature [21, 24]. Other forms of ettringite are carbonate ettringite that are made using calcium carbonate, and hydroxy ettringite made using calcium oxide as reactants in place of the calcium sulfate [24].

While OPC is a material that is quite versatile and heavily used in the construction industry, alternative cements are typically used for specialized situations where other project constraints result in OPC mixtures not being the preferred alternative. One situation where an alternative cement like C$A would be chosen is where high early strength is needed. The rapid strength gain in C$A cement systems due to the formation of ettringite. Other rapid hardening cements such as CAC have gained interest. CAC is of particular interest for repairs in cold weather climates due to the hydration reaction being able to happen at near freezing temperatures. Blended CAC systems have shown to be able to form ettringite as a primary hydrate [25].

1.3.9 Calcium Sulfoaluminate Cement (C$A)

C$A is an alternative cement that rapidly gains strength and hardening upon hydration. The characteristics of C$A result in use where rapid setting of the cement system is necessary as well as where sulfate resistance and freeze-thaw performance is needed. An overview of C$A, unhydrated composition, hydration, and stability of C$A is discussed in the following sections.

1.3.9.1 C$A Cement Overview. First mentioned in a French patent in the 1930s, C$A cement production developed during the 1970s and 1980s, primarily in China [26]. The original use of C$A cement was as an addition to OPC systems to compensate for shrinkage due to the expansive characteristics of this system. C$A, when used as a standalone cement, typically does not expand. The expansive nature of C$A is found when hydrated in an alkaline environment, presence of lime, or with high quantities of calcium sulfate [27]. C$A is primarily composed of tetracalcium trialuminate sulfate. This compound is more commonly referred to as “Klein’s compound” after American inventor Alexander Klein of

the University of California, Berkeley or ye'elimite [17]. C$A cement is starting to see more widespread use throughout the world and while a newer product, it is one of the commonly used types of cements in China. In the United States it has seen use as a rapid repair material for highways and airport runway replacements [28].

C$A based cements have become popular as a material to study due to the manufacture process releasing a third of the CO_2 released by the production of alite (C_3S); the firing temperature to produce the clinker is about 200^oC lower than that needed to produce OPC. In the creation of C$A, industrial by products can be used to produce the clinker, and grinding of the ye'elimite clinkers to produce the final cement fineness requires less energy than OPC [18].

The reduced CO_2 emissions is accounted by the combination of low calcium content relative to OPC requiring less heat to form the clinker products, the high level of interground gypsum (15-25%), and lower energy input needed to grind the clinker and gypsum to make the final cement. C$A cements are classified together as a group, though Alvarez-Pinazo et al. proposed that the C$A cements could be classified according to their ye'elimite content [18].

1.3.9.2 Composition of Un-hydrated C$A. Manufacture of C$A cements typically include the raw materials of limestone, bauxite or aluminous clay and gypsum [29]. A problem with the manufacture of C$A is the source of the alumina content, in which the primary source of the alumina, bauxite, can carry a high cost [30]. This high cost has resulted in other sources such as waste materials of fly ash, blast furnace slag, phosphogypsum, baghouse dust, scrubber sludge, and "red mud" from alumina purification to have been studied as alternatives [29–31]. Fly ash and blast furnace slag are already used

as supplementary cementitious materials with OPC. The raw materials are heated in a rotary kiln to a maximum temperature of approximately 1300°C to create the clinker. The main phase of C$A, ye'elimite, forms according to Equation (1.3) during the heating in the kiln at 1250°C and is stable to temperatures of approximately 1350-1400°C [17]. The ye'elimite crystal is tetragonal consisting of corners of AlO_4 tetrahedra, Ca^{2+} and SO_4^2 [17, 32, 33]. The second most common phase is calcium sulfosilicate with stability is between 1100 and 1180°C.

$$3CaCO_3 + 3Al_2O_3 + CaSO_4.2H_2O \rightarrow 4CaO.3Al_2O_3.SO_3 + 3CO_2 + 2H_2O \quad (1.3)$$

While C$A cement was originally used as an expansive additive, the calcium sulfoaluminate–belite cement was developed as a dimensionally stable type. In this type, the cement is primarily comprised of belite and ye'elimite. For the work performed in this dissertation, this type was used due to the non-expansive nature. For this cement, the clinker is inter-ground with gypsum at percentages between 16 and 25% depending on the C$A type and application. The phase composition of a standard commercial grade of C$A cement clinker and clinker inter-ground with gypsum is presented in Table 1.1.

Table 1.1 Phase Comparison of OPC and C$A Clinker Mineralogy

Comparison of clinker mineralogies

Phase/cement	OPC	$C\bar{S}A^{a}$
C_2S	Yes	Yes
$C_2(A,F)$	Yes	Yes
$CaSO_4$[b]	Yes	Yes
C_3S	Yes	No
C_3A	Yes	Trace
C_4A_3S	No	Yes

[a] Shorthand for calcium sulfoaluminate.

[b] Including gypsum and hemihydrate. Much or all the calcium sulfate is added in the course of grinding clinker.

Source: [29].

1.3.9.3 Hydration of C$A. C$A cements can exhibit rapid setting and high early strength. The primary hydration reactions related to C$A cements are shown by Equations (1.4) – (1.10) [34]. The reaction that forms ettringite is the hydration reaction of tetracalcium trialuminate sulfate ($C_4A_3\$$) and gypsum ($C\$H_2$) with water [21, 34–38] which is expressed by Equation (1.5). If the molar ratio of calcium hydroxide (CH) and gypsum is at least 1:2 then the dominant reaction results in the formation of ettringite and monosulfate according to Equation (1.9). After the depletion of calcium sulfate, primarily monosulfate will instead start to form in accordance with Equation (1.10). If depletion of $C_4A_3\$$ occurs faster than that of calcium sulfate ettringite may still form in the presence of aluminum hydroxide and calcium hydroxide according to Equation (1.7). A corresponding decrease in the concentrations of calcium and sulfate in the pore solution and an increase of the pH can be observed with the depletion [21, 22]. During hydration of the $C_4A_3\$$, it has been observed that 60-70% will react within 24 hours with full reaction by 28 days [39].

$$C\bar{S} + 2H \rightarrow C\bar{S}H_2 \quad (1.4)$$

$$C_4A_3\bar{S} + 2C\bar{S}H_2 + 34H \rightarrow C_6A\bar{S}_3H_{32} + 2AH_3 \quad (1.5)$$

$$C_4A_3\bar{S} + 8C\bar{S}H_2 + 6CH + 74H \rightarrow 3C_6A\bar{S}_3\,H_{32} \quad (1.6)$$

$$AH_3 + 3CH + 3C\bar{S}H_2 + 20H \rightarrow C_6A\bar{S}_3\,H_{32} \quad (1.7)$$

$$3C_4AF + 12C\bar{S}H_2 + 110H \rightarrow 4C_6(A,F)\bar{S}_3\,H_{32} + 2(A,F)H_3 \quad (1.8)$$

$$2C_4A_3\bar{S} + 2C\bar{S}H_2 + 52H \rightarrow C_6A\bar{S}_3H_{32} + C_6A\bar{S}_3H_{12} + 4AH_3 \quad (1.9)$$

$$C_6A\bar{S}_3H_{32} + AH_3 \rightarrow C_6A\bar{S}_3H_{12} + 2H \quad (1.10)$$

1.3.9.4 Stability of Hydration of C$A Cement. Ettringite formation in OPC is typically associated with the expansion and deterioration mechanisms of delayed ettringite formation and external sulfate attack. The formation of ettringite crystals is expansive in nature and, when formed within hardened OPC, can cause paste cracking and deterioration of the sample. As ettringite is the primary product of C$A cement systems, the dimensional stability must be considered. Papers on C$A cement systems have identified $C_4A_3\$$ content, pore structure, w/c ratio, sulfate content, free lime content, alkali hydroxide content, and cement particle fineness as factors that may impact the dimensional stability of the hardened paste [22, 34].

The more $C_4A_3\$$ that is available, the more ettringite that can be formed. This results in higher expansion with higher $C_4A_3\$$ content cement, the converse of lower $C_4A_3\$$ content resulting in little to no expansion has also been observed [34]. The dimensional stability of C$A can be observed in Figure 1.9 from Chen et al. [34] in which only high $C_4A_3\$$, (HS) exhibited large expansions at w/c 0.45 when close to the stoichiometrically required gypsum content was used. Janotka et al. [40] found that the lower $C_4A_3\$$ content

in their C$A-belite cement (20.2% $C_4A_3$$) had a higher porosity and coarser pore structure than PC at w/c 0.5 when both were tested at 90 days. Both were non-expansive.

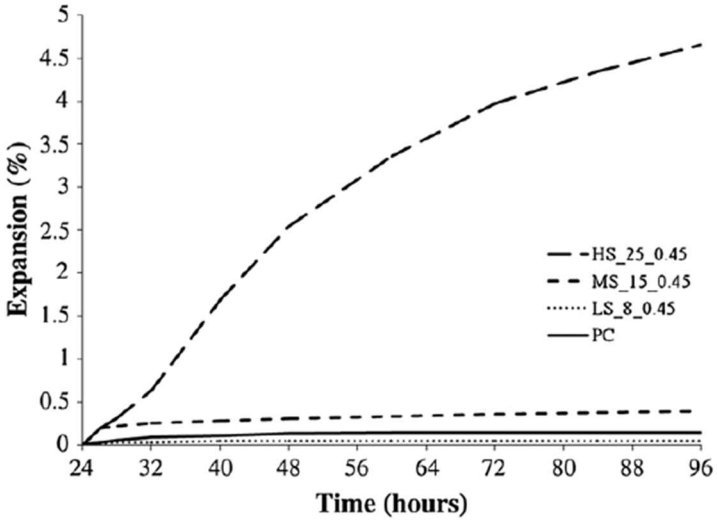

Figure 1.9 Dimensional stability of OPC and different $C_4A_3$$ content C$A cements.
Source: [34].

The hydration by Equation (1.5) to Equation (1.9) involve large quantities of water to be satisfied. If there is insufficient water to complete the reaction, the reaction is considered not to be stoichiometric, typically resulting from a low water to cement ratio (w/c). This low water state results in the hardened paste having unreacted cement that will react when exposed to more moisture [34]. Chen et al. [34] found that decreasing the w/c ratio results in expansion from two different mechanisms:

1. the lower w/c ratio results in a denser hydration space, when the products such as ettringite and AH3 do form their growth creates pressure inside the paste causing cracks and expansion, and

2. the low w/c ratios do not provide sufficient moisture for the cement to react before self-desiccation, the expansion occurs later due to the reaction of the cement and supplied external water [34].

Sulfate in the curing environment can increase the expansion of the C$A cement during hydration. When similar C$A content cements were cured in either a saturated $CaSO_4$ or a 5% Na_2SO_4 solution, the saturated $CaSO_4$ samples exhibited ~0.1% expansion after 91 days and the 5% Na_2SO_4 exhibited more than 5% expansion within 14 days, results from Chen et al. seen in Figure 1.10 [34]. Chen et al. interestingly noted that while a much greater expansion was seen in the 5% Na_2SO_4 cured samples, there was a similar amount of unreacted $C_4A_3\$$ in each. This led to the conclusion that the sulfate ions do not accelerate the $C_4A_3\$$ reaction but facilitate the precipitation of the formed ettringite. This addition to the precipitation would cause the rapid expansion observed. The stated reason by Chen et al. for the difference between the sulfate solutions is that the concentrations were not the same, with the Na_2SO_4 having a higher solubility as compared to the $CaSO_4$.

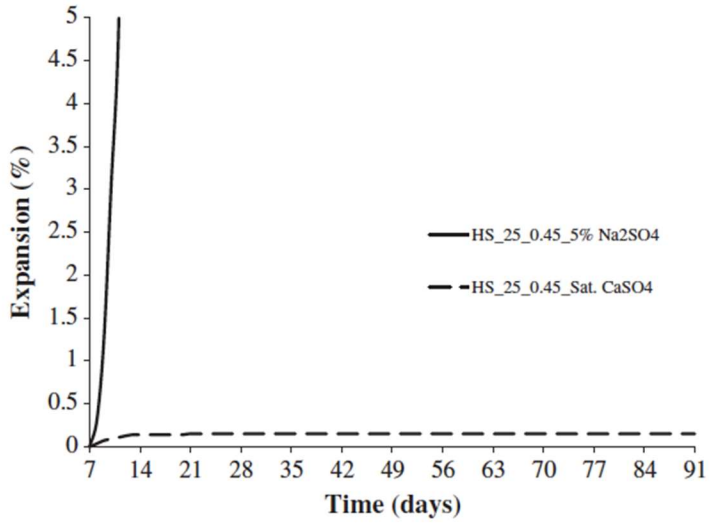

Figure 1.10 Sulfate resistance of the C$A under differing sulfate curing conditions.
Source: [34].

1.3.10 Calcium Aluminate Cement – Calcium Sulfate Blend (CAC-C$)

1.3.10.1 History of CAC. Calcium Aluminate Cements were originally developed to provide resistance against sulfate attack and chemical corrosion of the cement in the early 1900's by J.J. Bied who worked for J. & A. Pavin de Lafarge of France [41]. Sulfate attack in concrete was a known phenomenon in various regions of France at the time and thus, the development of a sulfate-resistance cement was needed to ensure longevity of the material [41]. The first patent for the manufacturing of CAC was in 1908 with the cement becoming readily available within ten years. The cement was known for its sulfate resistance and for its ability to rapidly gain strength. Due to these characteristics, the cement found use during WWI in the repair of gun emplacements [42]. CAC also found use as a liner in tunnels. In 1922 a tunnel in France was reinforced with CAC and another constructed for a railway running between Paris-Lyin-Marselle constructed through anhydrate used CAC to protect against sulfate attack.

Starting in the 1940's the use of CAC was expanded with the building code in the United Kingdom allowing the use for structural members. Due to the rapid strength gain of the material, it gained popularity for use in precast concrete construction during the 1950's. Though, due to three structural collapses of prestressed concrete beams made with CAC in the 1970s, the use of CAC for structural members has been limited. A contributing factor to the failures was the conversion of the CAC hydrates which formed upon initial hydration to a more stable state over a period of time. The stable hydrates are denser than the initial metastable states resulting in an increase in porosity and corresponding decrease in strength. In blended systems, the conversion process is not a concern because the metastable hydrates are not formed as a hydration product.

1.3.10.2 Composition of Unhydrated CAC. Calcium aluminate cement is manufactured through the heating of bauxite and limestone in a furnace. The clinker is pulverized in a ball mill to reach the desired particle size. There are different grades of CAC and the composition of each grade will vary. For standard grade CAC, the alumina content comprises approximately 40% of the cement with amounts of ferric or ferrous oxides of up to 20%. Purer CAC will contain higher amounts of alumina and lower amounts of iron oxides. Standard grade CAC was used in this study. The composition of the CAC differs significantly from OPC and the typical compositions are shown in Figure 1.11 and summarized in Table 1.2 [41, 43].

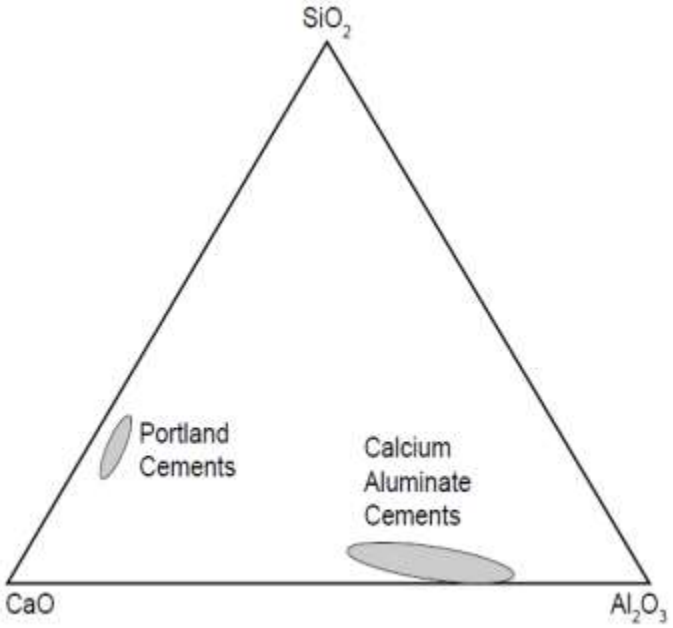

Figure 1.11 Comparison of composition of portland cement and calcium aluminate.
Source: [41].

Table 1.2 Range of Hydrates Formed by OPC and CAC Hydration

	Phase Hydrate	Ordinary Portland Cement	Calcium Aluminate
Silicates	C_3S	50--70	0
	C_2S	15--30	< 10
Aluminates	C_3A	5--10	0
	C_4AF	5--15	10--40
	CA	0	40--50

The main phase in the unhydrated system is monocalcium aluminate, typically comprising 40% or more of the CAC depending on the type [41]. Calcium dialuminate (CA_2) is also found in large quantities and its content increases with the amount of calcium oxide present [41]. Other constituents such as dodecacalcium heptaluminate ($C_{12}A_7$, manyenite), which increases the reactivity of the CAC, may also be present within the system. Minor constituents which form in CACs with higher alumina contents are dicalcium aluminate (C_2A) and hibonite (CA_6) [41]. For the work in this dissertation, the CAC cement was blended with C$.

1.3.10.3 Hydration of CAC-C$. The primary hydrates which form from CAC-C$ systems are ettringite and aluminum from the reaction between monocalcium aluminate and calcium sulfate. The form of calcium sulfate can alter the hydration and stability characteristics of the blended cement system [44]. The hydration reaction of monocalcium aluminate and calcium sulfate in the binary CAC-C$ system results in the formation of ettringite and aluminum hydroxide according to Equation (1.11) [17, 45]. If calcium hydroxide is added to the CAC-C$ system the hydration will result in the formation of only ettringite according to Equation (1.12) [46]. The value of x in Equation (1.11) and

Equation (1.12) depends on the type of calcium sulfate that is used; x = 0 for anhydrite, x = 0.5 for hemihydrate, and x = 2 for gypsum [46]. To ensure the formation of ettringite calcium sulfate is necessary, if the calcium sulfate is depleted, monosulfoaluminate will form from the reaction of the formed ettringite and the unreacted tricalcium aluminate according to Equation (1.13).

$$3CA + 3C\$H_x + (38 - 3x)H \rightarrow C_3A \cdot 3C\$ \cdot H_{32} + AH_3 \quad (1.11)$$

$$3CA + 9C\$H_x + 6CH + (90 - 9x)H \rightarrow C_3A \cdot 3C\$ \cdot H_{32} \quad (1.12)$$

$$C_3A \cdot 3C\$ \cdot H_{32} + 2C_3A + 4H \rightarrow 3C_3A \cdot C\$ \cdot H_{12} \quad (1.13)$$

1.3.10.4 Stability of CAC Based Systems. The formation of ettringite in a CAC-C$ system is heavily dependent on the ratio of CAC to C$. These cement systems have been found for use in self-leveling products, tile adhesives, and rapid repair products [47]. In work performed by Le Saout et al., the hydrated phases were found to be primarily ettringite and AH_3 when the CAC to C$ ratio was 1. When the ratio was increased to 2.3, less ettringite was found to form due to the reduction in the available calcium sulfate content [48–50]. At the higher ratio, other hydrates such as monosulfate phases and strätlingite were found. Martin et al. found similar results where the increase of the calcium sulfate content facilitated in the formation of ettringite [44]. Mixtures with a low quantity of hemihydrate were also found to form monosulfate and strätlingite. In their work C$·$H_2O$, or hemihydrate, was used as the calcium sulfate source due to its high kinetics of dissolution [44]. To promote the formation of ettringite sufficient sulfate was found to be needed as lower sulfate content was found to lead to an increase in the formation of

monosulfate [44]. Berger et. al studied the impact that the calcium sulfate type had on the hydration and properties of the ettringite system. Of the calcium sulfate characteristics studied, solubility best explained the variation in performance if the mixtures. The hemi-hydrates were found to result in quicker hardening, and better strength and shrinkage compensation than anhydrites due to the higher solubility of hemihydrates [51]. The lower solubility of anhydrides was found to result in less formation of ettringite and more precipitation of monosulfate.

1.3.11 Accelerated Ternary OPC-CAC-C$ System

The use of blended systems with OPC can be used to decrease the setting time compared to an only OPC system [52]. In these systems, the OPC is blended with a non-expansive cement to form ettringite at early ages. Two such cements that when blended with OPC and form ettringite are the binary blends of calcium aluminate cement and calcium sulfate or calcium sulfoaluminate cement blended with calcium sulfate [25]. For the work in this dissertation, only the OPC-CAC-C$ blend will be studied. The formation of ettringite in these systems results in the decrease in setting time along with the rapid gaining of strength as compared to a traditional OPC system. The ettringite crystal formed is discussed further in the following Section 1.3.12.

Depending on the use, the ternary systems will comprise primarily of OPC or the binary CAC blend. Applications of rapid repair and shrinkage compensation are typically OPC rich with a percentage of 70% OPC due to the low amount of calcium sulfate. This region is represented by area “1” in Figure 1.12. Systems where the binary CAC blend is the primary cement type are used in applications such as self-leveling screeds, tile

adhesives, and rapid-repair mortars and are characterized by rapid hardening, self-drying, and size variation control [45]. These systems are represented by area “2” in Figure 1.12.

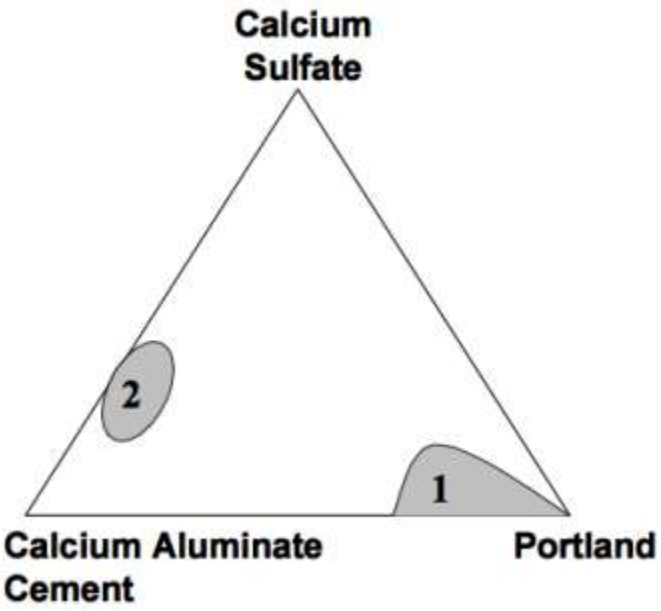

Figure 1.12 Cement blends of PC-CAC-C$.
Source: [45].

The hydration of the ternary systems is not characteristic of either pure OPC or CAC system. In OPC systems, the ettringite initially formed is of lower quantity than C$A systems and further converts to monosulfate during the remainder of the hydration reaction. The meta-stable hydrates of CAH_{10} and C_2AH_8 typically associated with the initial hydration of CAC are not formed due to the presence of OPC and additional amounts of C$. The addition of OPC in the system results in the formation of C-S-H, CH, ettringite, and monosulfate within the system. These reactions are presented in Equation (1.14) through Equation (1.19) [46, 53]. The presence of these OPC hydrates alters thermodynamics of the reactions of the binary CAC-C$ system described previously. The aluminum hydroxide formed from the binary system cannot co-exist thermodynamically

with the calcium hydroxide formed from the OPC. This results in other hydrates forming according to the following conditions. In the presence of calcium sulfate ettringite will form according to Equation (1.14), in the presence of calcium carbonate, monocarboaluminate will form according to Equation (1.15), and in the lack of presence of any other phase hydrogarnet will form according to Equation (1.16) [25]. Thus, to promote the formation of ettringite within the ternary system, sufficient calcium sulfate is needed to promote the reaction defined in Equation (1.14). The addition of OPC will also result in the presence of alite within the system. Alite can form strätlingite and calcium hydroxide (CH) according to Equation (1.17) in the presence of AH_3. In the presence of alite and calcium carbonate, ettringite may be consumed to form monocarobonate according to Equation (1.18) and hemicarboaluminate. according to Equation (1.19).

$$AH_3 + 3CH + 3C\$H_x + (26 - 3x)H \rightarrow 3C_3A \cdot 3C\$ \cdot H_{32} \quad (1.14)$$

$$AH_3 + 3CH + C\check{C} + 5H \rightarrow 3C_3A \cdot 3C\check{C} \cdot H_{11} \quad (1.15)$$

$$AH_3 + 3CH \rightarrow 3C_3AH_6 \quad (1.16)$$

$$AH_3 + C_3S + 6H \rightarrow C_2ASH_8 + CH \quad (1.17)$$

$$C_3A \cdot 3C\$ \cdot H_{32} + 2C_3A + 3C\check{C} + 7H \rightarrow 3C_3A \cdot 3C\check{C} \cdot H_{11} + 3C\$H_2 \quad (1.18)$$

$$C_3A \cdot 3C\$ \cdot H_{32} + 2C_3A + 1.5C\check{C} + 10H \rightarrow 3C_3A \cdot 3C\check{C}_{0.5} \cdot H_{12} + 3C\$H_2 \quad (1.19)$$

1.3.12 Ettringite Crystal Structure

The structure of ettringite has been widely studied and is based on columns and channels. The columns of the crystal have the empirical formula $[Ca_3Al(OH)_6*12H_2O]_{3+}$ and are parallel to the c axis [20]. The $Al(OH)_6$ octahedra alternate with triangular edge-sharing

groups of CaO_8 polyhedra. An OH- is shared. The cylindrical surface of the column is formed by each Ca atom being coordinated by four H_2O molecules. The channels between the columns are represented by the formula $[3(SO_4)*2H_2O]6-$ and comprise the sulphate and zeolitic water [20]. The column and channel formulas represent the chemical formula of ettringite: $[Ca_6Al_2(OH)_{12}*24H_2O]6+[3(SO_4)*2H_2O]_{6-}$ [20]. This formula represents the composition of ettringite per half unit cell. Other forms that this formula is typically represented by are $Ca_6A_{l2}(OH)_{12}*(SO_4)_3*26H_20$, $3CaO*Al_2O_3*3CaSO_4*32H_2O$, or $C_6A\$_3H_{32}$; the last is the form in cement notation [54–56]. These chemical formulas represent 32 molecules of water per half unit cell of ettringite structure, though it is important to note the reported water values many differ from 32 molecules based on actual measured values. While a water value of 32 is agreed by most researchers as the maximum value, there are reports in which water in the crystal containing 36 water molecules [13, 57–59]. A water content of 36 is typically associated with having six H_2O molecules of zeolitic water instead of the two molecules typically noted. The 32 molecule form of ettringite will be termed as fully saturated for the purposes of this work and termed Ett32, ettringite without zeolitic water at 30 molecules will be termed Ett30. The removal of the zeolitic water, whether two or six molecules, will not result in any noticeable changes in the ettringite crystal structure due to this water being located within the voids in the crystal structure [13, 58, 60]. The crystal structure of ettringite can be seen in Figure 1.13 and in Figure 1.14. Figure 1.13 represents the ettringite crystal structure along the C-axis while Figure 1.14 represents the 2x2x2 ettringite unit cell configuration as viewed down the c-axis.

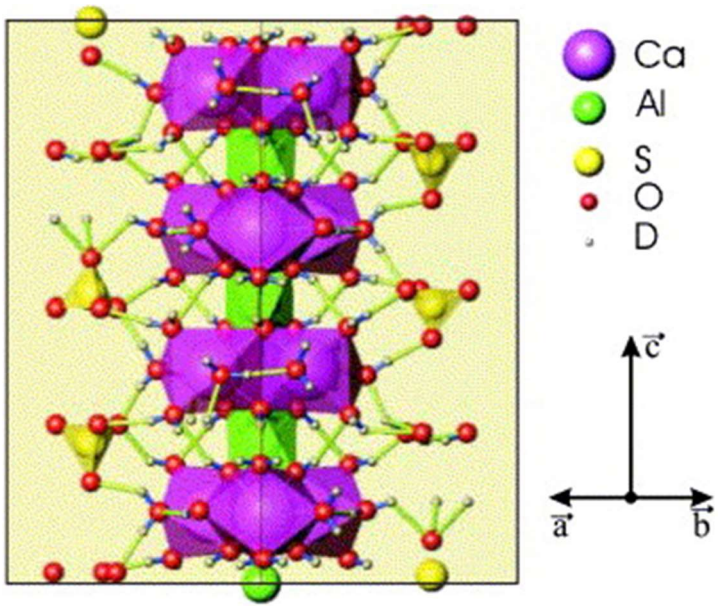

Figure 1.13 Ettringite crystal structure along the c-axis.
Source: [61].

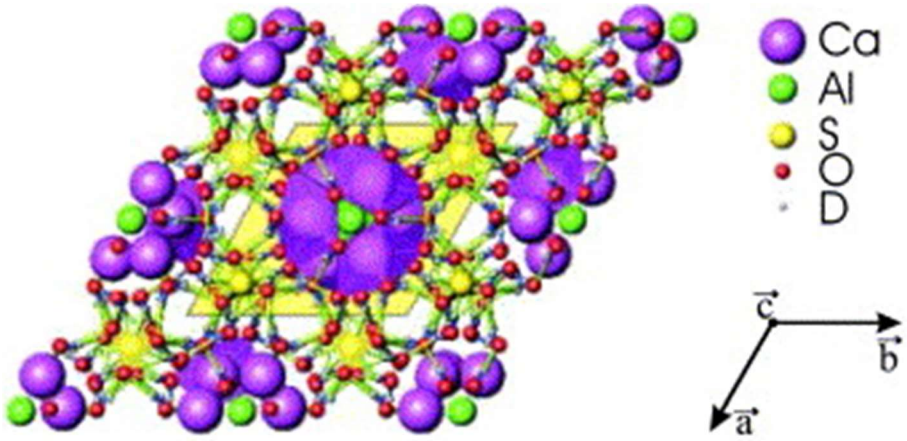

Figure 1.14 Ettringite crystal structure, 2x2x2 unit cell configuration viewed down the c-axis.
Source: [61].

Ettringite crystals are hexagonal in structure and are in the P31c space group. The lattice parameters of ettringite have been extensively studied with Table 1.3 summarizing the different results for parameters a and c. It is important to note that these values are only

for the wet ettringite crystal. The values for dehydrated ettringite will be discussed in Section 1.3.14.

Table 1.3 Unit Cell Parameters of Ettringite

Study Reference	Year	a_o (Å)	c_o (Å)
[62]	1970	11.26	21.48
[63]	1998	11.167+/- 0.005	21.260+/- 0.001
[63]	2005	11.229+/-0.001	21.478+/-0.003
[61]	2006	11.66881(82)	21.25266(22)
[63]	2008	11.240+/-0.001	21.468+/-0.006

1.3.13 Ettringite Dehydration

Dehydration of ettringite is primarily conducted through either application of heat, control of relative humidity, or a combination of the two. As dehydration conditions are applied, water is lost from the ettringite crystal structure. Depending on the degree of dehydration ettringite crystals may form the amorphous form called metaettringite or exhibit some decomposition to monosulfate [13, 58]. There is no consensus as to the mechanism of water loss from the Ett32 crystal. At lower degrees of dehydration, the water loss may not impact the ettringite crystal structure properties such as unit cell size and crystallinity [13]. This section will detail the dehydration process past this point and the structural changes that ettringite undergoes as the further water is lost from the system. In research conducted by Skobinskaya and Krasilnikov [60, 64] the decomposition of ettringite during dehydration is described as comprising of the loss of four different types of water the first being the loss of the zeolitic water, the second being a loss of 12 H_2O from the Ca polyhedral of the

crystal columns until n=18, where n represents the number of molecules of water in the crystal. During this stage, the basic structure of the crystalline ettringite was maintained but a large decrease in the a lattice parameter was observed. Diffraction line broadening during the drying may have impacted the determination of the lattice parameters [64]. The third stage comprises of the removal of the remaining 12 H_2O that are bound to the Ca atoms. From n=18 to n=16 the water removal took place at constant vapor pressure. After n=16 was reached, the vapor pressure continually decreased. When n=12 was reached, low vapor pressure and heat were needed to remove the last H_2O molecules from the Ca polyhedral, the vapor pressures needed for this last step were between 0.8 and 20 Pa and the temperatures were between 18 and 180^oC [64]. A decrease in the pressure and an increase in temperature was needed for the removal of each additional molecule. This step was able to reach n=6.

Work related to the stability of ettringite as a function of water vapor pressure and temperature by Zhou and Glasser also details the dehydration of ettringite [58]. At low water vapor pressures, the water content will drop below n=30 and reach a minimum value between n=10 and n=13. During the decrease in water content in the ettringite crystal, there is a corresponding progressive decrease in crystallinity reaching an amorphous state, or close to, when the minimum water content is reached. When the water vapor pressure was increased, the ettringite became more crystalline again. This reformation of the ettringite crystal is important as it demonstrates a hysteretic process. The dehydrated amorphous form was termed metaettringite and will be used to describe the dehydrated form of ettringite in this work [58]. Dehydration of the ettringite crystal primarily consists of three

different types, heating to drive off the water, storage in a low relative humidity environment, or storage in a low-pressure environment.

Renaudin et al. completed a comparative study of the crystal structure of wet and dried ettringite [54]. The dried ettringite studied was dried at 35% humidity. When the crystal structures were compared, there were very minor difference in the lattice parameters, further discussed in Section 1.3.14. Only when the 11% RH dried ettringite was also subjected to drying at 50°C were the water and hydroxyl molecules lost from the ettringite crystal, this simultaneous loss of water and hydroxyl molecules was also observed by Hartman et al. [54, 61]. This simultaneous loss of water and hydroxyl molecules does not conform to the step process described by Skobinskaya et al. and is refuted by Baquerizo et al. as the loss of the hydroxyl (OH)- should produce a collapse of the columnar structure of the suggested metaettringite structure, which was not observed [57, 60, 61, 64]. Baquerizo et al. also studied the dehydration of ettringite under heating and relative humidity which indicated that at 50°C, ettringite was preserved at relative humidity above 19%, though below 31% RH some decomposition to monosulfate was observed [57]. This result though is in line with Renaudin et al. as only when the ettringite was dried under 11% RH and subsequently at 50°C was water loss observed [54].

The weight loss of water from ettringite, when controlled by heat, has been observed to be possible when the temperature is in the range of 60 – 70°C [14, 65]. Shimada and Young found that with synthetic ettringite that there was not weight loss, thus water loss, when the sample was heated at 60°C [65]. Only when the temperature was raised to 70°C was weight loss found. When C$A cement was used where ettringite was the major

hydration product, Ndiaye et al. found that samples reached an invariant weight within three days when dried at 60ºC [14].

1.3.14 Dehydration Impact on Crystal Properties

The dehydration process of ettringite removes water from the crystal lattice, reducing the crystallinity until it reaches an amorphous state. As there is a change in crystallinity, there will be an impact on the properties. Zhou et al. demonstrated that in the conversion to metaettringite there is a great decrease in the a lattice parameter and a small change in the c lattice parameter [13]. Measurement of ettringite crystal lattice parameters that had water content reduced to 11-13 H_2O showed a c parameter of a range from 1.054 to 1.069 nm, this range is approximately half that of the 32 H_2O molecule ettringite c lattice parameter given of 2.1408 nm [13]. The a lattice parameter proved to be more complicated to measure. While an a lattice parameter of 0.849 nm (repeat of a* of 0.735 nm) was determined for one lattice streaking was present, indicating disorder parallel to a* [13].

In a study by Bannister et al., the a axis decreased from 1.124 to 0.84 nm while the c axis decreased from 2.145 to 1.021 nm when a single crystal of ettringite was dehydrated at 110ºC [66]. For this dehydration, Bannister et al. calculated that, of the 64 molecules of water in a unit cell of ettringite, there was a loss of 48 molecules of water. As previous references to the molecules of water in ettringite have been based on a half unit cell, this corresponds to 32 water molecules in the wet ettringite being reduced to 8 molecules in the dried state. While lower than more recent values, this dehydration amount does correspond well with the 10-13 molecules associated with metaettringite. This work was performed on naturally occurring ettringite instead of synthetically lab created ettringite as is typically studied. Bannister et al. also noted that the reduction in the c axis corresponded to halving

the initial value. In the dehydrated state Bannister et al. wrote that all the zeolitic water channels would be collapsed sideways from the original ettringite crystal in which the 48 water molecules were located within these channels [66]. When collapsed, the ettringite structure would preserve the same pattern along the c-axis. Though in observation this was not in agreement with the observed x-ray peak intensities. This suggested that the zeolitic water molecules cannot be neglected [66].

Work by Hartman et al. also studied the impact that thermal decomposition has on the structure of ettringite. The authors found that the a axis increased by 0.2% while the c axis decreased by 0.4%. With analysis using pulsed neutron time of flight (TOF) diffraction analysis no splitting or merging of the diffraction lines was noted [61]. This indicates that there is a lack of phase transformation and that the ettringite unit cell symmetry remains unchanged, results backed up by the small change in the a and c axis parameters. As noted, this result is contrary to the observations of Bannister et al. discussed previously.

Shimada and Young found that the a axis parameter increased from 1.122 nm to 1.152 nm and the c axis parameter decreased from 2.146 nm to 2.104 nm when 15 molecules of water were removed [65]. The c parameter was noted as being in line with previous studies but the a parameter was noted as being quite different. The difference was attributed to the different behavior of natural and synthetic ettringite. When the water content was reduced to a value of about 12 molecules, the samples being analyzed became amorphous the X-ray analysis. These values for the lattice parameters closely align with the changes found by Hartman et al. [61].

1.3.15 Ettringite Dehydration-Rehydration Loop Impact on Sample Stability

While dehydration of ettringite to metaettringite has been shown to be a reversible hysteretic reaction, it is necessary to understand what is happening to the ettringite crystal as it decomposes.

If the ettringite decomposes to a form other than metaettringite such as monosulfoaluminate hydrate, basanite, and/or katoite; the hysteresis loop between ettringite and metaettringite will cease to continue [67]. This decomposition is exhibited when the ettringite is heated to elevated temperatures around 100ºC, though other conditions such as drying treatment condition and pressure can impact this temperature value [57, 58, 67]. Decomposition will result in an instable crystal structure that will crack and disintegrate the sample [67]. As highlighted Kaufmann et al., the conditions that the dehydration is done under will play a large role in determining if the system is reversible [67]. Kaufmann et al. examined 21 condition setups using two different types of C$A cement paste cubes which were exposed to differing curing procedures. In four of the trials the samples included a curing procedure that rehydrated the sample after it had been dehydrated, where each specimen was visually different after the set of curing procedures. Three of these trials were made using the same type of C$A cement and will be discussed here. These samples were cured in 20ºC water for both the initial curing and rehydration process. In-between, the samples were first exposed to steam at different temperatures and then dried at different temperatures. The steam was at 70, 90, and 100ºC with drying being 110 or 90ºC. The sample exposed to the 70ºC steam and 110ºC drying had visually cracked, the sample exposed to 100ºC steam and 110ºC drying had seriously deteriorated, and the sample exposed to 90ºC steam and 90ºC drying had some observed cracking [67]. A

comparison of a stable and unstable system can be seen in Figure 1.15. With these samples, it can be seen that the dehydration process can greatly impact the stability of the system when it is rehydrated. Thus, while systems can be designed that are stable, it is important to acknowledge what the expected conditions may be and if the conditions are averse to the system stability, those factors need to be controlled or mitigated.

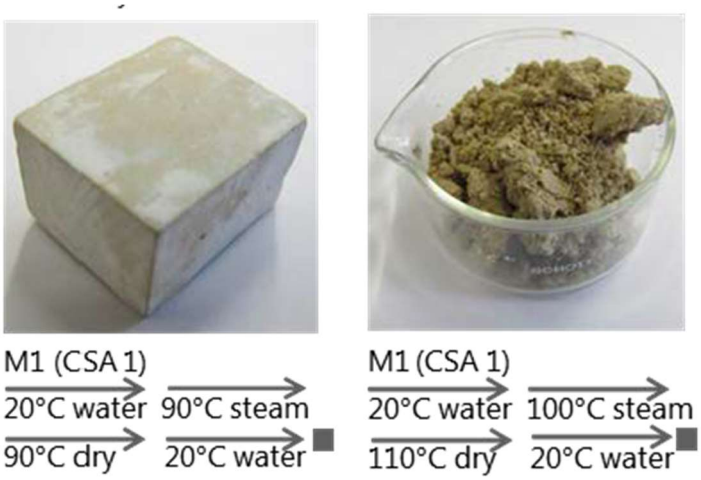

Figure 1.15 (left) Stable C$A system after one cycle, (right) unstable C$A system after one cycle.
Source: [67].

If properly designed, the ettringite-metaettringite cycle has been shown have a stable macrostructure over one as well as several cycles. Multiple studies have been completed that show that this rehydration loop of ettringite is reversible and produces a hysteretic loop [57, 58, 67]. Figure 1.16 shows one cycle of this loop where the number of moles of water per formula weight is equivalent to the number of molecules of water in one half of a unit cell of ettringite crystal. Skoblinskaya et al. shows this initially when samples of ettringite were rehydrated and subsequently dehydrated again. The rehydrated samples showed a higher n value of up to 36.5 but when dehydrated for the second time

the water removal from the crystallohydrate again started at around n=30 [60]. This dehydration again at n=30 is important as if the sample decomposed to other forms the H_2O value at which the water starts to be removed from the crysallohydrate would be reduced. The hysteretic loop of ettringite was tested by Zhou and Glasser were they tested pure phase ettringite under isothermal conditions while varying the temperature. The results showed that a reversible reaction does take place and that the reversibility at temperatures of 117.5 ± 2.5ºC can be achieved [58]. Further Ndiaye et al. showed that this reaction can be stable when applied to multiple cycles when C$A cement paste samples after 28 day curing and subjected to seven cycles of dehydration at 60ºC and rehydration at 20ºC there was a stable macrostructure of the binder [14]. The macroscopic stability was assessed based on no macroscopic cracks of collapse being observed [14]. The seven cycles were stated to represent the system undergoing seven years of service life where the material would be used for seasonal heat storage (one cycle per year). Though this longer cyclic testing is important to note in that samples can remain stable, determination it is still unclear as to whether these systems will stable over a more regular level of cycling each year.

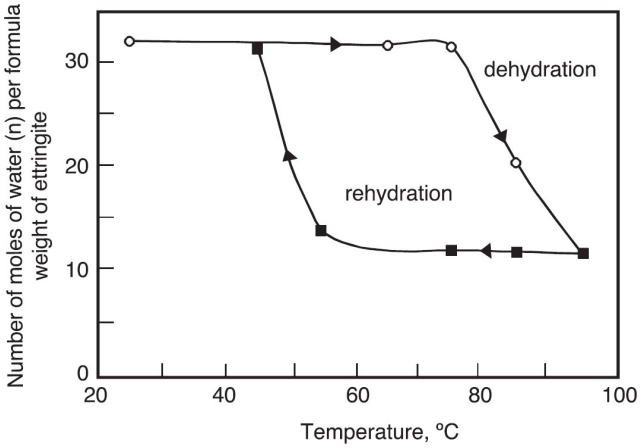

Figure 1.16 Ettringite dehydration and rehydration hysteresis.
Source: [13].

The stability of ettringite may be a function of its morphology and thus, when synthesis of the ettringite is performed it is important to understand what bias may be introduced. Ettringite used for analysis typically comes from three typical sources; it is sourced from a mine containing naturally formed ettringite (natural), it is created as a pure phase synthetically in the lab (synthetic), or as a product from a chemical reaction such as the hydration of C$A cement (product). In each method ettringite crystals are found with the natural and lab created being a pure single phase and the chemical reaction ettringite product typically being a heterogeneous makeup with other products.

In a comparison of natural and synthetic ettringite, Jimenez and Prieto noted that due to the better crystallinity of the natural ettringite it was more resistant to dehydration than a typical synthetic sample [68]. When exposed to elevated temperatures, Jimenez and Prieto observed that at >50ºC the synthetic ettringite reflections were lost, while the natural ettringite was unaltered up to 75ºC and remained present until 100ºC [68]. This impact of crystallinity on thermal stability is also observed by Shi et al. [69] Shi et al. studied the impact that superplasticizers have on the stability of ettringite. Of the four superplasticizers studied, the addition of a naphthalene sulfonate superplasticizer was observed to have a larger crystal size and better stability below 100ºC as compared to ettringite found in the C_3A – gypsum hydration system. The three other tested superplasticizers were found to decrease the d-space as compared to the C_3A – gypsum system. For amino sulfonate and aliphatic superplasticizers, this resulted in a lower thermal stability. For polycarboxylic acid, while the crystal size was reduced, there was an improvement of the stability, this increase is attributed to calcium complex chelate compounds, these formed in a dense structure and linked particles together resulting in a more compact and stable product [69].

Other studies have also found admixtures to greatly impact the crystal structure and formation of ettringite, examples from Cody et al. are seen in Figure 1.17 [70–72]. Figure 1.17 (A) is a six sided needle-like crystal grown without any admixtures, (B) is a short pointed crystal formed from the addition of arabinic acid, and (C) is an elongated thin ettringite crystal grown with Alizarin Red S exhibiting growth defects [71]. Thus, any change to the ettringite crystal size and morphology my result in a change in system thermal stability.

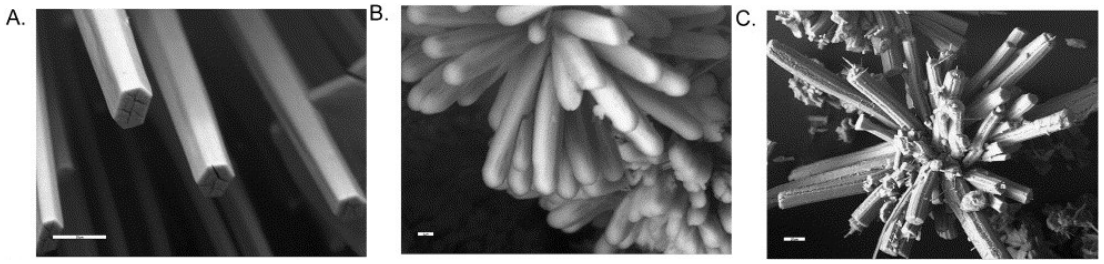

Figure 1.17 Examples of synthetic ettringite.
Source: [71].

1.3.16 Ettringite Carbonation

Carbonation of cements is typically associated with the corrosion of reinforcing steel but in systems with high ettringite content the ettringite itself may decompose through carbonation. The decomposition kinetics of ettringite by carbonation is given by Equation (1.20) which was suggested by Kuzel and Strohbauch and used for analysis by Nishikawa et al. [73, 74].

$$3CaO \cdot Al_2O_3 \cdot 3CaSO_4 \cdot 32H_2O + 3CO_2 \rightarrow 3CaCO_3 + 3(3CaSO_4 \cdot 2H_2O) + Al_2O_3 \cdot xH_2O + (26 - x)H_2O \quad (1.20)$$

Xiantou et al. studied the impact of different partial pressures of H_2O, CO_2 and different temperatures had on the carbonation rate [75]. When subjected to temperatures of 10, 20, and 30ºC at 100% RH, it was observed the higher temperature the quicker the carbonation rate [75]. When testing samples with low relative humidity, Xiantou found that as the temperature was increased from 10 to 50ºC the carbonation reaction rate considerably slowed, with it almost being nonexistent at 50ºC [75]. If just the partial pressure of CO_2 is changed, an increase of partial pressure of CO_2 increases the carbonation kinetics of ettringite linearly. The conclusion for this result was that the activation energy of the carbonation reaction is negative, meaning that in this condition the ettringite is in an unstable state.

Ndiaye et al. also conducted tests to determine the impact carbonation may have on C$A based ettringite cement pastes. Tests were completed on aerated and non-aerated samples. The aerated samples were to increase the exchange surface area of the C$A paste in order to promote dehydration and rehydration of the samples. When subjected to 4% CO_2, 65% RH, and 25ºC for one month, the aerated samples showed a carbonation layer of 16mm while the non-aerated samples only showed surface carbonation (layer less than 0.5mm) [14]. The high carbonation of the aerated C$A cement paste is attributed to its high gas permeability as compared to only hardened C$A paste, 8.8x10-14 m^2 and 3.6x10-16 m^2 respectively. This represents an increase by a factor of 250 [14]. The ettringite decomposition due to the carbonation reaction was according to Equation (1.21). This reaction results in hemihydrate being formed instead of the generally reported gypsum.

$$3CaO \cdot Al_2O_3 \cdot 3CaSO_4 \cdot 32H_2O + 3CO_2 \rightarrow$$
$$3CaCO_3 + 3\left(CaSO_4 \cdot \frac{1}{2}H_2O\right) + Al_2(OH)_3 + 27.5H_2O \quad (1.21)$$

Typically, in the decomposition of ettringite gypsum ($CaSO_4$ $2H_2O$) is observed and given by Equation (1.22), experiments by Ndiaye et al. observed hemihydrate instead [14]. The explanation given for this discrepancy was that there was probably insufficient water in the cement matrix or relativity humidity during the test resulting in the production of hemihydrate and not gypsum [14].

$$3CaO \cdot Al_2O_3 \cdot 3CaSO_4 \cdot 32H_2O + 3CO_2 \rightarrow$$
$$3CaCO_3 + 3(CaSO_4 \cdot 2H_2O) + 2Al_2(OH)_3 + 23H_2O \quad (1.22)$$

After ten days of carbonation of crushed C$A paste, the ettringite content had decreased from 66.7% to 19.4% while the hemihydrate content had increased from 0.0% to 23.9% and the calcium carbonate content had increase from 0.6% to 10.8% [14]. These values result in a carbonation rate of 71% [14]. When C$A paste samples were placed in air, 0.04% CO_2, for one year, the carbonation rate of the paste was 86% [14]. This high carbonation rate under both accelerated conditions and under natural atmospheric CO_2 conditions shows that ettringite is highly susceptible to carbonation. As the carbonation reaction relies on the water in the ettringite, further testing of the susceptibility of the C$A cement paste under accelerated and atmospheric CO_2 conditions when the ettringite is in the dry state would better represent the expected conditions when stored. As seen in Equations (1.6) – (1.8), large quantities of water molecules are present in decomposition side of the reaction. Metaettringite in the typical form of 10-13 molecules of water would

still present a concern as there is enough present on the reactant side to drive the reaction presented in the equations.

While a dehydrated state may provide a degree of protection against carbonation during rehydration, or discharge, careful consideration to counter or mitigate the carbonation reaction may be necessary. If the ettringite is allowed to carbonate, the hysteretic conversion process between ettringite and metaettringite will stop. Other research by the authors seek to use moist nitrogen instead of moist air for the discharge humidification process to avoid the ettringite carbonation [14].

1.4 Summary

This chapter summarized the literature related to the different high ettringite cement systems of C$A, CAC-C$ and PC-CAC-C$ that will be used in this dissertation. Presented were history, composition, hydration, and stability of the cements. The literature review further discussed the hydrate of interest, ettringite, in detail. The crystal structure dehydration, impacts of dehydration, and carbonation were discussed. An overview of energy methods and storage was presented with the focus on TCES process that was used for this work.

In conclusion, previous work has studied the characteristics of high ettringite cements and have seen that they may be applicable for use in energy storage. The instability of the TCES reaction of ettringite and how the cement systems that may be used to generate the necessary ettringite are still not well understood. In response, this work seeks to improve the understanding of the TCES reaction of ettringite generated from different types of high ettringite producing cements. The stability of these cements was measured to

assess the viability for use. This work is also intended to determine the applicability of these cements for use in TCES by measuring the heat that is able to be recovered from the system. The work is intended to be able to provide guidance for further research related refinement and development of this storage medium.

CHAPTER 2

MEANS AND METHODS

2.1 Materials

Three types of cement were used for in this work. The C$A cement was a standard commercially available type used for rapid work and situations were fast setting and strength gain is needed. The binary CAC-C$ and ternary OPC-CAC-C$ were procured from a supplier pre-blended. The oxide analysis for each of the three cement types used is provided in Table 2.1. Water used in the hydration of the cements was deionized water.

Table 2.1 Oxide Analysis of Cements

Oxide (wt %)	Na_2O	MgO	Al_2O_3	SiO_2	P_2O_5	SO_3	Cl	K_2O	CaO	TiO_2	Cr_2O_3	MnO	Fe_2O_3	CuO	ZnO	SrO	ZrO_2	LOI**
C$A	0.17	1.57	14.19	14.51	0.11	15.63	0.11	0.57	50.23	0.60	*	*	0.69	0.03	0.03	0.14	*	1.45
CAC-C$	*	0.24	20.97	2.89	0.05	23.63	*	0.12	44.79	1.21	0.04	*	3.15	*	*	0.10	0.06	2.77
OPC-CAC-C$	0.18	2.89	10.01	16.58	0.18	7.65	*	1.00	57.10	0.56	0.05	0.11	2.01	*	0.05	0.23	*	1.41

Notes: *not detected, **accounts for loss due to C, CO_2, H_2O, OH, organic compounds and/or other

2.2 Specimen Preparation

2.2.1 Cube Specimens

Specimens used for testing in this study were cast as 50 mm x 50 mm x 50 mm (2 in x 2 in x 2 in) cubes as shown in Figure 2.1. These specimens were used for stability testing and were broken down to create the specimens for XRD and SEM-EDS testing. For this work, paste mixtures, comprising of just the cement and water, were used as addition of aggregate would reduce the total amount of hydrates formed per unit volume. The cement paste mixtures were mixed according to ASTM C 305 Section 5 with one modification [76]. Due to the fast setting nature of the cement pastes, placement into the

molds was done in one lift instead of the prescribed two. After placement in the molds, excess paste was removed from the top using a straight edge. The pastes were covered with wet burlap and sealed with plastic and let to cure at ambient temperature for 24 hours before being demolded. Once demolded cubes were then placed in a moist curing room at 95%+ relative humidity and 23 +/- 3 ºC temperature until 28 days from casting had elapsed.

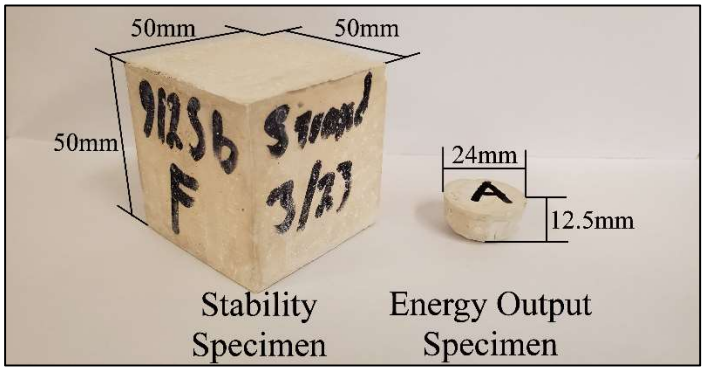

Figure 2.1 Specimens used for this work, larger cube specimens were used for stability testing, smaller hemispherical specimens were used for calorimetry work.

2.2.2 Hemispherical Specimens

For testing of energy recoverable from the system, smaller specimens sized 24mm in diameter x 12.5mm in height, shown in Figure 2.1, were used. The smaller specimens were used due to constraints in the calorimeter where larger sizes maxed out the sensor. Due to the small volume used for each mixture, a mixing procedure was developed as follows.

1. The cement was added to a plastic bag through a funnel
2. The water was added, rinsing remaining cement on the funnel into the bag.
3. Mixing was done by shaking the bag up and down at speed of two full shakes per second (one shake being a completed cycle of up and down), with one shake being a distance of about 100 mm (4 inches) for 30 seconds.
4. The mixing was followed by a 15-second rest period.

5. Mixing of the paste then resumed at a faster speed of four full shakes per second for 60 seconds.

6. After mixing was completed, a corner of the bag was cut and the cement paste was squeezed into each of the specimen plastic moulds.

7. Consolidation of the specimens was accomplished by tapping the filled moulds on the table top from a height of 5mm.

8. Initial curing was done through wet burlap for 24-hours under plastic before the samples were demoulded and placed in the moist curing room (>95% RH and 23+/-2 degrees) for 28 days.

2.3 Stability Testing

2.3.1 Dehydration/Rehydration Cycle of Specimens

After 28 days of curing, specimens were put through dehydration and rehydration cycles to convert between ettringite and metaettringite. For each cement and temperature combination, three specimens were tested in which the mass of the sample was measured as a representation of the amount of water that could be removed from the system. For each data point, the average mass of the specimens was found and reported. Stability testing started with heating in an oven at 40ºC for two hours to remove the zeolitic water. This water is not bound within the ettringite crystal and does not factor into the thermochemical reaction. After the two hours, the mass of the specimen was measured and recorded as the initial mass, representing a fully charge system. An image of the specimen in this initial state was also taken. Specimens were then placed in glass dishes to capture any material that may fall off of the specimen during oven drying. The weight of the empty glass dish measured and along with the specimen ID was written on each dish. Specimens were then placed into ovens at either 60, 75, 90, 105, or 120ºC for three days to dehydrate the specimens, removing the bound water from the ettringite crystal. During the dehydration

process, the mass of the specimens was measured each day. To protect the scale from heat damage during measurement of dehydrated specimens, the scale was zeroed with a separate glass dish placed on top. The mass of the specimen was calculated by subtracting out the mass of the glass dish.

After the three days of dehydration, specimens were removed from the oven and the mass of each specimen was measured. The specimens were then allowed to cool to ambient temperature to prevent thermal shock during rehydration. For rehydration, specimens were placed into 475ml (16 oz.) plastic cups where deionized water was added to completely cover the specimen. Due to the rapid adsorption of water of some of the specimens, the level of water was continually checked to ensure that the samples stayed completely submerged. More water was added as needed. After five minutes, lids were placed on the cups to prevent evaporation of the water. Specimens were rehydrated for three days. On each day, the specimen was removed from the cup and placed in a glass dish. The specimens were then placed in an oven at 40^{o}C for two hours to remove the zeolitic water. The mass of the specimens was then measured and the specimen was returned to its cup. If needed, additional deionized water was added to ensure the sample was fully covered.

2.3.2 Testing for Long Term Reversibility

For testing the long term reversibility of the systems, the procedure outlined in Section 2.3.1 was repeated. After rehydration for three days, the specimens were dehydrated in the oven at the prescribed dehydration temperature for that specimen. This process of measurement of mass of the specimens in their dehydrated and rehydrated condition was repeated until the specimen was no longer able to hold together. At this point, the day and

cycle that the specimen was recorded. An image was collected of the specimen in the final state to compare against the initial condition of the specimen.

2.3.3 Long Term Storage of C$A Specimens

Discharge of the energy from the system due to water in the form of moisture in the air was studied. For this test, relative humidity's below 50% were analyzed. 0, 13, 25, 35, and 45% RH were used. A desiccator and vacuum pump were used to maintain 0% RH while saturated salt solutions were used to control the relative humidity of the other conditions. The saturated salt solutions were lithium chloride for 13% RH, potassium acetate for 25% RH, magnesium chloride for 35% RH, and potassium carbonate for 45% RH. The saturated salt solutions were placed into buckets into either a plastic container or on the bottom of the bucket were a perforated piece of plastic that was fitted to the bucket. This was done to prevent the specimens from coming into contact with the salt solution. Temperature and humidity were measured through Lascar EL-USB-2-LCD data loggers during the duration of the experiment.

Testing was completed using C$A cement cube paste specimens. These specimens were cast and cured according to the procedure in Section 2.2.1. After curing for 28 days, the specimens were placed in an oven at 40^{o}C for two hours to remove the zeolitic water. The mass of the cubes was then measured to determine the initial base line of the specimen in its initial state. The cube specimens were then dehydrated at 60^{o}C for seven days to convert the ettringite to the metaettringite phase, charging the system. After the seven days, the specimens were removed from the oven and the mass of the specimen in the dehydrated state was taken. Specimens were then placed into the buckets containing the saturated salt solutions and the lid was sealed with tape to prevent moisture from entering or leaving the

bucket. The buckets were then left in a secluded location in the laboratory to prevent any disturbance to the specimens. The mass of the specimens was measured weekly for the first 15 weeks and then every 15 weeks until laboratory work was suspended due to the COVID-19 pandemic. One final reading was taken after 181 weeks.

2.4 Calorimetry Testing

Isothermal calorimetry was used to compare the heat output of specimens upon rehydration. The experiments were conducted in a I-CAL 2000 HPC isothermal calorimeter by Calmetrix at 20˚C, shown in Figure 2.2. A test method procedure to measure the energy released during the rehydration of the specimens was developed for this testing and was as follows. Dehydration of hemispherical specimens described previously was conducted at 60˚, 75˚, 90˚, 105˚, or 120˚C in standard, uncontrolled humidity conditions in laboratory ovens for three days to dehydrate (charge) the specimens. One set of specimens was kept in the hydrated state and run through the calorimeter as a baseline for the amount of energy introduced to the test through the addition of the specimens. Rehydration was done with 50 grams of water. Dehydrated specimens and water to be used in rehydration were conditioned to 20.0ºC to minimize the impact of thermal energy other than from the rehydration of the ettringite. The mass of the specimens was measured one hour before the start of testing. The mass of the specimens ranged from six to nine grams depending on dehydration condition. The specimen was added to the water and data collection of the calorimeter was then started and run for 24 hours. Data collection was done every ten seconds for the first hour, then every one minute until 24 hours had elapsed. The data obtained from the calorimeter were the voltage, power, and heat of each specimen. Heat

outputs were normalized based on specimen mass after dehydration and averaged between the two testing chambers.

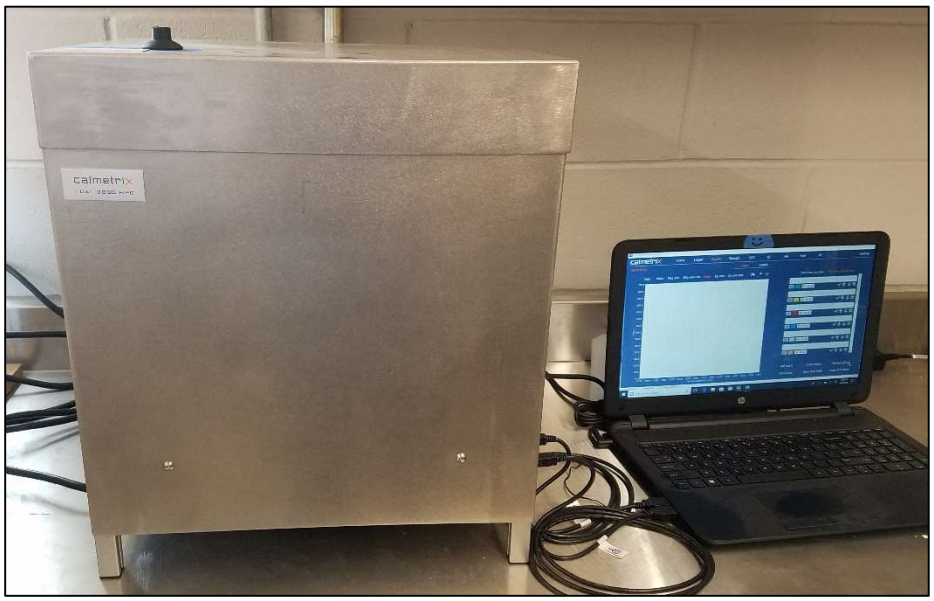

Figure 2.2 Isothermal calorimetry setup with Calmetrix I-CAL 2000 HPC.

2.5 Compression Strength Testing

Compression strength testing was completed on all three cement types following ASTM C109 [77]. Compression strength testing was completed on 50 mm x 50 mm x 50 mm cubes cast as described in Section 2.2.1. The tested conditions were initial after 28 days of hydration; in the dehydrated state after three days of oven drying at either 60, 75, 90, 105, or 120^{o}C; and in the rehydrated state after three days of rehydration. For specimens at 28 days and rehydrated, the specimens were placed in an oven for two hours at 40^{o}C to remove the zeolitic water prior to compression testing. If the specimens failed before compression testing could be completed than no compression result was recorded. The area of the cube was determined through the measurement of the top and bottom of the cube

were measured with a caliper with two perpendicular measurements per side. The area of the cube surface was calculated by taking the average of the four distances and squaring the result. The compression testing was carried out in a Forney Test Pilot compression machine (FHS-700 B-T PILOT) at a loading rate between 90 and 180 kg/s (200 and 400 lbs/s), shown in Figure 2.3. For each condition, three specimens were tested and the average compressive strength was calculated.

Figure 2.3 Forney Test Pilot compression machine (FHS-700 B-T PILOT).

2.6 Arresting Hydration

Preparation of the samples for XRD and SEM-EDS analysis required the arresting of the hydration of the sample. Due to the sensitive nature of the ettringite crystal, the widely

used technique of microwave and vacuum drying may induce damage into the crystal [78]. Also, as for this study the drying of the specimens through use of ovens is part of the experimental procedure an alternative method of solvent exchange was used to arrest the hydration. Different solvents have been studied for use in the exchange process and for ettringite the use of isopropyl alcohol has been found to be effective [78].

In the solvent exchange process, paste specimens were broken down to smaller chunks which were cut into slices sized three millimeters thick. Cutting of specimen slices was accomplished through use of Struers Minitom precision saw fitted with a diamond coated blade. During this procedure, isopropyl alcohol was used as a lubricant to ensure that no rehydration occurred from contact with water. For the solvent exchange, the slices were then stored in isopropyl alcohol for 24 hours at which time the isopropyl alcohol was replaced. The slices were then allowed to sit for another seven days. The slices were then removed from the isopropyl and placed into a desiccator to evaporated the isopropyl for two days. After the two days, the specimens could then be prepared for either XRD or SEM-EDS analysis.

2.7 XRD Analysis

For preparation of hydration arresting, slices for XRD analysis were ground in a mortar and pestle into fine particles using isopropyl alcohol as a lubricant. The resulting slurry mixture was placed into a desiccator in a labeled plastic Petri dish to evaporate the isopropyl alcohol. After the isopropyl alcohol had evaporated, the sample remained in the desiccator until testing could be performed to prevent carbonation and exposure to moisture of the powder samples. The storage setup is shown in Figure 2.4

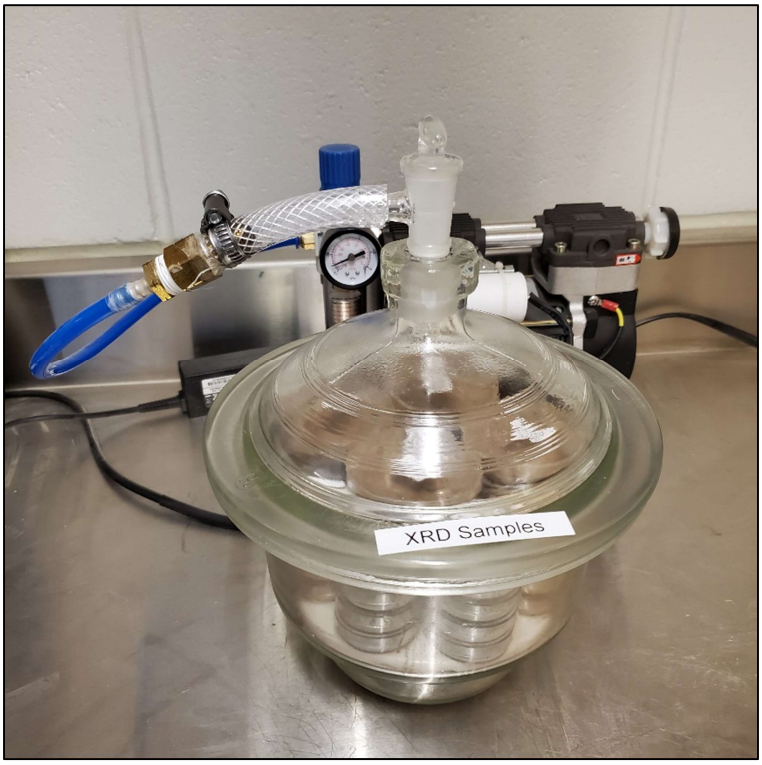

Figure 2.4 Desiccator setup for XRD sample storage.

X-ray diffraction analyses were done using a Philips EMPYREAN multi-purpose research X-ray diffractometer, shown in Figure 2.5. Bragg-Brentano geometry with a 2-Theta of 5º to 65º with an X-ray source of 45kV and 40mA. An angle step of 0.026º with a time step of 97.6 seconds was used for the experiments. Dry powders were used for analysis and were back loaded into the sample holder. A 27mm diameter sample holder was used unless there was not enough powder, in this case a smaller 16mm diameter sample holder was used instead. Quantification of the crystalline composition was not done through a Quantitative Rietveld analysis. HighScore Plus was used to identify the composition of the powder based on locations of the peaks by comparison with known powder diffraction file (PDF) numbers for the hydrates.

Figure 2.5 Philips EMPYREAN multi-purpose research X-ray diffractometer.

2.8 SEM-EDS Analysis

Samples were taken from cube specimens, which were cut and had their hydration arrested according to the procedure described in Section 2.6. After the isopropyl solvent was removed via the vacuum desiccator, the samples were mounted in epoxy to stabilize the system. A two-part clear epoxy, EpoFix, was used to mount the samples due to its slow curing nature and specialty design use for delicate specimens like cement pastes. Samples were mounted and impregnated using a Struers CitoVac vacuum impregnation unit shown in Figure 2.6.

Figure 2.6 CitoVac vacuum impregnation unit.

The epoxy was allowed to cure for at least 48 hours before being polished. Polishing was done on two separate phases, coarse and fine. First, a coarse polish was done to remove the epoxy and expose the surface of the samples using a Struers LaboPol-30. For this, a 200 μm grit sandpaper disk was used with the LaboPol-30 rotating the sandpaper at 300 rpm. During this process, the samples were held by hand and isopropyl alcohol was used as a lubricant. After the cement paste surface had been exposed, the specimens were placed in isopropyl and cleaned using an ultrasonic cleaner. Storage of specimens was done in a vacuum desiccator.

The second fine polishing phase was accomplished using a Struers LaboPol-30 with a LaboForce-Mi counter-rotation sample holder, shown in Figure 2.7. Up to eight samples were polished at a time. A Struers MD-Largo polishing disk was used and rotated at

150 rpm during the polishing, the counter-rotation sample holder rotated at 8 rpm. Diamond polishing spray was applied to the disk with the succession of grits being 9µm, 3µm, and 1µm to create a smooth surface of the cement paste for SEM examination. The time spent polishing under each successive grit was increased, staring at 1.5 hours for 9µm, three hours for 3µm, and six hours for 1µm. The grits were reapplied once every hour with the samples and disk being removed and cleaned every two hours or when there was a change of grit. Samples were cleaned in isopropyl in the ultra-sonic cleaner and brushes used for cleaning the disk were segregated per grit level. Lubrication of the disk and samples was done with an alcohol based lubricant, DP-Lubricant Yellow supplied by Struers. The lubricant is for use with soft water sensitive materials. After the fine polishing process was complete, samples were placed in the vacuum desiccator for a minimum of 48 hours to remove any remaining volatiles in the sample that may damage the SEM.

Figure 2.7 LaboPol-30 with LaboForce-Mi counter-rotation sample holder.

Before analysis in the SEM samples were coated with carbon. Copper tape was added around the edge of the sample to ensure conductivity of the sample and prevent charging. SEM analysis was done using a JEOL JSM-7900F SEM machine equipped with a retractable backscatter detector and INCA energy system Energy Dispersive X-ray (EDS) detector for semi-quantitative elemental analysis, shown in Figure 2.8. A beam acceleration voltage of 15kV and a working distance of approximately 10 mm was used for examining the samples. A 30 second collection time was used per EDS collection point.

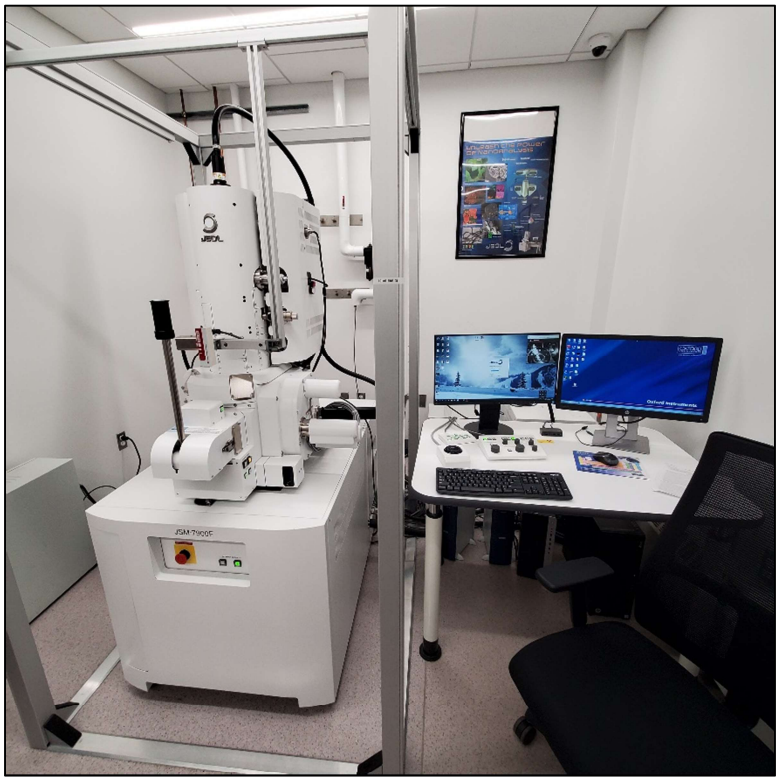

Figure 2.7 JEOL JSM-7900F SEM.

CHAPTER 3

ENERGY OUTPUT OF DEHYDRATED HIGH ETTRINGITE PRODUCING CEMENTS FOR USE IN ENERGY STORAGE

3.1 Abstract

Novel energy storage methods, such as thermal storage, are an important part of meeting increasing energy needs and improving the sustainability and security of energy systems. Thermochemical energy storage (TCES), a subset of thermal energy storage methods, have higher energy storage densities than is found in more traditional storage mediums and have the capability of storage of energy from renewables. Ettringite based cement systems are a potential material for use in TCES that is created using raw materials that are inexpensive and abundant. Ettringite based cement systems are a special type of hydraulic binder that, when mixed with water, result in the hydration product known as ettringite ($3CaO{\cdot}Al_2O_3{\cdot}3CaSO_4{\cdot}32H_2O$). Ettringite crystals can undergo a reversible thermochemical conversion that may be a viable tool for energy storage. However, the amount of energy able to be recovered from these systems is still not well understood due to the influence of many different factors. The objective of this work was to examine the energy output of three different high ettringite cement paste systems at different dehydration temperatures. During the rehydration process, isothermal calorimetry was used to determine the peak heat flow and cumulative heat for each condition. These were normalized by the amount of dehydrated paste. The impact of multiple dehydration and rehydration cycles on the heat output was also measured for one of the cement types at three different dehydration temperatures. The results indicate that the type of cement will

play a role in the amount of heat returned, dehydration temperature can have an impact on heat return, and increasing cycles results in the loss of returned energy.

3.2 Introduction

Energy is an essential component of modern society and demand is constantly increasing due to an increasing population and an increase in living and comfort standards. Since 1965, the world's energy consumption has quadrupled [2]. More than half of the energy used in residential buildings is used for heating and cooling needs [2]. For heating, many different energy sources can be utilized though for cooling, electricity is the primary source [2]. During peak utilization of, especially, cooling systems, the strain on the grid infrastructure can be immense. The interest in the use of renewable energy sources has increased, particularly in regards to national interests of energy security and sustainability [2]. Storage solutions of the energy generated from these systems are needed to compensate for the flux in generation [79]. A 2013 report by the United States Department of Energy (USDOE) focused on how energy storage will play a role in the modernization of the energy grid in order to meet projected energy needs [1]. The primary concerns outlined in the report are that as of 2013 the U.S had 24.6 GW of energy storage which approximated around 2.3% of total electricity production capacity, a percentage that lags behind other developed countries and regions such as Japan and Europe [1, 6]. As of June 2018, the storage capacity had been marginally increased to 25.2 GW of energy [7, 8]. At the average national usage rate of 867 kWh per month, this storage capacity represents power for one month for approximately 29,000 households [9]. To compound this problem, 95% of current storage is from the singular method of pumped hydro storage, a form of mechanical

energy storage that requires significant elevation changes not necessarily available near renewable energy sources [1, 6]. Increasing the diversity of our energy storage options is necessary to make energy production more economical and sustainable, as well as to increase national energy security.

Practical applications of energy storage can be broken into six different branches with each branch having many different sub-applications; chemical, thermal, mechanical, electrochemical, biological, and magnetic and electromagnetic energy storage. Each method has advantages and disadvantages depending on usage with many different techniques being studied and improved upon [2]. Storing energy through heat (thermal) processes, otherwise known as thermochemical energy storage (TCES), has a wide range of applications. The study of these systems is important and promising due to most irreversible losses within systems being in the form of heat, and more than half of the energy generated and consumed in the world occurs through thermal processes [11]. With this method of energy storage, higher energy storage densities can be realized than are found in more traditional storage mediums [2]. TCES systems also have the capability of storage of energy produced from renewables [2]. In TCES, the safety of the system is based on both the material that is used for storage and the process to convert the medium between the energy states. The medium used for storage can be of any physical state; liquid, solid, or gas. When compared to other heat energy storage methods such as sensible heat and latent heat storage systems, TCES systems result in a high heat storage capacity without minimal to no losses during storage if properly stored [2]. An example of TCES is found in the dehydration of salt hydrates. For magnesium hydroxide, the application of heat results in the removal of water from the salt forming magnesium oxide [12]. In the cement-

based systems a thermochemical reaction occurs through the chemical binding and unbinding of water within a hydrate commonly found called calcium trisulfoaluminate hydrate, also known as ettringite.

Ettringite is a mineral that, while found rarely in nature, is a common hydration product found in ordinary portland cement (OPC) and other hydrated hydraulic cements [16, 17, 22, 80, 81]. Ettringite forms early in OPC systems, but then converts into monosulfate during later hydration ages. In the hardened OPC systems ettringite is found in relatively low amounts compared to the silicate hydrates that provide the majority of strength for OPC systems [16, 19, 82]. In a OPC system calcium sulfoaluminate hydrates occupy 15 to 20 percent of the hardened cement paste volume [16], with ettringite occupying ten percent of the paste volume [14]. In hardened OPC systems, the early dissolution of the ettringite crystal due to high temperatures followed by delayed reformation in the hardened OPC system is associated with extensive cracking and damage. The damage is caused from the ettringite crystal exerting significant pressure when reforming in the capillary porosity of the cement paste [67, 71, 83]. In other binders, such as calcium sulfoaluminate (C$A) cement and calcium aluminate cements (CAC) blended with sulfates (C$), ettringite content in the hardened paste has been seen to be up to 80 percent of the hardened paste by weight [14, 22, 23, 30, 67, 81]. The fast hydration kinematics of the anhydrite materials into ettringite means that these systems are typically used in situations where rapid hardening is required [84–86]. The solubility of the ettringite crystal has been studied extensively due to the damage caused by delayed ettringite formation and the fact that it is the main hydrate present in several alternative cement systems [14, 23, 67, 68, 71, 83, 87–91]. Much less understood is the dehydration of the

ettringite crystal into the low water state form known as metaettringite. The conversion to metaettringite is reversible and can occur without full decomposition or dissolution [13, 57, 59, 67]. Despite the loss of water during conversion, previous work has shown that the crystal does not undergo significant volume change and can remain stable depending on the vapor pressure, temperature, and mechanical stresses of the surrounding environment [14, 58]. The dehydration of ettringite can be accomplished through heating at temperatures as low as 60°C [14]. Metaettringite can be rehydrated to ettringite, which is accompanied by an exotherm, and could be harnessed as a thermochemical energy storage option.

For use as an energy storage system, the ettringite-metaettringite system would be charged through dehydration of the ettringite crystal (heat and dehumidification). Energy release would occur through rehydration of the system and collection of the heat from the exothermic reaction [13, 14, 92]. This process is described in Figure 3.1. Ettringite devices can be made as a standalone reactor to store thermal energy or be incorporated into building systems through the use of architectural panels. The energy released can either be used to create electricity which would be fed back into the grid or released as thermal energy for hot water and heating. This work presents novel information regarding energy storage using concrete, as most prior work on using concrete as energy storage has focused on sensible heat storage and thermal inertia [93–101].

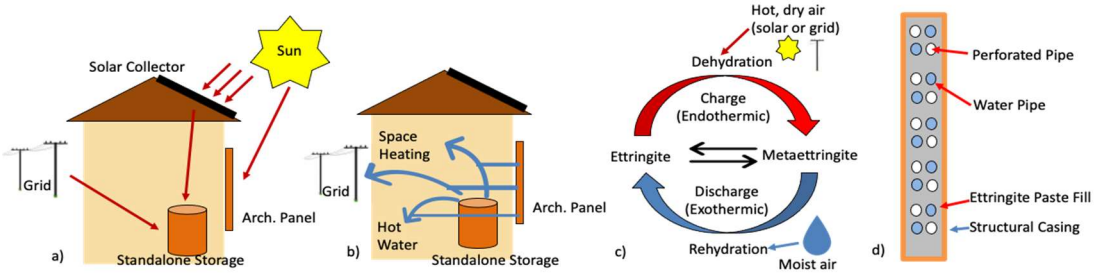

Figure 3.1 Schematic of system a) being charged b) discharging, c) cycle of charging/discharging of ettringite/metaettringite storage, and d) cross section of architectural panel

For use as a TCES medium, the energy input into the system must be able to be recovered and this should be able to occur over multiple cycles of dehydration and rehydration. Where the macro-stability stability of the system is needed for structural applications of the system, energy can be recovered from the system even in a deteriorated macro-structure state. Thus, energy can be recovered from either a structural system or self-contained reactors setup designed to make use of granular material.

Previous work studying the enthalpies of dehydration and rehydration of ettringite was focused on the pure ettringite crystals and not the crystal as a part of a heterogeneous hydraulic cement system [57, 58, 68, 92, 102, 103]. Thus, for the use of the hydraulic cement systems to generate the ettringite for TCES the enthalpies of dehydration and rehydration of the heterogeneous cement paste system is needed. The dehydration enthalpies between the ettringite and metaettringite states have been found to be between 630 and 1878 kJ/mol [57, 68, 92, 103, 104]. For rehydration, the enthalpy change was been found to be between 205 and 1316.1 kJ/mol [57, 103, 104]. Work by Ndiaye et al. has shown that for C$A pastes energy can be recovered after a second rehydration cycle when humid nitrogen gas is used [14]. Work by Chen et al. presented an investigation of protype reactor using granules produced from the hydration of a ternary OPC-CAC-C$ cement [105]. In the work by Ndiaye et al. and Chen et al. the temperature rise of the system was measured during rehydration. Multiple cycles were tested by Ndiaye et al. though only two rehydration cycles were conducted [14, 105]. More research is needed into the impacts of multiple rehydration cycles on the expected amount of heat output.

This work seeks to address gap related to the study of enthalpy of the ettringite dehydration and rehydration when heterogeneous materials are used. For this, three

different cement based materials which have been previously found to generate ettringite in the hardened paste were used. As ettringite has been found to dehydrate to metaettrigntie at temperature between 60 and 120^{o}C, each paste type was subjected to dehydration at a different temperature between 60 and 120^{o}C before being rehydrated. Rehydration of the pastes was done in an isothermal calorimeter where the heat flow and cumulative heat were measured to determine the characteristics of the rehydration reaction. For use in TCES, energy should be able to be recovered during rehydration from the paste over multiple dehydration and rehydration cycles. Previous work has only tested up to two rehydration's of the C$A paste dehydrated at 60^{o}C. This work address this gap through the testing of C$A paste for heat flow and cumulative heat during rehydration on seven subsequent dehydration and rehydration cycles at three different temperatures.

3.3 Materials and Experimental Methods

3.3.1 Cement Types

Three different cement types were examined in this study. A commercially available C$A cement (referred to herein as C$A), a sourced binary blend of CAC and C$ (referred to herein as CAC-C$), and a sourced ternary blend of OPC, CA and C$ cements (referred to herein as OPC-CAC-C$). The CAC-C$ system comprised of a 2.2 to 1 parts ratio of a standard grade CAC and C$. The OPC-CAC-C$ system comprised of the 2.2 to 1 parts ratio CAC and C$ blended at 30% of the cementitious material with a Type I portland cement making up the remaining 70% of the blend, by mass (per ASTM C150 [106]). An oxide analyses for the three cement systems are presented in Table 3.1.

Table 3.1 Oxide Analysis of Cements

Oxide (wt %)	Na_2O	MgO	Al_2O_3	SiO_2	P_2O_5	SO_3	Cl	K_2O	CaO	TiO_2	Cr_2O_3	MnO	Fe_2O_3	CuO	ZnO	SrO	ZrO_2	LOI**
C$A	0.17	1.57	14.19	14.51	0.11	15.63	0.11	0.57	50.23	0.60	*	*	0.69	0.03	0.03	0.14	*	1.45
CAC-C$	*	0.24	20.97	2.89	0.05	23.63	*	0.12	44.79	1.21	0.04	*	3.15	*	*	0.10	0.06	2.77
OPC-CAC-C$	0.18	2.89	10.01	16.58	0.18	7.65	*	1.00	57.10	0.56	0.05	0.11	2.01	*	0.05	0.23	*	1.41

Notes: *not detected, **accounts for loss due to C, CO_2, H_2O, OH, organic compounds and/or other

3.3.2 Paste Mixtures

Paste mixtures were used in this study as the crystal of interest, ettringite, is formed as a hydration product of the cement hydration. A water to cement ratio of 0.65 was used for all pastes to ensure that there was sufficient water in the system to form ettringite from the hydration of the cement.

3.3.3 Mixing and Casting Procedure

Due to the small volume of the paste for each batch, a table top mixer was not able to be used for mixing. A modified procedure based on ASTM 305 was used [76]. The casting procedure used was as follows: The cement and water mass were measured out. The cement was added to a plastic zip-top bag through a plastic funnel with the water being then added into the funnel to wash any cement residue on the funnel into the bag. The funnel was removed, and the bag closed tightly When the water was added, a timer was started and the mixture was allowed to sit for 30 seconds. The bag was then agitated by shaking the bag two times per second by hand for 30 seconds. For this procedure, one shake of the bag corresponded to a height of 100mm though complete cycle up and down. The mixture was then let to sit for 15 seconds making sure that all the mixture was combined on one area of the bag. The bag was then agitated again through shaking at the rate of four times per second for 60 seconds. After this mixing procedure was completed, a corner of the bag was cut and the paste mixture was squeezed out of the bag through the hole into the mold. Consolidation of the specimens was done through taping of the mold on the table from a

height of 5mm ten times. Excess paste was then removed from the top of the molds. The mold was covered by wet burlap and was cured for 24 hours before being demolded. Once demolded specimens were then placed in a moist curing room at 95%+ relative humidity and 23 +/- 3°C for 28 days before any testing was started.

3.3.4 Specimen Size

Specimens used for calorimetry testing were approximately hemispherical with a height of 12 mm and a diameter of 24 mm. This specimen sized ensured that the rehydration of the specimen in the calorimeter did not result in exotherms that exceeded the capacity of the calorimeter. The specimen and the mold used for casting can be seen in Figure 3.2.

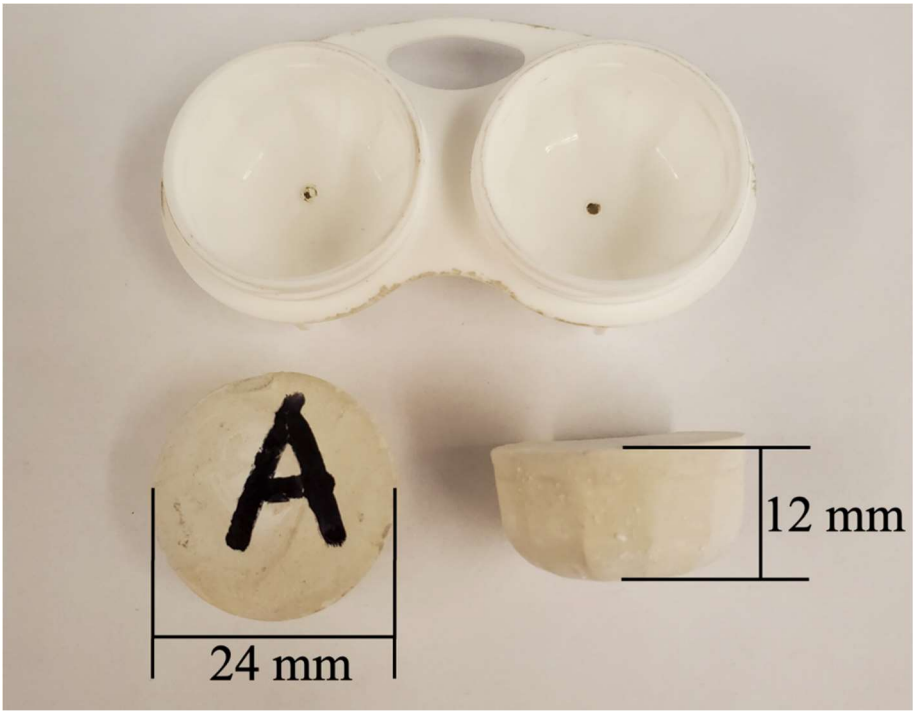

Figure 3.2 Calorimetry specimen mold and specimen dimensions

3.3.5 Specimen Dehydration

Dehydration of the specimens was conducted at one of five different temperatures. The lowest temperature was 60ºC. This value was selected as in literature this temperature was been found to be able to dehydrate ettringite based cement systems [14]. The upper dehydration temperature used for this work was 120ºC. This temperature was selected as from literature at this temperature decomposition of the ettringite is expected [58, 66]. The other selected dehydration temperatures of 75, 90 and 105ºC were selected at 15ºC increments between the two boundary temperatures. After the specimens had cured for 28 days, dehydration was performed through the heating of specimens in ovens at one of five temperatures of either 60, 75, 90, 105, or 120ºC. Dehydration of the specimens was for three days before being removed from the oven for testing in the calorimeter.

3.3.6 Sample Preparation for XRD Analysis, SEM Imaging, and EDS Analysis

Preparation of the samples for XRD and SEM-EDS analysis required the arresting of the hydration of the sample. Due to the sensitive nature of the ettringite crystal, the widely used technique of microwave drying may induce damage into the crystal [107], and, since the drying of the specimens through use of ovens is part of the experimental procedure of this work and drying through ovens to arrest hydration may impact the sample, an alternative method was used. The solvent exchange method using isopropanol has been found to be a more gentle way of arresting the hydration and better preserving the microstructure [78]. This method has been used successfully to arrest the hydration for of specimens to study the microstructure of C$A and CAC systems [108, 109]. Different solvents have been studied for use in the exchange process and for ettringite the use of

isopropyl alcohol has been found to be effective [78]. The solvent exchange process followed the procedure described by Zhang and Scherer [69].

Sampling of specimens was done by cutting 3 mm thick slices, approximately 15 mm by 15 mm in size from larger cube specimen. After the solvent exchange process was completed, the slices were then removed from the isopropyl alcohol and placed into a desiccator for two days to remove the isopropyl. After the two days, the samples could then be prepared for either XRD or SEM-EDS analysis.

Samples used for XRD analysis are ground in a mortar and pestle into fine particles using isopropyl alcohol as a lubricant. The resulting slurry mixture was placed into a labeled plastic Petri dish and the Petri dish was placed into a desiccator to evaporate the isopropyl alcohol. Once the isopropyl alcohol had evaporated, the sample remained in the desiccator until testing could be performed to prevent carbonation of the powder samples.

Samples for analysis through SEM-EDS were first into epoxy resin using EpoFix from Struers. Polishing was done on two separate phases, coarse and fine following the procedure listed in Chapter 8 in *A practical Guide to Microstructural Analysis of Cementitious Materials* [110]. After the polishing process was complete, samples were placed in the vacuum desiccator for a minimum of 48 hours to remove any remaining volatiles in the sample that may damage the SEM.

3.3.7 Isothermal Calorimetry

Isothermal calorimetry is the measure of heat output during a reaction through the measure of the amount of heat it takes to keep the system at a constant temperature. As a reaction occurs in the calorimeter, a temperature gradient will develop between the specimen and the heat sink used to keep the device at constant temperature. The temperature gradient will

generate a voltage which is measured through a sensor placed between the specimen and the heat sink. The voltage is proportional to the heat flow across the sensor and also the rate of the reaction. Integration of the heat flow allows for the determination of the total heat generated by the reaction. Isothermal calorimetry is useful for the energy testing work as the rate of the reaction and the total heat generated can be measured simultaneously. Also, the results allow for the comparison of the energy output during rehydration to be compared to the energy needed to dehydrate the system to determine the efficiency of the system. From isothermal calorimetry the reaction can be quantified by the amount of energy released per unit of material.

For testing, dehydrated paste specimens were placed in an I-CAL 2000 HPC isothermal calorimeter by Calmetrix at 20.0˚C to measure the cumulative heat during rehydration. The water and specimens to be used in the calorimeter were conditioned to 20.0˚C overnight to minimize any impacts from environmental heat (from water) or latent heat (from specimens). The sample mass of each specimen was measured within one hour prior to starting the calorimetry run. Mass of the specimens ranged from 6-9 grams depending on dehydration condition. The calorimeter collected data for the first 24 hours of rehydration with measurements being every ten seconds for the first hour and every minute after online the 24 hours had elapsed. Calorimetry results were normalized to specimen mass after dehydration and averaged between two specimens. The voltage change was measured by the calorimeter and the heat flow (displayed as power) and cumulative heat (displayed as heat) were calculated from this value.

3.3.8 XRD Analysis

X-ray diffraction analyses were done using a Philips EMPYREAN multi-purpose research X-ray diffractometer. Bragg-Brentano geometry with a 2-Theta of 5º to 65º with an X-ray source of 45kV and 40mA. Dry powders were used for analysis and were back loaded into the sample holder. A 27mm diameter sample holder was used unless there was not enough powder, in this case a smaller 16mm diameter sample holder was used instead. An angle step of 0.026º with a time step of 97.6 seconds was used for the experiments. HighScore Plus was used to identify the composition of the powder based on locations of the peaks by comparison with known powder diffraction file numbers in the International Centre for Diffraction Data (ICDD) Database Version 4+.

3.3.9 SEM-EDS Analysis

SEM imagine and EDS analysis was done using a JEOL JSM-7900F SEM machine equipped with a retractable backscatter detector and INCA energy system energy dispersive X-ray (EDS) detector for semi-quantitative elemental analysis. A beam acceleration voltage of 15kV and a working distance of approximately 10 mm was used for examining the samples. A 30 second collection time was used per EDS collection point.

3.4 Results

3.4.1 Impact of Dehydration Temperature on Total Heat Output During Rehydration

After dehydration of specimens was completed to promote conversion of the ettringite to metaettringite, the specimens were rehydrated by placing them in water. The rehydration of the samples was done in an isothermal calorimeter in order to study the heat released during rehydration of the samples. The data of interest was the peak heat flow, time to peak

heat flow, and the cumulative heat generated over 24 hours. The peak heat flow relates to the peak instantaneous amount of energy from rehydration. The time to the peak heat flow relates to the discharge characteristics of the pastes. The cumulative heat is the amount of energy that was able to be recovered from the reaction.

The heat flow for the three cement paste systems during the first 30 minutes of rehydration when first dehydrated between 60ºC and 120ºC are presented in Figure 3.3 A-E. The cumulative heat during rehydration for the three cement paste systems when first dehydrated between 60ºC and 120ºC are presented in Figure 3.3 F-J. Included on each graph for each cement type are curves for paste specimens that did not experience any dehydration prior to the calorimetry process (denoted by Baseline in the legend).

The heat flow observed during rehydration for each of the three cement pastes after dehydration at 60ºC for three days is presented in Figure 3.3 A. For all three of the tested cement systems, it is found that the peak heat flow of the reaction occurs within the first six minutes after being placed in water. The heat flow spikes on initial hydration before decreasing at a relatively constant rate from the peak. The specimens made with C$A cement resulted in the largest observed heat flow of 0.18 watts/gram of dehydrated cement paste and the longest time after commencing the test before peak heat flow was reached. The heat flow after the peak value decreased at the quickest rate of the three cement paste systems. The peak heat flow during rehydration of the CAC-C$ paste was found to be 0.013 watts/gram. For the OPC-CAC-C$ paste, the peak heat flow on rehydration was found to be 0.014 watts/gram.

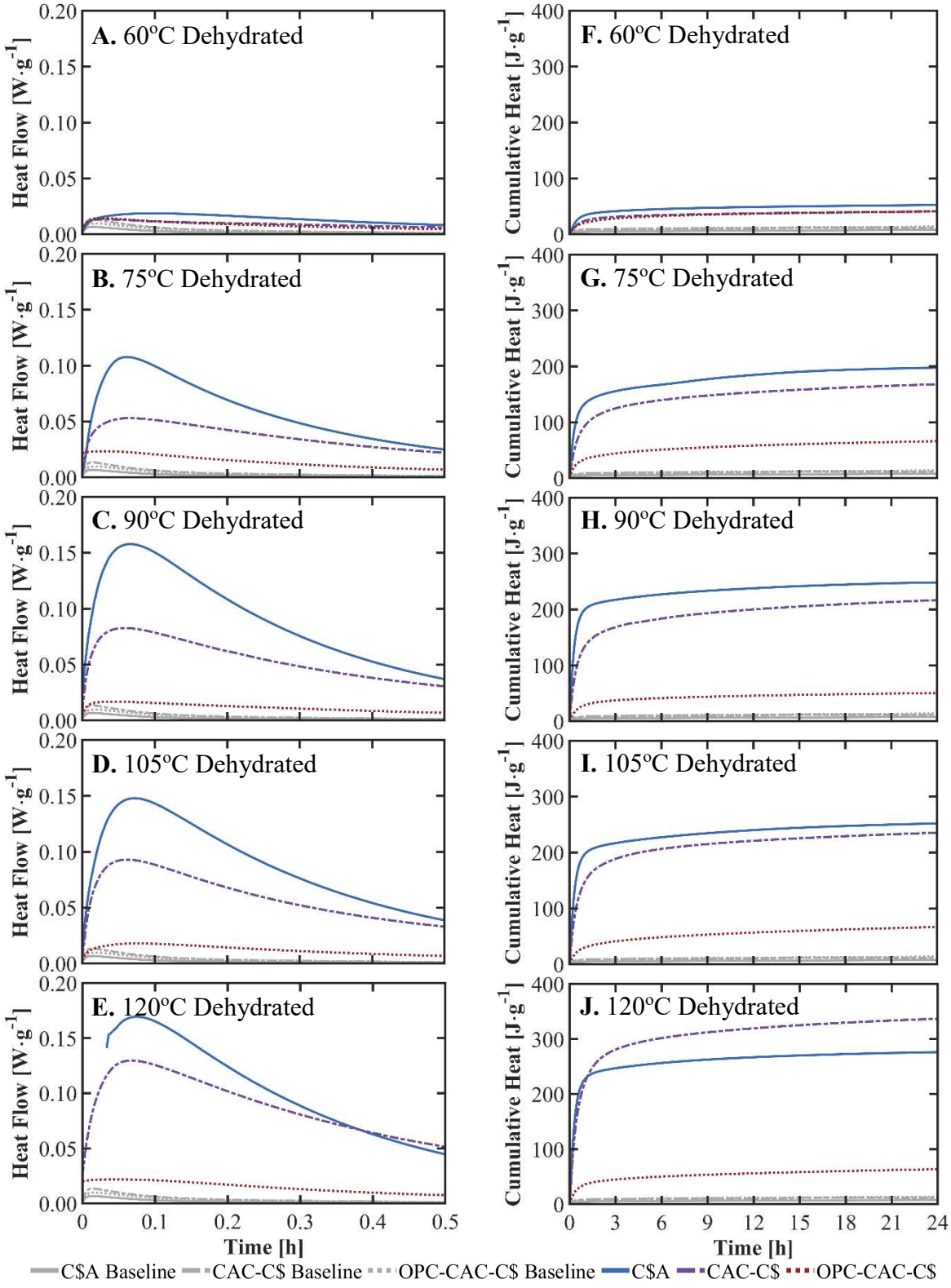

Figure 3.3 Heat flow during first 30 minutes of rehydration of pastes when first dehydrated at (A) 60°C, (B) 75°C, (C) 90°C, (D) 105°C, or (E) 120°C; Cumulative heat during rehydration of pastes when first dehydrated at (F) 60°C, (G) 75°C, (H) 90°C, (I) 105°C, or (J) 120°C.

The heat flow observed during rehydration for each of the three cement pastes after dehydration at 75ºC for three days is presented in Figure 3.3 B. For the cement paste specimens dehydrated at 75ºC, a noticeable difference in the heat flow peaks was observed between the three cements. The C$A paste specimens returned the largest peak heat flow of 0.1 watts/gram of dehydrated paste at 3.5 minutes after the start of rehydration. The peak power of the CAC-C$ paste system was found to be about half that observed for the C$A paste specimens at 0.05 watts/gram and reached this after four minutes of rehydration. The heat flow was observed to be similar for both the C$A and CAC-C$ paste specimens after 30 minutes. The OPC-CAC-C$ paste resulted in the lowest peak output of 0.02 watts/gram.

The heat flow for the three cement pastes first dehydrated for three days at 90ºC are presented in Figure 3.3 C. Rehydration of the 90ºC dehydrated OPC-CAC-C$ paste resulted in specimens that resulted in a heat flow peak 0.007 watts/gram greater than that observed in the baseline paste specimens. The heat flow after the peak was not observed to rapidly decrease past the peak, instead decreasing at a constant rate after the peak. The peak OPC-CAC-C$ heat flow was observed to be 0.016 watts/gram of dehydrated paste. This value was reached 2.5 minutes after rehydration was started. The CAC-C$ paste reached a peak heat flow of 0.083 watts/gram after 3.5 minutes of rehydration. The rehydration of the C$A paste resulted in the greatest heat flow of 0.158 watts/gram four minutes after the start of rehydration. The peak heat flow of the C$A paste specimens was observed to be double that found in the CAC-C$ paste system.

The heat flow during rehydration for the three cement pastes first dehydrated for three days at 105ºC are presented in Figure 3.3 D. The baseline curves for each of the cement types are included as reference. The peak heat flow was observed to be greatest for

the C$A paste specimens. The peak heat flow was found to be 0.148 watts/gram of dehydrate paste and the time of rehydration of the peak was 4.5 minutes. The peak value observed for C$A paste was found to be double that found for the CAC-C$ paste system. The CAC-C$ paste system was observed to have a peak heat flow of 0.093 watts/gram after four minutes of rehydration. The heat flow rate decreased the fastest after the peak in the C$A paste specimen, reaching a similar heat flow observed in the CAC-C$ paste after 30 minutes.

The heat flow during rehydration is presented in Figure 3.3 E for the highest tested dehydration temperature condition of 120^{o}C for three days. Error in the setup resulted in the data for the first minute of the C$A paste not being recorded. This was corrected and the peak heat flow was observed to be 0.169 watts/gram of dehydrated paste at 4.5 minutes after the start of rehydration. The peak heat flow of the CAC-C$ paste system was observed to be 0.13 watts/gram after four minutes of rehydration. The heat flow decreased quicker in the C$A system than in the CAC-C$ paste system resulting in a higher observed heat flow in the CAC-C$ paste system compared to the C$A paste system after 23 minutes. After this point, the heat flow of the CAC-C$ paste system remained above the C$A paste system.

The 24-hour cumulative heat during rehydration for the three cement pastes first dehydrated at 60^{o}C are presented if Figure 3.3 F. In Figure 3.3 F it is shown that the C$A paste specimens resulted in the highest returned heat after 24 hours or rehydration at 52.4 joules/gram of paste. Both CAC based paste systems resulted in similar cumulative heats of 40.9 joules/gram of dehydrated paste. For all pastes systems, the primary cumulative heat occurs within the first hour after stating rehydration. At this point, the C$A paste had

released 65% of the observed 24-hour heat total. The CAC-C$ paste system had release 59% and the OPC-CAC-C$ paste system had released 50% of the total 24-hour heat amount. At two hours, the percent of 24-hour heat that had been release was found to be 75% for C$A paste, 72% for CAC-C% paste, and 62% for OPC-CAC-C$ paste. At six hours, one quarter of the total testing time, the percentage of total heat that had been released was 86% for C$A paste, 84% for CAC-C$ paste, and 80% for OPC-CAC-C$ paste.

The cumulative heat during 24 hours of rehydration for the three cement pastes first dehydrated at 75^{o}C for three days are presented in Figure 3.3 G. The baseline heat curves for each cement are also presented. Of the three cement pastes the C$A and CAC-C$ resulted in much greater cumulative heat after 24 hours compared to the OPC-CAC-C$ paste system. For 24 hours of rehydration, the C$A paste system resulted in a cumulative heat of 197.8 joules/gram of paste and the CAC-C$ paste system resulted in 168.2 joules/gram of paste. In the OPC-CAC-C$ paste system, the 24-hour cumulative heat was found to be 66.2 joules/gram of paste. The majority of the cumulative heat was observed early on in rehydration, steadying at later ages. After one hour of rehydration, the C$A paste system was observed to have released 67% of the heat generated over the 24-hour testing time. At one hour, 56% of the CAC-C$ paste and 52% of the OPC-CAC-C$ paste 24-hour heat was observed. After two hours of rehydration, the percentages were found to be 75% for C$A paste, 68% for CAC-C$ paste, and 61% for OPC-CAC-C$ paste. At six hours, the percentages had increased to 85% for C$A paste, 83% for CAC-C$ paste, and 77% for OPC-CAC-C$ paste.

Presented in Figure 3.3 H are the observed heat curves during rehydration of the three cement paste systems after first being dehydrated at 90°C for three days. Also, presented are the baseline heat curves for each paste type. All three cement pastes were found to have a cumulative heat greater than that of the baseline paste specimens. The C$A paste specimens were found to have a 24-hour cumulative heat of 248 joules/gram of paste. For the CAC based cement pastes after 24 hours of rehydration, the CAC-C$ paste was found to have a cumulative heat of 216 joules/gram and the OPC-CAC-C$ paste was found to have a cumulative heat of 50 joules/gram. The cumulative heat for C$A paste was found to be five times that of the OPC-CAC-C$ paste system while the CAC-C$ paste system was found to result in four times the cumulative heat of the OPC-CAC-C$ paste system. For the C$A paste system after one hour of rehydration, 80% of the 24-hour cumulative heat had occurred. At two hours, this had increased to 86% and at six hours, one-quarter of testing time, 91% of the total amount of heat released during testing had occurred. For the CAC-C$ paste specimen after one hour, 62% of the 24-hour heat had already occurred; by two hours 73% had occurred; and by six hours 85% had been released. In the OPC-CAC-C$ paste system the percentage of heat released was found to be 57% after one hour, 69% after two hours, and 82 percent after six hours.

The cumulative heat during the rehydration of the three cement pastes first dehydrated at 105°C are presented if Figure 3.3 I. All specimens were observed to result in greater energy release than found in the baseline specimens. The C$A and CAC-C$ pastes resulted in similar heat release after 24 hours and were found to release a greater amount of heat over the test compared to the OPC-CAC-C$ paste. The C$A paste release 252 joules/gram and the CAC-C$ paste released 235 joules/gram during the 24 hours that heat

was observed. These represent a 3.5 to four times increase in heat released compared to the 64 joules/gram found in the OPC-CAC-C$ paste system. During the rehydration, the primary release of heat was found to occur during the initial stages of rehydration. When compared to the heat release during the 24 hours, the C$A paste was found to have released 78% of the total after one hour of rehydration. At two hours, this percentage had increased to 84% and at six hours 90% of the total 24-hour heat had been released. For the CAC-C$ paste at one hour, it was found that 63% of the total heat had been released. The percentage released at two and six hours was 75 and 88 percent, respectfully. The percentage of total measured heat for the OPC-CAC-C$ paste at one, two, and six hours was found to be 45, 55, and 73 percent, respectfully.

The cumulative heat over the first 24-hour period of rehydration for paste specimens dehydrated the prior three days at 120ºC are presented in Figure 3.3 J. The baseline reference heat curves for each of the pastes are also included as reference. The three cement pastes all were found to release more heat over the 24-testing time than their corresponding baseline. The CAC-C$ paste specimens resulted in the largest 24 cumulative heat of 336 joules/gram of paste. The C$A paste was found to release 276 joules/gram and the OPC-CAC-C$ paste 64 joules/gram over this period. The C$A paste was found to release four times the heat and CAC-C$ paste five times as much as the OPC-CAC-C$ paste. The primary energy release occurred during the initial rehydration. The C$A paste was found to have released 82% of the total found heat after one hour. After two hours, the percentage of total heat released was 88% and at six hours was 93%. For CAC-C$ paste at one hour of rehydration, 65% of the total heat was found to already have been released. This increased to 75% at two hours and 88% by six hours. The

OPC-CAC-C$ paste system was found to have released 57, 66, and 79 percent of the found energy by one, two, and six hours, respectfully, after rehydration.

Presented in Figure 3.4 are the cumulative heat results for each of the cement pastes and dehydration temperatures divided by the cement type. This comparison is to show how the dehydration temperature impacted the cumulative heat released of each cement paste type.

The cumulative heat curves for the 24-hour rehydration of C$A pastes are presented in Figure 3.4 A. It was found that the highest cumulative heat on rehydration was in the specimens first dehydrated at 120^{o}C. Where the cumulative heat was found to be 276 joules/gram of paste. At the dehydration temperatures of 105 and 90^{o}C, similar cumulative heats during rehydration were observed at 252 and 248 joules/gram of paste, respectfully. The paste specimens dehydrated at 75^{o}C resulted in a cumulative heat of 168 joules/gram of paste during rehydration. The lowest cumulative heat during rehydration was observed in the specimens dehydrated initially at 60^{o}C. At this dehydration temperature, 52 joules/gram of paste were observed during rehydration. This represents 20% of the heat observed during rehydration when dehydrated at 120^{o}C and 30% the heat at 75^{o}C.

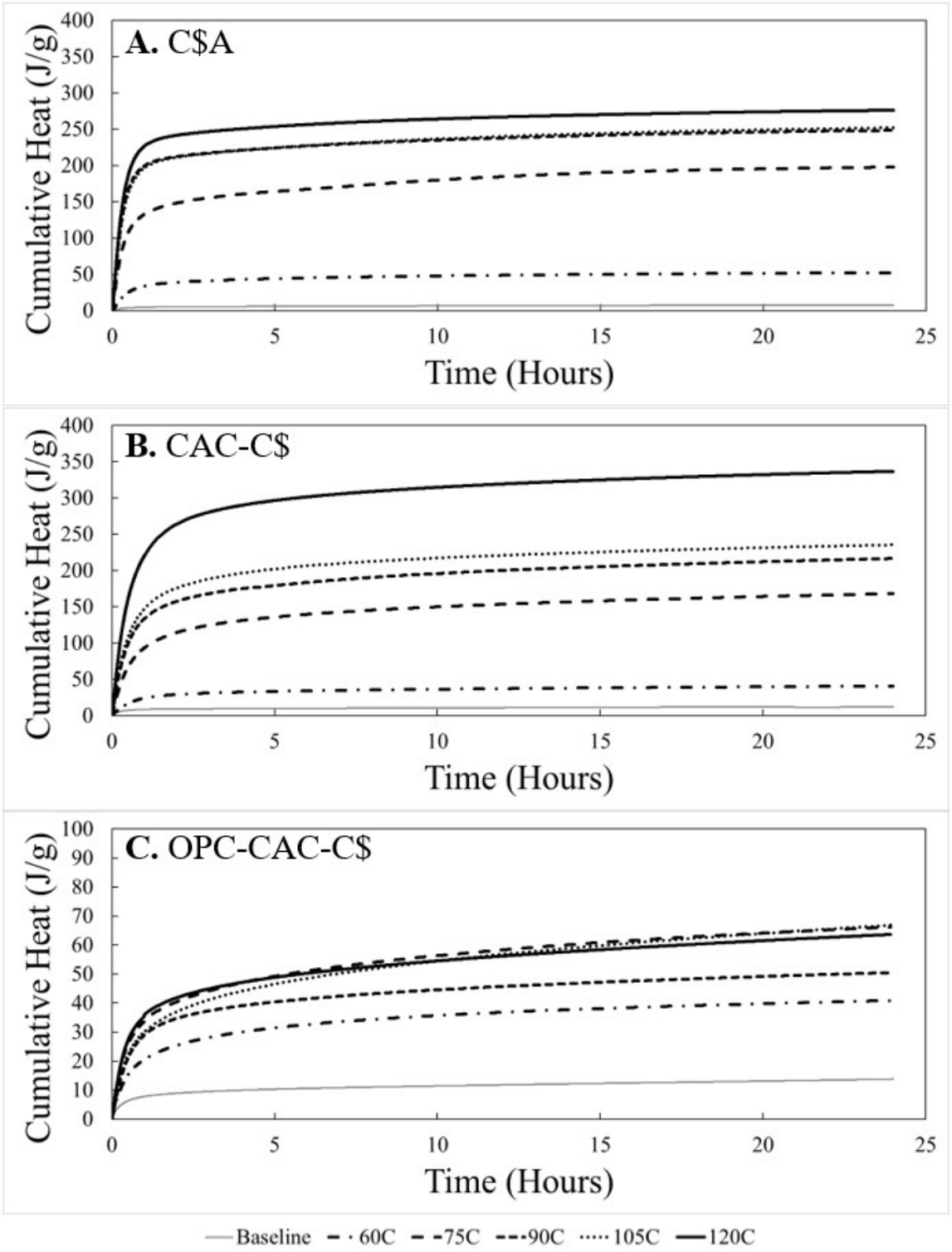

Figure 3.4 Cumulative heat during rehydration when initially dehydrated at 60ºC, 75ºC, 90ºC, 105ºC, and 120ºC for (A) C$A paste samples, (B) CAC-C$ paste samples, (C) OPC-CAC-C$ paste sample.

The cumulative heat observed during rehydration for the CAC-C$ paste specimens is presented in Figure 3.4 B. The trend observed between the dehydration temperatures is increasing the dehydration temperature will result in a higher cumulative heat on rehydration. The cumulative heat during rehydration of paste specimens dehydrated at 120ºC was found to result in an output of 337 joules/gram of paste after 24 hours. At 105ºC, the cumulative heat from rehydration was observed to drop to 235 joules/gram, a decrease of 30%. Dehydration of 90ºC was found to be 217 joules/gram of paste, a result like the heat produced from rehydrating specimens that were dehydrated at 105ºC. The cumulative heat from rehydration of the specimens dehydrated at 75ºC of 168 joules/gram of paste was 50% of that of the cumulative heat found from rehydration of the specimens dehydrated at 120ºC. The lowest cumulative heat from rehydration of the dehydrated paste specimens was found in the specimens first dehydrated at 60ºC where 41 joules/gram of paste was observed. This result for 60ºC was 12% of the cumulative heat found from rehydration of the specimens dehydrated at 120ºC and 3.3 times that found in the baseline specimen.

Presented in Figure 3.4 C are the rehydration heat curves for the OPC-CAC-C$ specimens for each initial dehydration temperature. From Figure 3.4 C, it is seen that all heat curves were of similar values after 24 hours of rehydration. With the low cumulative heat for each curve the differences observed are not as significant as those observed in the C$A and CAC-C$ curves presented previously.

3.4.2 Heat Released During Rehydration of C$A Specimens Over Multiple Cycles

For TCES use, the energy input into the system needs to be able to recovered from multiple cycles. The energy should be able to be recovered with minimal decrease in output on subsequent cycles. During the dehydration-rehydration cycling of specimens, the power

and cumulative heat during rehydration was measured for each cycle. The results for C$A pastes are presented in this section for the dehydration temperature of 60, 75 and 90ºC. These conditions were tested as from the stability testing detailed in Chapter 4, lower dehydration temperatures resulted in more stable systems and the C$A pastes resulted in the largest cumulative heat of the three pastes tested at these three temperatures when rehydrated the first time. Seven cycles has been previously used for multiple cycle testing by Ndiaye et al. [14].

Figure 3.5 presents the heat flow during the first 30 minutes of the 24-hour measurement period for specimens dehydrated at 60ºC. The power data curves show that as the cycle count increased the time to the peak heat flow decrease. The general trend of the heat flow increasing starting with cycle two was observed. A large decrease in heat flow was observed during cycle four. The increase in the heat flow prior to the peak was observed to occur at a faster rate at higher cycles. This is shown through the steeper slope and less rounded peak of the lines of the high cycles compared to the lower cycles. The increase in the observed peak heat flows of 0.093 watts/gram of paste for cycle one and 0.141 represents a 50% increase between the two cycles. The peak heat flow of 0.036 watts/gram observed in cycle four represents a peak 40% that observed during cycle one and 25% of the maximum observed peak during cycle seven. The time to peak heat flow was observed to decrease as the cycle count number increased. During the first rehydration, the time to peak heat flow was 5.25 minutes, for cycle seven the time to peak heat flow had decreased to 2.58 minutes after the start of rehydration.

The cumulative heat measured for each rehydration cycle during the first 24 hours of the three-day rehydration for 60ºC dehydration are presented in Figure 3.6. In the first

few cycles the cumulative heat was found to decrease though this varies as increased are seen on cycles three and five. These cycles were found to all result in cumulative heat values below that of cycle one. For cycles six and seven, the cumulative heat was found to increase for each cycle and above that of cycle one. The maximum cumulative heat was observed in cycle seven at 198 J/g an increase of 28 J/gram over cycle one. The lowest observed cumulative heat was observed in cycle four at 77 J/g, a decrease of 93 J/g from cycle one.

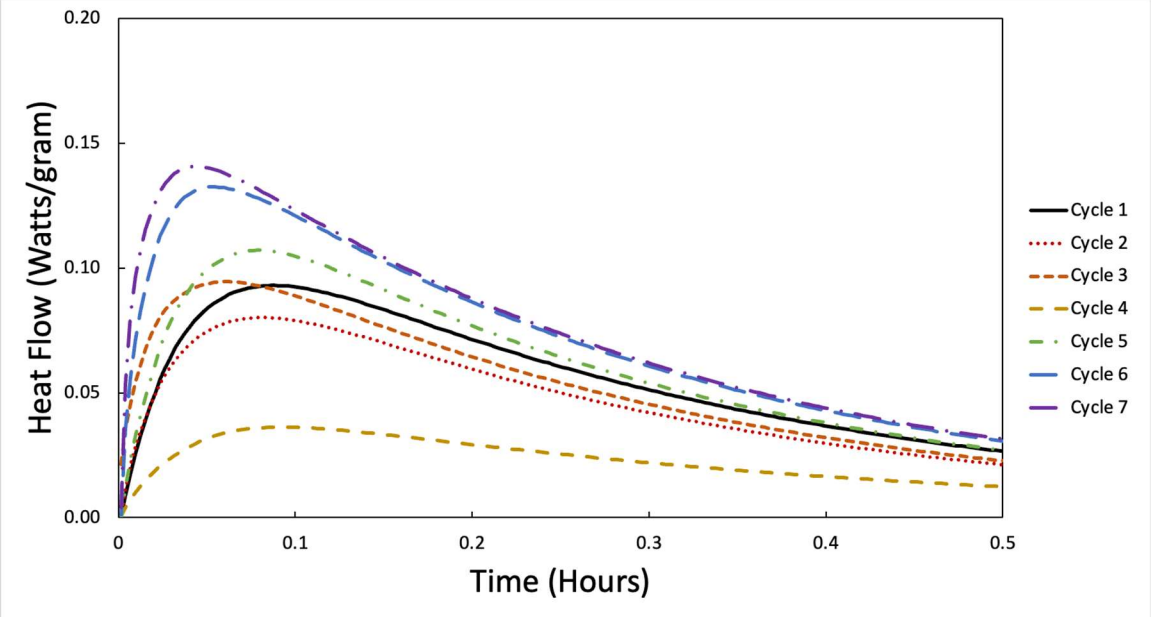

Figure 3.5 Heat flow during rehydration of C$A cement paste samples undergoing dehydration-rehydration cycles where dehydration was conducted at 60°C.

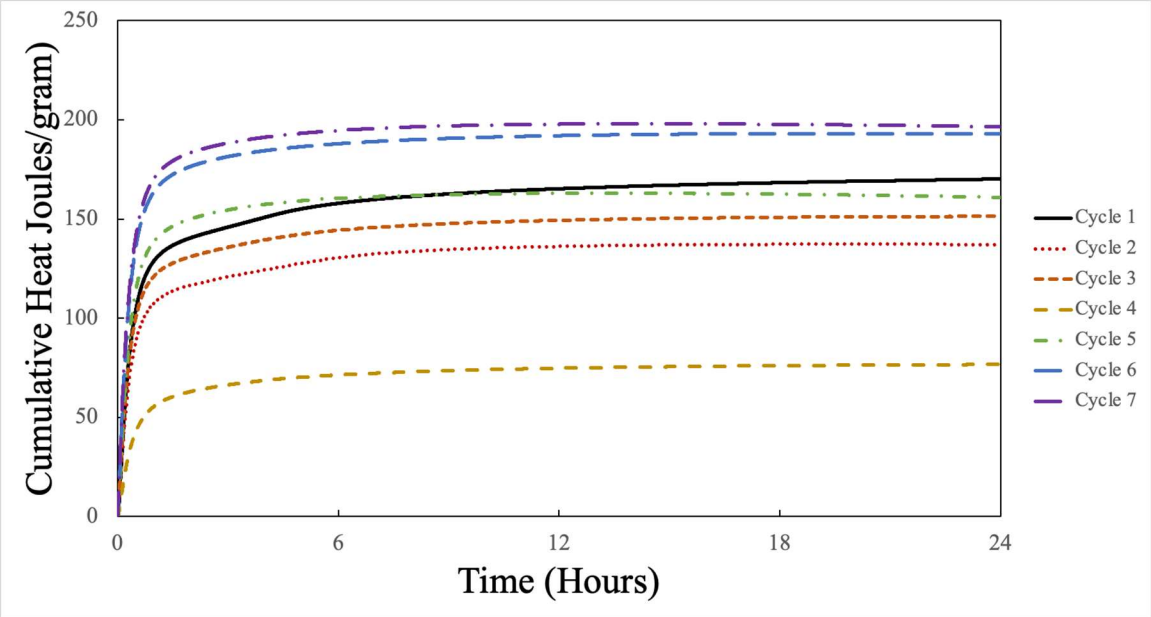

Figure 3.6 Cumulative heat during rehydration of C$A cement paste samples undergoing dehydration-rehydration cycles where dehydration was conducted at 60ºC.

The heat flows observed during progressive rehydration cycles for specimens dehydrated at 75ºC are presented in Figure 3.7. The highest observed heat flow of 0.173 watts/gram of paste was observed during cycle two. A progressive decrease in the heat flow was observed on subsequent rehydration cycles. The initial rate of heat flow was observed to be similar for each of the cycles. After 30 minutes of rehydration, the heat flow was observed to be a similar rate for each of the cycles. The time to peak heat flow was observed to decrease as the cycle count number increased. During the first rehydration, the time to peak heat flow was 5.08 minutes, for cycle seven the time to peak heat flow had decreased to 2.25 minutes after the start of rehydration.

The cumulative heat observed during the rehydration cycles are presented in Figure 3.8. A slight increase was observed between cycles one and two where the cumulative heat increased tom 234 watts/gram to 244 watts/gram. After cycle two, a decreasing trend was observed in the observed heat on each rehydration. A slight increase

was observed during cycle four. The cumulative heat observed for cycle seven of 193 watts/gram represents a 17% decrease from cycle one and a 21% decrease form the maximum cycle cumulative heat in cycle 2.

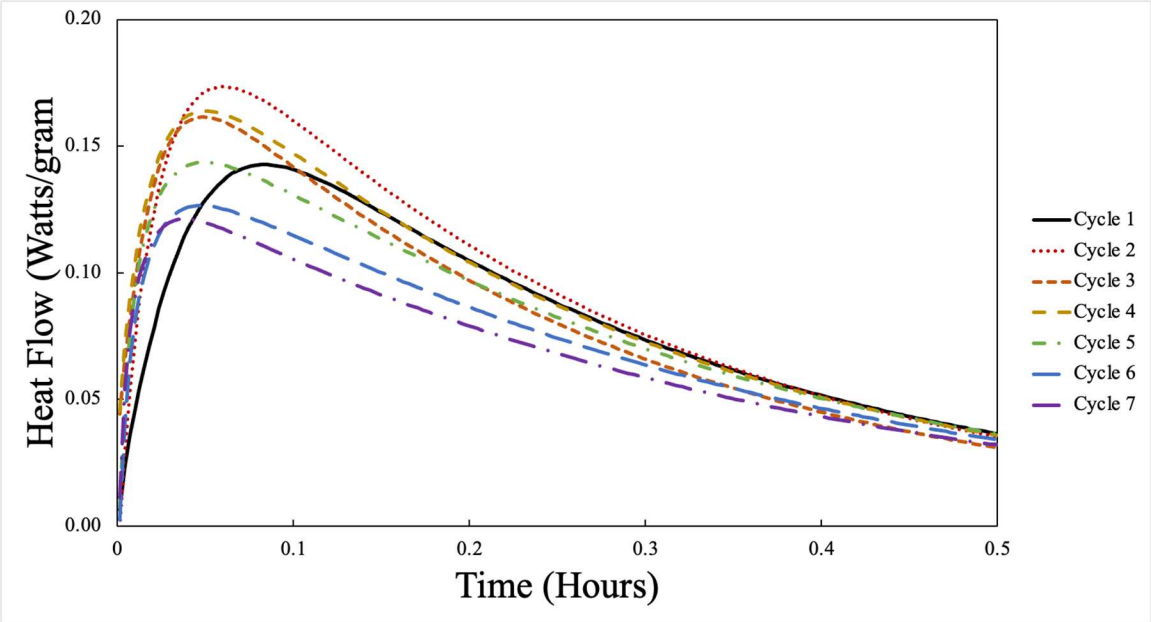

Figure 3.7 Heat flow during rehydration of C$A cement paste samples undergoing dehydration-rehydration cycles where dehydration was conducted at 75ºC

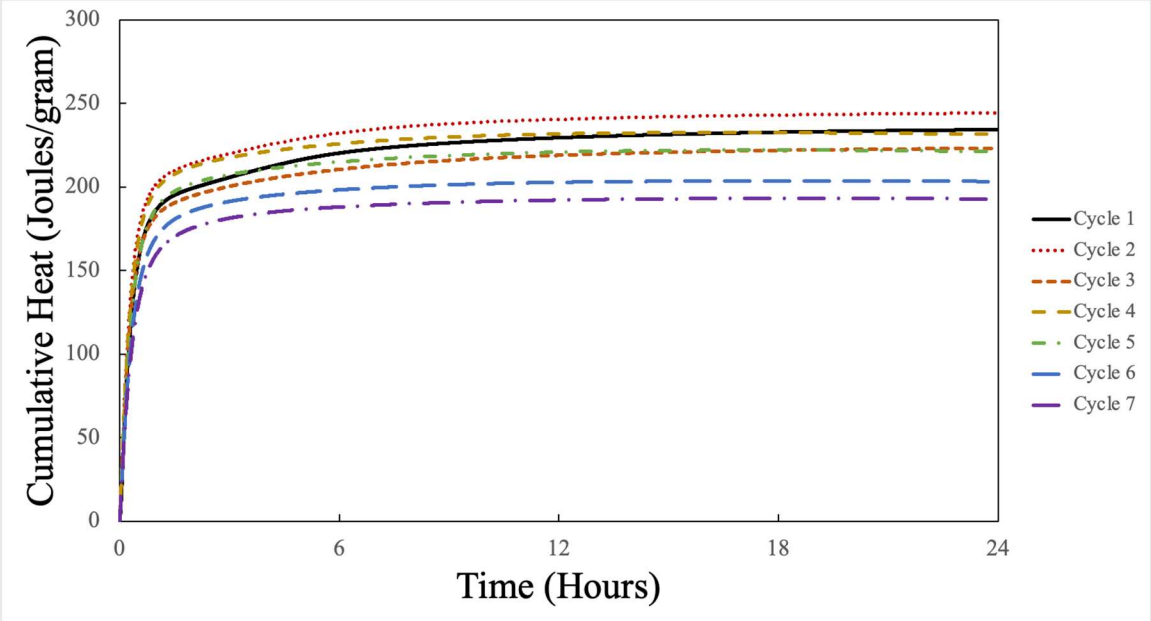

Figure 3.8 Cumulative heat during rehydration of C$A cement paste samples undergoing dehydration-rehydration cycles where dehydration was conducted at 75ºC.

The heat flow for the first 30 minutes of each rehydration cycle are presented in Figure 3.9 when 90ºC was used for dehydration. The peak output increased between cycle one and cycle two from 0.143 watts/gram to 1.68 watts/gram. Each subsequent cycle resulted in a lower peak heat flow. As the cycle number increased, the time to the peak heat flow was observed to decrease while the initial rate of heat flow increase was similar for cycles two on. During the first rehydration, the time to peak heat flow was 5.42 minutes, for cycle seven the time to peak heat flow had decreased to 3.42 minutes after the start of rehydration. Cycle one resulted in a slower rate of power increase. After 30 minutes of rehydration, all cycles were observed to have similar heat flows. The cumulative heat observed for each rehydration cycle is presented in Figure 3.10. The maximum cumulative heat was observed in cycle two at 266 J/g, a marginal increase of 9 J/gram from the first cycle. As the cycle count increased, a decrease in the cumulative heat values was observed. At cycle seven, the cumulative heat had decrease by 41 J/g from the first cycle and 50 J/g from the observed maximum cumulative heat in cycle two.

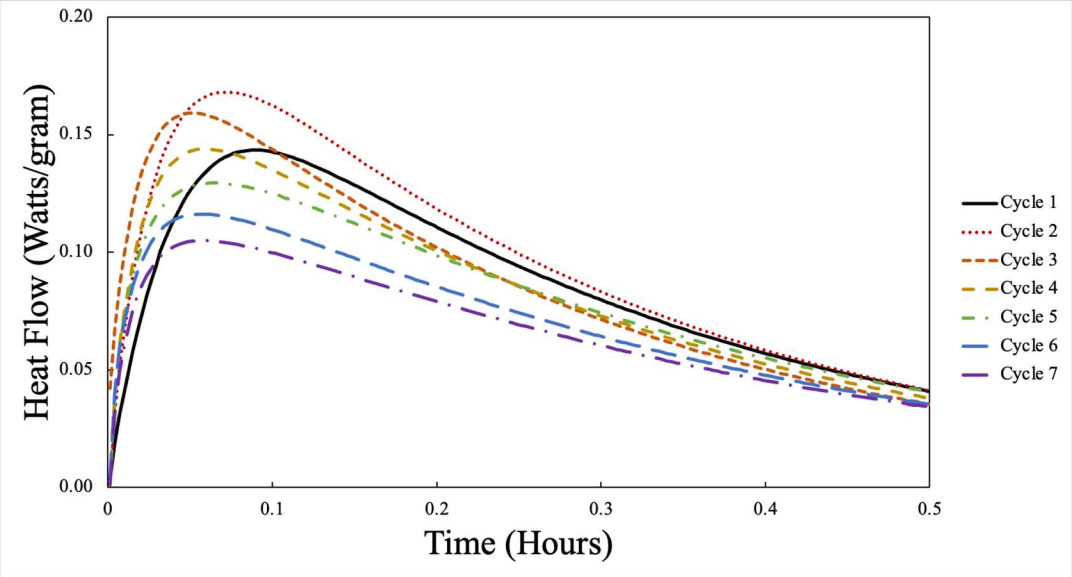

Figure 3.9 Heat flow during rehydration of C$A cement paste samples undergoing dehydration-rehydration cycles where dehydration was conducted at 90ºC.

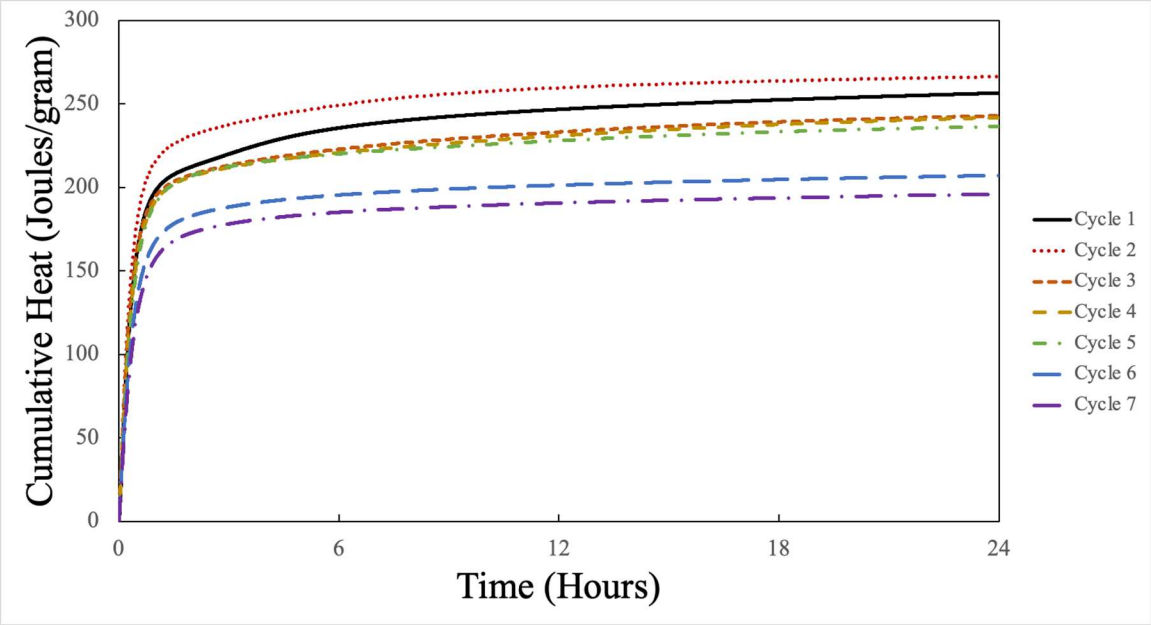

Figure 3.10 Cumulative heat during rehydration of C$A cement paste samples undergoing dehydration-rehydration cycles where dehydration was conducted at 90°C.

Presented in Figure 3.11 are the cumulative heats for each of the three dehydration temperatures used grouped based on cycle number. For the first five cycles, it was observed that the 90°C dehydration resulted in the highest cumulative heat on rehydration. The 75°C dehydrated specimens were found to result in a cumulative heat similar but lower than that of the 90°C specimens. In these five cycles dehydration at 60°C resulted in the lowest cumulative heat of the three cements with a difference in cumulative heat between the 60°C and 75°C larger than that observed between the 75°C and 90°C specimens. In cycles six and seven, all three cements were found to result in similar cumulative heats of 200 joules/gram of cement.

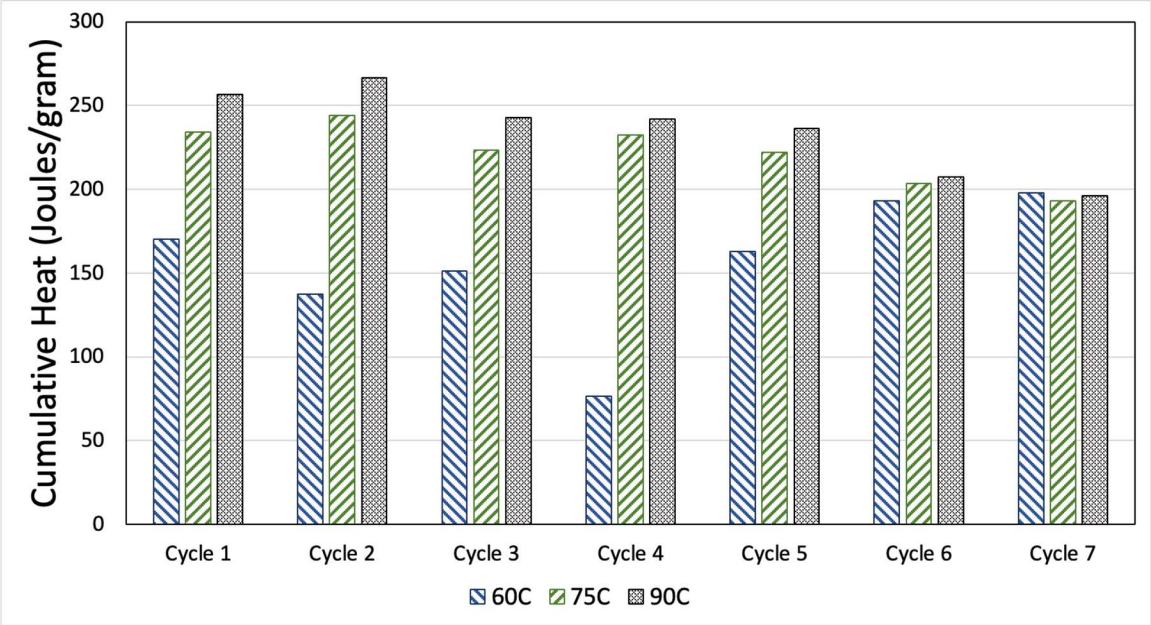

Figure 3.11 Comparison of cumulative heat per cycle for C$A specimens dehydrated at 60, 75, or 90°C.

A comparison of the cumulative heat during rehydration of cycle C$A paste specimens is presented in Figure 3.12, where the cumulative heats for each cycle are grouped per cement type. The observed cumulative heats for the rehydrated paste dehydrated 60°C are observed to be variable, where starting with cycle two a general increase in cumulative heat on each subsequent cycle is observed. Though, cycle four resulted in a cumulative heat of around half that observed for the other cycles. For rehydrated pastes first dehydrated at 75°C and 90°C, an increase in the cumulative heat was observed for cycle two before a decreasing trend of cumulative heat for each subsequent cycle was observed.

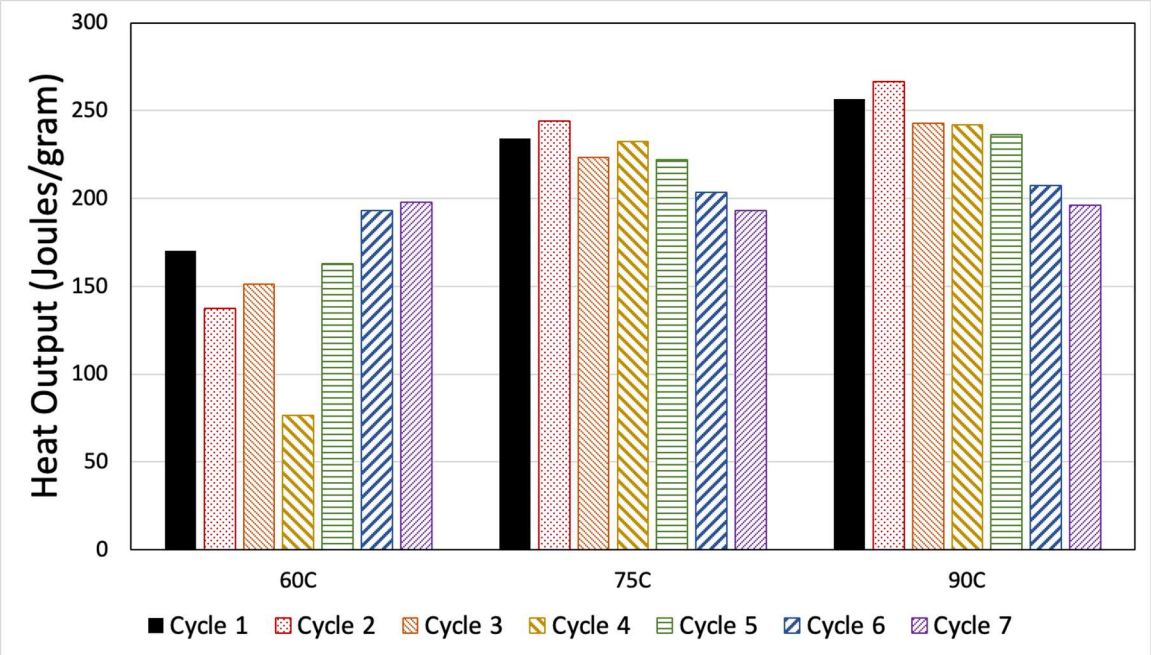

Figure 3.12 Comparison of C$A specimen cumulative heat per dehydration temperature for each cycle.

During progressive cycling of the specimens, the samples were observed to break apart into smaller piece. The initial and broken states of the specimens is presented in Figure 3.13. The failure of the specimens was first observed in the 90ºC specimens after cycle two. This was followed by cycle three for 75ºC and cycle five for 60ºC. Both specimens of each dehydration temperature failed on the same cycle. As seen in the cycle power curves, a progressive decrease to the time of peak power was observed. There was no noticeable decrease in the time to maximum power when the specimen failed.

Figure 3.13 Comparison of C$A paste calorimetry specimens in initial state and broken state after seven dehydration and rehydration cycles.

3.4.3 X-Ray Diffraction Results

XRD profiles for OPC-CAC-C$ specimens are presented in Figure 3.14. The conditions presented are the initial; dehydrated at 60ºC for three days, and then rehydrated; and dehydrated at 120ºC for three days, and rehydrated. In can be seen that in the OPC-CAC-C$ pastes ettringite is only present in the initial condition. Ettringite is not found in the dehydrate or rehydrated conditions at either of the boundary dehydration temperatures tested.

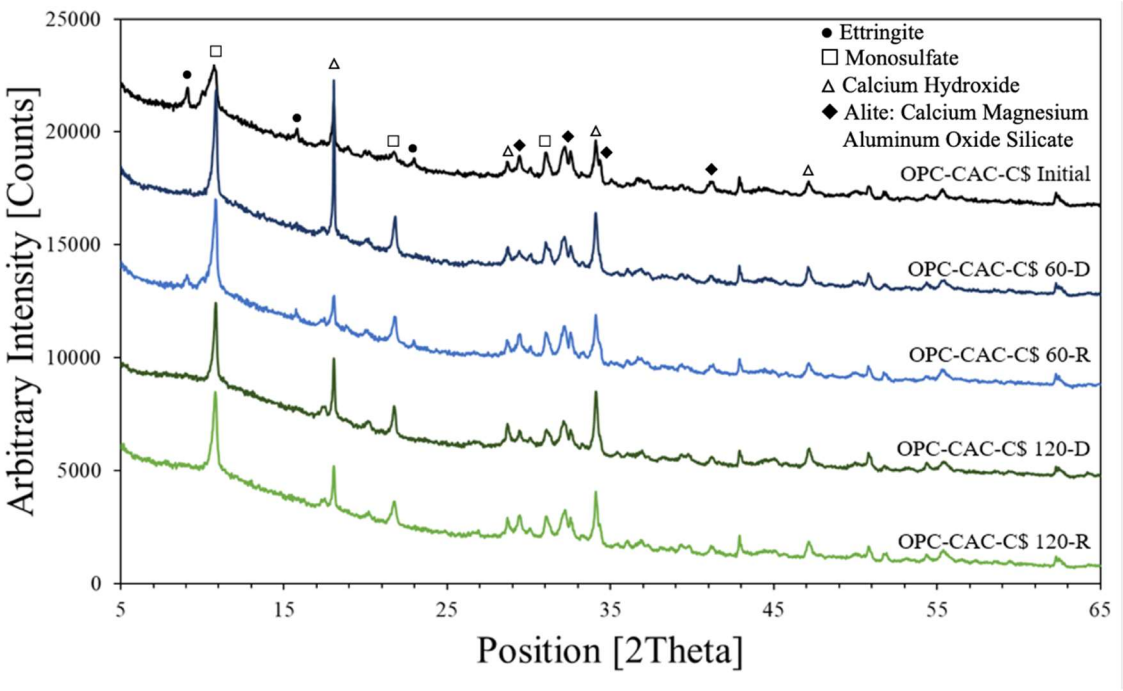

Figure 3.14 XRD scans of OPC-CAC-C$ paste at the initial condition and dehydrated and rehydrated conditions for specimens dehydrated at the boundary temperatures of 60°C and 120°C.

3.4.4 SEM-EDS Results

The ratios of EDS point analysis for OPC-CAC-C$ in the initial condition is presented in Figure 3.15. All data points lie below the monosulfate line with no data point in alignment with the line indicating ettringite nor in the region between the ettringite and monosulfate. The primary cluster of points near the line for monosulfate is around a Ca/Al ratio of 2.25 and an S/Al ratio of 0.45.

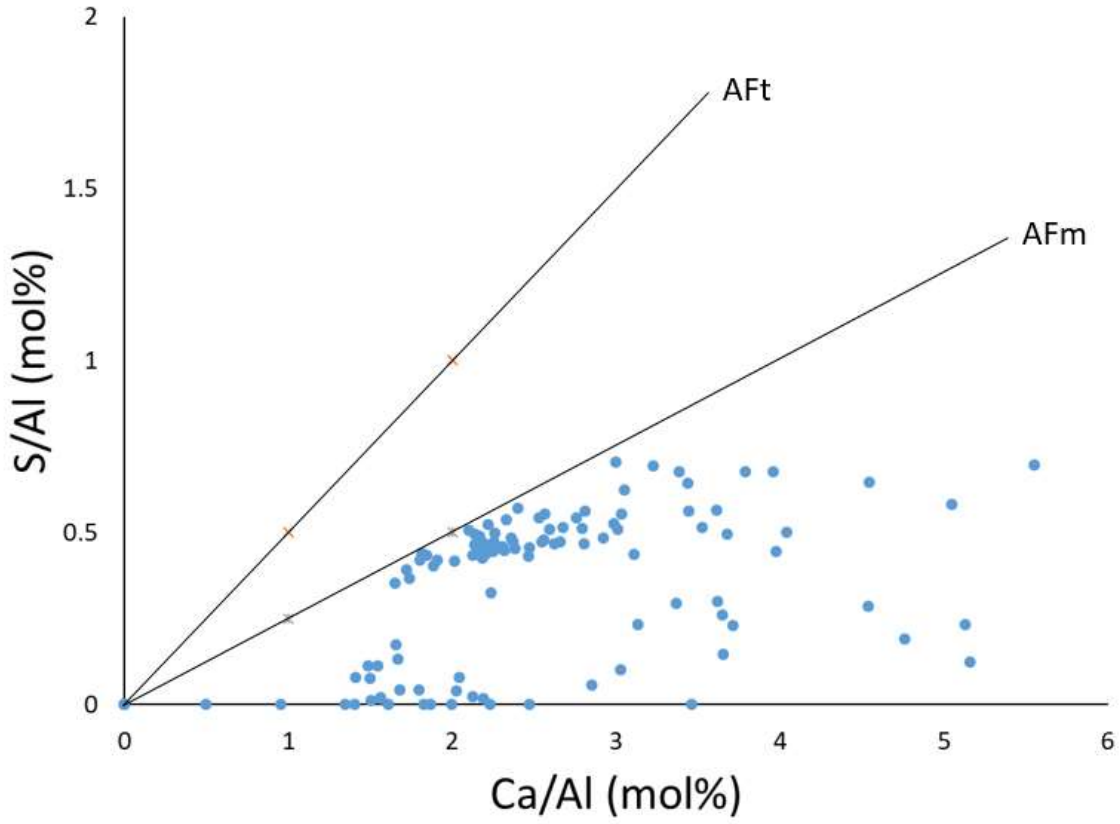

Figure 3.15 SEM-EDS point analysis for initial condition OPC-CAC-C$ specimen

3.5 Discussion

For use in TCES, heat energy input into the system needs to be able to be recovered when discharged. For the cement paste systems, the release of heat occurs when the dehydrated pastes are rehydrated. The important factors are the rate at which the discharge reaction happens and the amount of energy output during the rehydration. The rate of the discharge is measured by the peak rate of heat that is output from the paste during rehydration and the time it takes from the start of rehydration to reach this value. The total amount of heat output during the reaction is the amount that is able to be recovered from the rehydration of the paste. This can then be related to the amount of energy needed to dehydrate the

system to determine the efficiency of the storage reaction. For use as a TCES system, the reaction needs to be able to release the heat quickly on rehydration, most of the energy should be released together, and how efficient the heterogeneous paste material is compared to a pure ettringite system. The amount of energy that can be recovered on subsequent rehydration's indicate the rate that the reaction degrades. These factors are influenced by the cement paste type and the temperature used to dehydrate the cement pastes.

The temperature used to dehydrate the cement pastes was found to have an impact of the observed heat flow during rehydration. For the C$A and CAC-C$ pastes, there was an observed increasing trend of the peak heat flow values between the lower and higher tested dehydration temperatures. This trend was not observed in the OPC-CAC-C$ heat flow results. A significant change was observed between dehydration temperatures of 60ºC and 75ºC for the C$A and CAC-C$ paste systems. The C$A paste was observed to have the largest change with a peak heat flow of five times that when dehydrated at 75ºC than at 60ºC This change was observed to be less for the CAC-C$ system with three times increase between 60ºC and 75ºC. The OPC-CAC-C$ paste only saw a marginal increase of 33%. When the dehydration temperature used was increased to 90ºC, a marginal increase of 50% was observed in the heat flow during rehydration of the C$A pastes than at 75ºC. When the dehydration temperature was further increased to 105ºC and 120ºC, the observed peak heat flow was similar to the observed value for systems dehydrated at 90ºC. Specimens dehydrated at 90ºC had, on average, a 6.3% higher peak heat compared to specimens dehydrated at 105ºC, and a 7% higher peak heat than systems dehydrated at

120ºC. This indicated that, in the range of tested dehydration temperatures, there is a limit to the amount of heat flow from the samples if a sufficient dehydration temperature is used.

In the CAC-C$ pastes, an increase in peak heat flow was observed was the dehydration temperature was increased. Specimens dehydrated at 90ºC had on average a 57% higher peak heat compared to specimens dehydrated at 75ºC. Specimens dehydrated at 105ºC had on average a 12% higher peak heat compared to specimens dehydrated at 90ºC. Specimens dehydrated at 120ºC had on average a 39% higher peak heat compare to specimens dehydrated at 105ºC.

The OPC-CAC-C$ specimens peak heat flow results indicated no trend as the dehydration temperature was changed with all peak values, including the baseline, being within 0.013 watts/gram of each other. Excluding the baseline this difference in peak heat flow of all the tested temperatures did not vary more than 0.009 watts/gram. Peak heat flow is not a parameter that has been previously studied but is important to consider when designing a reactor to use these materials. A similar rapid increase of heat release was observed by Ndiaye et al. at early rehydration ages with a trailing decrease after the peak [14].

When comparing the peak heat flow between the various cement types, the OPC-CAC-C$ resulted in the lowest peak heat flow values of the three tested cements. The low heat flow values and no significant change of the peak heat flow value as the dehydration temperature was increased for the OPC-CAC-C$ pastes indicate that there was minimal amount of ettringite present in the system. This is reinforced through the chemical analysis of the cement paste as ettringite was minimally present in the initial OPC-CAC-C$ XRD profile and absent in the SEM-EDS analysis. Of the other two cement systems studied in

this work, the C$A system resulted in the highest peak heat flow during rehydration at all the tested dehydration temperatures. Though at 120ºC, the CAC-C$ system was observed to have a slower decrease in heat flow compared to the C$A after 20 minutes' dehydration. This indicates that, in the C$A system, the metaettringite is able to rehydrate at a faster rate and/or has more ettringite present in the system. To further understand this relationship a quantitative analysis of the amount of ettringite present in the pastes is needed. The amount of energy released is primarily realized at early rehydration ages with the heat flow values returning to similar values by 30 minutes. This indicates that the primary reaction occurs on initial rehydration and that systems should be designed for instantaneous release of heat rather than gradual.

It is also important to understand cumulative heat released from the pastes on rehydration to determine the systems' energy storage potentials. The results indicate that C$A and CAC-C$ pastes will see an increase in the cumulative heat released on rehydration as the dehydration temperature for each is increased. This trend was not observed for OPC-CAC-C$ pastes. For all three cement systems, the largest increase in cumulative heat during rehydration occurred between the pastes dehydrated at 60ºC and the pastes dehydrated at 75ºC. The C$A paste cumulative heat increased by 146 joules/gram between these temperatures, a 280% increase. The cumulative heat of the CAC-C$ was found to increase by 128 joules/gram between the same temperatures, though had a larger 320% increase. The lowest increase was observed in the OPC-CAC-C$ specimens where only a 25 joules/gram increase was observed, a 61% increase. There was no observable overarching trend in the change in cumulative heat as the dehydration temperature was increase. This is shown as while the percent increase of cumulative heat

for C$A and CAC-C$ were lower between dehydration at 75ºC and 90ºC than between 60ºC and again between 90ºC and 105ºC; a larger increase was found between 105ºC and 120ºC for both cements. The lack of trend was different in the OPC-CAC-C$ cement as the cumulative heat was found not increase or decrease by more than 25%.

The largest cumulative heat during rehydration for the C$A and CAC-C$ pastes was found in the specimens dehydrated at 120ºC. The largest cumulative heat at this temperature was observed in the CAC-C$ paste specimen at 337 joules/gram of paste. This was an increase of 22% compared to the C$A paste specimen.

An average American household used 38,574 MJ (10,715 kWh) of energy in 2020. This corresponds to a daily usage rate of 105.68 MJ (29.35 kWh). Dividing the daily usage by the 337 joules/gram for the cumulative heat from rehydration of the CAC-C$ paste dehydrated at 120ºC results in 313.6 kg (700 lb) of dehydrated paste needed to power an average American house for one day. This translates, using a typical unit weight of 2,402 kg/m^{3}1 (50 lb/ft^3), to a paste cube with sides of 0.51 meters (1 foot 8 inches) per house for one day of energy. For a C$A paste dehydrated at 75ºC, the density of 198 joules/gram would result in a typical daily house energy usage being stored in a paste cube with sides of 0.61 meters (2 feet).

The energy used to dehydrate the specimens was not measured as a part of this work, but previous work related to natural and synthetic ettringite has found the heat enthalpy needed to remove the water. Jiménez and Prieto found that for natural ettringite 2066 J/g was needed to remove 23 molecules of water at 190ºC and in synthetic ettringite less energy of 1298 J/g was needed to remove 19 molecules of water [68, 104]. For synthetic ettringite systems, Baquerizo et al. used a dehydration temperature of 60ºC, 973.3

J/g was needed to form metaettringite with 9.3 molecules of water and at 65ºC 997.2 J/g were needed to form metaettringite with 8.3 molecules of water [57, 104]. Using this data, the efficiency of the C$A system would be between f and 28% if 973.3 J/g is needed to remove water and 2-14% if an enthalpy of 2066 J/g is used. For the CAC-C$ system, the efficiency would be 4-34% for an enthalpy of 973.3J/g and 2-16% for an enthalpy of 2066 J/g. The efficiency of the OPC-CAC-C$ was the lowest at 4-7% for enthalpy of 973.3 J/g and 2-3% for an enthalpy of 2066 J/g.

While the C$A paste system produced higher cumulative heat, the CAC-C$ system did not produce extremely lower levels of cumulative heat when rehydrated. The results indicate that more heat is produced at higher dehydration temperatures, though the gains in output may not overcome the amount of excess energy required to dehydrate the system. Thus, the next step is the study of the efficiency of these systems specifically, since much of the previous work looking at the energy required for dehydration has focused on natural or synthetic ettringite [57, 68, 104]. The CAC-C$ pastes were also found to reach peak heat output in a shorter time from the start of rehydration than the C$A pastes. Though, this may be due to the lower peak heat flow values of the CAC-C$ pastes compared to the C$A pastes. The cumulative heat on rehydration of the OPC-CAC-C$ pastes was similar for all the tested dehydration temperatures. The cumulative heat observed for the OPC-CAC-C$ was found to typically be at a lower value than that of the other two cements, though this was not the case at dehydration of 60ºC where the CAC-C$ and OPC-CAC-C$ systems resulted in similar cumulative heat results. The difference between the OPC-CAC-C$ paste and the C$A and CAC-C$ pastes was found to increase as the dehydration temperature increased. The low cumulative heat and lack of trend as the temperature increased indicates

that the quantity of ettringite present in the OPC-CAC-C$ system may be minimal. This is confirmed through the XRD where ettringite was only found to be slightly above background levels in the initial state and in SEM-EDS where ettringite was not found to be present.

The long-term impact of cycles on the energy output from the paste on rehydration was studied for the C$A paste systems when a dehydration temperature of 60ºC, 75ºC, or 90ºC was used. Previous work by Nidaye et al. has shown that energy can be recovered from rehydration of the system after a second dehydration cycle at 60ºC though a decrease in the amount of energy was noted [14]. The results indicate that multiple cycles of the C$A paste at different dehydration temperatures are possible and energy is still able to be recovered from specimens after degradation of the macro-structure. For all three tested dehydration temperatures, an increase was observed in the peak heat flow and cumulative heat between cycles one and two. A similar increase in heat released was observed by Ings and Brown when pure ettringite was subjected to dehydration and rehydration cycling [102]. This may indicate that during the first cycle not all the ettringite has converted to metaettringite. This is indicated for the conditions tested as through the XRD analysis, peaks for crystalline ettringite were observed for the dehydrated C$A pastes when dehydrated at 60ºC, 75ºC, and 90ºC. Both 75ºC and 90ºC dehydration temperatures resulted in a decreasing trend for the peak heat flow and cumulative heat as the cycle count increased. The cumulative heat of the 90ºC dehydrated specimens was greater than that of the 75ºC specimens for each cycle though the difference was not more than 25 joules/gram between them a 9.3% difference.

The peak heat flow and cumulative heat for rehydration of specimens dehydrated at 60ºC resulted in more variable results than seen at 75ºC and 90ºC. As the cycle count increased, the peak heat flow and cumulative heat results were found to increase at the later tested cycles. For rehydration in cycle seven, a similar cumulative heat was observed for all three of the dehydration temperatures tested. This indicates that the most efficient dehydration temperature is likely the lower dehydration temperatures. The increase in energy needed to dehydrate the pastes at higher temperatures may result in a less efficient storage system as the increase in energy needed to charge the systems and the increase in energy released may not be proportional. This effect would also be compounded as at higher cycle counts the heat output on rehydration from all three temperatures was the same. The rate of decrease in cumulative heat per cycle at 90ºC for C$A is similar to that observed of pure ettringite dehydrated at 100ºC before rehydration performed in work performed by Ings and Brown [102]. Though, the decrease of 27% observed in the presented work was greater than that of 20% observed by Ings and Brown [102]. The lower temperature change observed by Ndiaye et al. during a second rehydration cycle while not what was observed in this study does indicate that even in the first couple of cycles a loss in the recovered energy should be expected for these systems [14].

However, for the multiple cycle testing of the C$A paste system, at a dehydration temperature of 60ºC, a larger peak heat flow of 0.093 watts/gram was observed than the 0.018 watts/gram presented in Figure 3.3 A. This would represent a 16% increase between the 60ºC heat flow from the cycle testing and the 75ºC peak heat flow shown in Figure 3.3 B. This inconsistency could be due to unknown issues with the oven during dehydration as the same oven was also used for the other pastes in Figure 3.3. This is

highlighted where a low heat flow was observed in the CAC-C$ paste at 60ºC compared to the other four dehydration temperatures. The CAC-C$ specimen dehydrated at 60ºC also resulted the same peak heat flow as that observed in the non-dehydrated baseline specimen. A higher cumulative heat was only observed due to the slower decrease in heat flow of the 60ºC dehydrated specimen compared to the baseline. Further investigation is needed to understand the heat release during rehydration of specimens dehydrated first at 60ºC. In the OPC-CAC-C$ paste the lack of ettringite and low heat output indicates that this cement system is not viable for use in TCES. As this type of cement has been found previously to result in ettringite in the hardened system, more testing of the blended system cast in different conditions is needed to see if the cement can be viable for TCES.

From the presented research, the energy results indicate that C$A and CAC-C$ paste systems are able to be used for TCES. Energy was able to be recovered from the pastes systems on rehydration and the bulk of the energy release was found to occur at early rehydration ages. Key components for use as a storage medium. The C$A paste system was found to still release energy on rehydration after multiple dehydration and rehydration cycles. The energy release from the rehydration of the best performing system of CAC-C$ paste dehydrated at 120ºC was found to result in a volume that is reasonable for practical use. The next steps are expansion of the multiple cycle calorimetry to the higher dehydration temperatures and CAC-C$ paste to determine the rate of loss in heat output from the systems. Also, the efficiency of the dehydration and rehydration cycle of the pastes is still needed to be determined as the presented work did not measure the energy do dehydrate the paste systems.

3.6 Conclusion

This work has shown the energy that can be recovered during rehydration of the tested pastes and dehydration temperatures and these factors can significantly change the amount of energy that can be recovered. The greatest impact was observed in the type of cement used. The OPC-CAC-C$ paste was found to result in significantly reduced recovery of energy at higher dehydration temperatures compared to the C$A and CAC-C$ systems. This was likely due to the minimal presence of ettringite in the hardened paste observed from microstructural analysis. At the lowest dehydration temperature of 60°C, heat energy was still able to be recovered from the system. Increasing the dehydration temperature was found to increase the energy released on rehydration. The heat energy recovered from the paste systems was found to less than that typically found in systems made of pure ettringite.

Further work is needed to understand the efficiency of the dehydration and rehydration cycling of these systems. The cyclic testing of these pastes should be further expanded in the scope of cements, temperatures, and cycle count to develop a comprehensive understanding of the performance of prolonged cycling of the systems.

CHAPTER 4

STABILITY OF HIGH ETTRINGITE PRODUCING CEMENTS FOR USE IN THERMOCHEMICAL ENERGY STORAGE

4.1 Abstract

New and novel methods for energy storage are an important part of meeting increasing energy needs and improving the sustainability and security of energy systems. Grid energy systems are designed to consistently meet peak energy demand situations, resulting in costly, inefficient systems that waste energy during low demand periods. Novel methods of storing energy are required to meet load-leveling needs of efficient energy systems. To date, much of the research on energy storage has focused on battery storage solutions; however, the U.S. Department of Energy (USDOE) has noted the need for more revolutionary materials and solutions. Ettringite based cement systems offer a potential solution to this issue using raw materials that are inexpensive and abundant. These cements are a special type of hydraulic binder that, when mixed with water, result in the hydration product known as ettringite ($C_6A\$_3H_{32}$). The ettringite crystals can undergo a reversible, stable, thermochemical conversion that may be a viable tool for energy storage. However, the conditions that these systems are stable at without decomposing are not well understood as they are influenced by many different factors. The objective of this work was to examine stability of three different high ettringite cement paste systems under different conditions. The macro integrity of the systems was measured through, (i) time to failure when cycled, (ii) change in mass when cycled, (iii) change in compressive strength during a cycle, (iv) mass change over time of stored dehydrated systems, and (v) microstructural changes observed from XRD and SEM-EDS analysis. The results indicate lower dehydration temperatures result in a system that performs longer before failure, the systems can

maintain a dehydrated state over an extended period of time, and that the state of the system impacts the compressive strength.

4.2 Introduction

The demand for energy has been constantly increasing. Since 1965, the world energy consumption has quadrupled from $40x10^3$ MWh to $160x10^3$ MWh in 2018 [2]. During peak utilization periods, the strain on energy infrastructure can be immense. A recent event related to this are high temperatures causing rolling blackouts in California in 2020 where the system was expected to be short 4,400 megawatts of power in the late afternoon [4]. In Texas in 2021 grid power failures were seen due to the icing of natural-gas processors with the entire Texas power grind close to completely going offline [111]. An issue which has not been resolved and is unique to Texas as it has a separate grid to the rest of the country and must generate its own power. The governor's plan is to increase the generation capacity for crypto-mining in the state with the extra capacity able to be leveraged for the need of the state when another event occurs [111]. The excess capacity is stated to be years away and a storage method of using personal electric trucks as batteries has a waitlist of years [111]. Storage of the energy is a possible solution to future events. A storage concept called load leveling can be implemented where the energy generated when demand is low is released to compensate during high demand periods [112]. Through storage of energy generated during lower demand periods the following three primary benefits are found.

1. Load leveling where the existing generation capacity does not need to be expanded immediately to meet the new demand [112].
2. The generation facility will require less maintenance and upkeep as generation levels do not need to constantly match demand [112]

3. Storage provides for redundancy within the system. [112]

The primary current concerns for energy storage in the United States outlined in a 2013 report from the U.S. Department of Energy are that, as of 2013, the U.S had 24.6 GW of energy storage which equaled about 2.3% of electric production capacity at the time, a percentage that lagged behind other developed countries and regions such as Japan and Europe [1, 6]. As of June 2018, the storage capacity had been marginally increased to 25.2 GW of energy, showing that energy storage increases have been slow and new technologies and methods are required to meet energy storage needs [7, 8]. Less than 30 GW (power for 29,000 households) of the United States national energy output is able to be stored at any single time for later use, and 95% of that storage capacity is realized through pumped hydroelectric, an option that is only available in some geographic regions [1, 6, 7]. One potential energy storage technology that still needs significant investment to be understood is thermochemical energy storage [1, 2, 113].

Thermochemical energy storage is of interest as an emerging technology that's primary benefit over other methods is its very high energy density, 5 to 20 times conventional storage [1] . Storing energy through heat (thermal) processes has a wide range of applications and can be deployed in varied situations and on multiple spatial scales [114]. The study of these systems is important and promising as most irreversible losses within energy systems occur in the form of heat and more than half of energy generated and consumed in the world occurs through thermal processes [11].

One potential thermochemical energy storage system can be created using a high water content crystal called ettringite. In the thermochemical reaction some of the bound water is removed through a form of dehydration such as elevated temperatures, though

other methods to remove the water such as vacuum drying can also be used [103]. The dehydrated form of ettringite is termed metaettringite and comprises between 10 and 13 molecules of water compared to the 32 associated with ettringite [58]. To complete the thermochemical energy storage cycle heat is released with the rehydration of the metaettringite. Hydraulic cement systems, utilizing the hydration and dehydration of water from ettringite crystals formed during the cement hydration process can be used to generate ettringite [13, 14, 58, 67, 104, 115–117].

The dehydration and rehydration of ettringite to the dehydrated form can be repeated if the ettringite crystal and the system remain stable [58]. While this has been shown to be a reversible hysteretic reaction, understanding of what happens to the system during the reversible reaction is still not well understood [13]. Dehydration at temperatures between 60ºC and 120ºC has been found in previous studies to result in the loss of water from the ettringite crystal [13–15, 57–59, 67]. Decomposition is exhibited when the ettringite is heated to elevated temperatures around 100ºC, though other conditions such as drying treatment condition and pressure can impact the temperature at which ettringite will decompose [57, 58, 67]. If the ettringite decomposes to a form other than metaettringite such as monosulfoaluminate hydrate, basanite, and/or katoite, the hysteresis loop between ettringite and metaettringite will cease to continue [61, 67, 118, 119]. Decomposition will result in an instable crystal structure that will crack and disintegrate the sample [67].

Ettringite as a rarely occurring crystal naturally though is commonly found in the hydration of cement systems. In ordinary portland cement (OPC) based systems ettringite is a common product that is formed during the early stages of hydration, however in OPC the ettringite will later convert to monosulfoaluminate [120]. In mature portland cement

systems (older than 28 days), ettringite comprises only 10% of the hydrated cement paste [14]. In other binders such as calcium sulfoaluminate cements (C$A) and calcium aluminate cements (CAC) blended with sulfates, the ettringite content in the mature hardened paste has been observed to comprise up to 80% of the hardened paste by mass[14]. The hydration of OPC systems blended with CAC and a form of calcium sulfate have also been found to form ettringite in the hardened paste [15, 49, 51, 121]. This ternary system is advantageous as it is primary composed of OPC, the dominant cement currently in use.

The high ettringite content from these cements have seen their use in previous studies assessing their viability for use as a thermochemical energy storage medium. Studies related to ettringite have looked at the lower temperature where ettringite forms metaettringite and found that this occurs around 60ºC [13]. Ettringite has been found to be stable to up to between 100ºC and 125ºC where decomposition has been found to occur [13–15, 57–59, 67]. Previous work has primarily focused on synthetic and systems C$A cement created ettringite [14, 15, 26, 116, 122]. The application of the CAC-C$ high ettringite cement system has been studied for the use in an isolated reactor setup [15, 105]. The ettringite-metaettringite reaction has been shown to be stable for multiple cycles and energy has been found to be able to be released on a second rehydration [14].

The application of these cement systems is still needed to be understood to ensure the proper use. For use as an energy storage medium, a question is, can these systems be incorporated into the structure or architectural elements of a building or do they systems need to be self-contained reactors? In a structural or architectural system, the systems would need to be able to maintain strength and integrity over multiple cycles or else

specialized systems would be needed. They energy able to be recovered from the system is also of importance as a stable system which energy is not able to be recovered from would be unsuitable. This reaction also needs to be able to release energy on subsequent rehydration cycles. Thus, the stability of the macro-structure throughout the dehydration and rehydration cycle and the energy of the system is needed to be understood to ensure proper use of the ettringite cements. For optimal use, the relationship between the stability and energy is needed.

The results on the stability of ettringite based cement systems are presented. The three cement systems of C$A, CAC-C$, and OPC-CAC-C$ were all studied as they have been shown to produce high amounts of ettringite in the hardened paste [14, 15, 52]. The study of different systems is important as while ettringite is the primary hydrated of interest, the pastes systems are not homogeneous. This factor may impact the performance of the systems. The dehydration and decomposition of the ettringite has shown to be temperature dependent and alter the state of the ettringite [13–15, 57–59, 67]. Thus, different temperatures were used in this work to dehydrate the systems. Microstructural analysis of the pastes when cured, dehydrated, and rehydrated are presented to understand the impact of the different dehydration temperatures and cement types. For use as a structural or architectural element, the systems will be required to remain stable. Therefor the time to failure of the system when cycled and the compressive strength when different dehydration temperatures are used are important parameters studied in this work. Presented are the results for the macrostability of the three cement systems measured by the time to failure when subjected to dehydration and rehydration cycles of the paste. The compressive results for each paste in the three states of initial before testing, dehydrated, and rehydrated

are also included. The time that the systems can remain in the dehydrated state storing energy is important as a quick discharge will not allow for long term storage of energy. As the systems are discharged from the presence of water, the storage RH is of concern. The work presents the percent mass change of charged C$A specimens when stored at different RH below 45% for an extended period of time.

4.3 Materials and Experimental Methods

4.3.1 Cement Types

Three different cement types were examined in this study. A commercially available C$A cement (referred to herein as C$A), a sourced binary blend of CAC and C$ (referred to herein as CAC-C$), and a sourced ternary blend of OPC, CA and C$ cements (referred to herein as OPC-CAC-C$). The CAC-C$ system comprised of a 2.2 to 1 parts ratio of a standard grade CAC and C$. The OPC-CAC-C$ system comprised of the 2.2 to 1 parts ratio CAC and C$ blended at 30% of the cementitious material with a Type I portland cement the other 70% of the blend (per ASTM C150 [106]). An oxide analyses for the three cement systems are presented in Table 4.1.

Table 4.1 Oxide Analysis of Cements

Oxide (wt %)	Na_2O	MgO	Al_2O_3	SiO_2	P_2O_5	SO_3	Cl	K_2O	CaO	TiO_2	Cr_2O_3	MnO	Fe_2O_3	CuO	ZnO	SrO	ZrO_2	LOI**
C$A	0.17	1.57	14.19	14.51	0.11	15.63	0.11	0.57	50.23	0.60	*	*	0.69	0.03	0.03	0.14	*	1.45
CAC-C$	*	0.24	20.97	2.89	0.05	23.63	*	0.12	44.79	1.21	0.04	*	3.15	*	*	0.10	0.06	2.77
OPC-CAC-C$	0.18	2.89	10.01	16.58	0.18	7.65	*	1.00	57.10	0.56	0.05	0.11	2.01	*	0.05	0.23	*	1.41

Notes: *not detected, **accounts for loss due to C, CO_2, H_2O, OH, organic compounds and/or other

4.3.2 Mixture Design

Cement paste mixtures were used for all experimental work in this study. The three cement paste systems were used for this work were as follows, (1) a C$A cement cast with 0.65 w/cm, (2) a binary blend of CAC-C$ cast with 0.65 w/cm, and (3) a ternary blend of OPC-CAC-C$ cast with 0.40 w/cm. A higher w/cm was used for the C$A and CAC-C$ systems to ensure that there was sufficient water in the system to fully hydrate the cement powder. A 0.65 w/cm ratio was chosen as under stoichiometric conditions this is the ratio for the highest possible hydration and avoid segregation of the cement pastes [14]. A 0.4 w/cm ratio was chosen for the OPC-CAC-C$ system as this ratio is commonly used for OPC control mixtures and this blend is primarily OPC.

4.3.3 Mixing and Casting Procedure

The cement past mixtures were mixed according to ASTM C 305 section 5 in a five liter countertop mixer [76]. Specimens used for testing in this study were cast in 50 mm x 50 mm x 50 mm cube molds according to a modified version of ASTM C109 [77]. Due to the fast setting nature of the cement pastes, placement into the molds was done in one lift instead of the prescribed two. After finishing, the fresh cubes were covered with wet burlap and sealed with plastic and let to cure at ambient laboratory temperature (23 ± 4ºC) for 24 hours before being demolded.

4.3.4 Sample Curing and Conditioning

Samples underwent several different curing regimes as a part of this work in order to study different aspects of the stability of the system through hysteretic dehydration and rehydration of ettringite and metaettringite. For all specimens, once they were demolded they were placed into a moist curing room at >95% relative humidity (RH) and 23 +/- 4ºC

until 28 days from casting had elapsed. After this initial curing period, further conditioning and testing was completed as described in the following sections.

The ettringite-metaettringite conversion process requires the dehydration of ettringite to form metaettringite [58]. Using heat to dehydrate the ettringite is the charging phase of thermochemical energy storage using the ettringite based systems. When the metaettringite crystals are rehydrated, they will release heat, or discharge the stored energy [14]. The work presented studies the impact of this conversion process on the stability of the system, therefore a dehydration cycling process was developed to examine this. After initial curing (through 28 days after casting), the specimens were dehydrated using different dehydration temperatures to understand the impact of dehydration temperature on system stability. Following dehydration, some specimens were then rehydrated and dehydrated again to study how many cycles samples could undergo this process before failing. The dehydration and rehydration processes are described in the following section.

The casting and curing of specimens for use in energy output is previously described previously in this dissertation in Chapter 3 Section 3.3.4. The procedure for isothermal calorimetry for determining energy output is described previously in this dissertation in Chapter 3 Section 3.3.6.

4.3.5 Dehydration and Rehydration Cycling of Specimens

The cycling through dehydration and rehydration was not started until 28 days from casting had elapsed. At 28 days, the specimens were removed from the moist curing environment and subjected to dehydration and rehydration cycling to simulate the ettringite-metaettringite conversion process that would be necessary to use these systems for

thermochemical energy storage. For each cement system and temperature combination, three cube specimens were subjected to the conversion cycling process, though two cubes were used for three dehydration temperatures of the OPC-CAC-C$ pastes (75°C, 105°C, and 120°C). Mass measurements were done in 24-hour increments and averaged across the specimens. The following procedure was followed for the dehydration/rehydration cycling:

1. After removal from the moist curing chamber, the specimens were placed in an oven at 40°C for two hours to remove the zeolitic water.

2. The mass of the specimen was measured and recorded as the initial mass.

3. Specimens were then placed in glass dishes of known masses to capture any material that may fall off of the specimen during the cycling process.

4. Specimens were placed into ovens at one of five difference temperatures, either 60°C, 75°C, 90°C, 105°C, or 120°C for three days to dehydrate the specimens, removing the bound water from the ettringite crystal. During dehydration, each day the mass of the specimens was measured.

5. The specimens were then allowed to cool to ambient temperature to prevent thermal shock when rehydrated.

6. Specimens were placed into 475ml specimen containers and submerged in water. Due to the rapid absorption of water of some of the specimens, the level of water was continually checked to ensure that the samples stayed completely submerge. More water was added as needed. After five minutes, lids were placed on the cups to prevent evaporation of the water. Specimens were maintained in the water rehydrated for three days at 23 +/- 4°C.

7. After rehydration, the samples were removed from the water, dried, and the mass was recorded before beginning the process again. The cycling process was halted when a specimen reached failure, as described in the following section.

Initial heating of the specimens at 40°C for two hours before testing of hydrated specimens was done to ensure the free and zeolitic water was removed from all samples. This did not impact the rate of dehydration between samples [14]. This was necessary to ensure that measurements were of only the water rebound during rehydration. Five different dehydration temperatures were selected to be used in this study: 60°C, 75°C,

90ºC, 105ºC, or 120ºC. The lower bound of this range was selected from literature, which indicated that dehydration and reversibility of the ettringite-metaettringite reaction could occur at temperatures as low as 60ºC [92]. The upper bound of 120ºC was also selected as from literature temperatures between 110 to 120ºC have been found to decompose the ettringite crystal beyond the metaettringite phase resulting in the halting of the reversibility of the reaction [58, 119]. Previous work on the ettringite–metaettringite system for use in thermochemical energy storage has been done at temperatures of 60ºC to 110ºC [14, 122, 123]. Though, previous work on stability of ettringite at elevated temperatures has found that the decomposition limit may be between 110ºC and 125ºC [58, 119, 124].This range of temperatures was chosen to show how dehydration temperature impacted system stability, and to understand if optimum temperatures for stability may differ depending on the cement system used to create a high ettringite system. Failure of the specimens was defined as the loss of 10% of the specimen volume. An example is if the specimen broke into two equal pieces this would be defined as loss of 50%.

4.3.6 Environmental Conditions for Long-term Storage Capacity Measurements

One potential benefit of thermochemical energy storage systems is that they can provide long-term energy storage as the energy is stored in the chemical bond [12]. The disadvantage is that this bond obtained when charging the systems is unstable [2]. Thus, as long as this bond remains stable, the energy can be stored. In the ettringite base cement storage system the instability in the charged bond is satisfied in the presence of water. Therefore, understanding how resistant the system is to rehydration in different environments is vital for understanding what storage conditions may be needed to maintain long-term storage capacity. To study this, 50 mm cubic specimens made of C$A cement

paste were dehydrated and then maintained in controlled environments with specific relative humidity (RH) of 0, 13, 25, 35, and 45% at ambient temperature that varied between 15.5ºC and 28.5ºC. Temperature and humidity in the buckets were monitored using Lascar EL-USB-2-LCD data loggers with accuracy of ±0.5°C and ±2.25% RH during the duration of the experiment at one hour intervals. After curing for 28 days, the specimens were placed in an oven at 40ºC for two hours to remove the zeolitic water. Initial dehydration at 60ºC for seven days was done prior to storage in the specified RH environments. A desiccator and vacuum pump were used to maintain 0% RH while saturated salt solutions were used to control the relative humidity of the other conditions. The saturated salt solutions were lithium chloride for 13% RH, potassium acetate for 25% RH, magnesium chloride for 35% RH, and potassium carbonate for 45% RH [125]. The RH values found are within the error of the datalogger of the expected RH values for each solution. The salt solution was placed into the bottom of the bucket where a perforated piece of plastic was fitted to prevent the specimens from coming into direct contact with the salt solution.

To determine the rate of rehydration of the specimens, the mass of the cubes was measured directly after removing them from the high RH curing room to determine the initial mass. The mass was measured again after the initial dehydration process. After dehydrating for seven days, the specimens were removed from the oven and the mass of the specimen in the dehydrated state was taken. Specimens were then placed into buckets and the lid was sealed with tape to prevent moisture from entering or leaving the bucket. The mass of the specimens was measured weekly for the first 15 weeks and then every 15 weeks for 24 months. Due to laboratory closures associated with the COVID-19 Pandemic,

measurements were suspended for several months, with a final measurement taken after the laboratory reopened, 42 months after starting testing.

4.3.7 Compressive Strength Measurements

Compression testing was completed on 50 mm cubic paste specimens cast with each of the three cement systems according to ASTM C109 [77]. Three replicate specimens were tested at each testing day for each system. Initial compressive strength measurements were made after the initial 28 days of curing in a high RH curing room; compressive strengths measurements were also done on samples that had been dehydrated for three days; and again, on samples that had been dehydrated for three days and then rehydrated for three days. For specimens at 28 days and rehydrated, the specimens were placed in an oven for two hours at 40^{o}C to remove the zeolitic water prior to compression testing. Due to volumetric changes in some systems during dehydration and rehydration, the compressive strength specimens failed before compression testing could be completed, and so no measurements were made.

4.3.8 Sample Preparation for XRD analysis, SEM Imaging, and EDS Analysis

Preparation of the samples for X-ray diffraction (EDX), scanning electron microscope (SEM) imaging, and scanning electron microscope – energy dispersive spectrometry (SEM-EDS) analysis required the arresting of the hydration of the sample. Due to the sensitive nature of the ettringite crystal, the widely used technique of microwave drying may induce damage to the microstructure [126]. Given the sensitive nature of the ettringite crystal to oven dehydration and that this study focuses on the dehydration and rehydration of ettringite, an alternative method of solvent exchange with isopropyl alcohol was used to arrest the hydration. This method has been used successfully to arrest the hydration for of

samples to study the microstructure of C$A and CAC systems [127]. While ethanol was used as the solvent instead of isopropyl, Lui et al. found that solvent exchange followed by vacuum drying preserved the composition and microstructure of C$A cement hydrates best [128]. The solvent exchange process followed the procedure described by Zhang and Scherer [69].

Sampling of specimens was done by cutting 3 mm thick slices, approximately 15 mm by 15 mm in size from larger cube specimen. After the solvent exchange process was completed, the slices were then removed from the isopropyl alcohol and placed into a desiccator for two days to remove the isopropyl. After the two days, the samples could then be prepared for either XRD or SEM-EDS analysis.

Samples used for XRD analysis are ground in a mortar and pestle into fine particles using isopropyl alcohol as a lubricant. The resulting slurry mixture was placed into a labeled plastic Petri dish and the Petri dish was placed into a desiccator to evaporate the isopropyl alcohol. Once the isopropyl alcohol had evaporated from the sample remained in the desiccator until testing could be performed to prevent carbonation of the powder samples.

Samples for analysis through SEM-EDS were first into epoxy resin using EpoFix from Struers. Polishing was done on two separate phases, coarse and fine following the procedure listed in Chapter 8 in *A practical Guide to Microstructural Analysis of Cementitious Materials* [110]. After the polishing process was complete, samples were placed in the vacuum desiccator for a minimum of 48 hours to remove any remaining volatiles in the sample that may damage the SEM.

4.3.9 XRD Analysis

X-ray diffraction analyses were done using a Philips EMPYREAN multi-purpose research X-ray diffractometer. Bragg-Brentano geometry with a 2-Theta of 5º to 65º with an X-ray source of 45kV and 40mA. Dry powders were used for analysis and were back loaded into the sample holder. A 27mm diameter sample holder was used unless there was not enough powder, in this case a smaller 16mm diameter sample holder was used instead. An angle step of 0.026º with a time step of 97.6 seconds was used for the experiments. HighScore Plus was used to identify the composition of the powder based on locations of the peaks by comparison with known powder diffraction file numbers in the International Centre for Diffraction Data (ICDD) Database Version 4+.

4.3.10 SEM Imaging SEM-EDS Analysis

SEM imagine and EDS analysis was done using a JEOL JSM-7900F SEM machine equipped with a retractable backscatter detector and INCA energy system energy dispersive X-ray (EDS) detector for semi-quantitative elemental analysis. A beam acceleration voltage of 15kV and a working distance of approximately 10 mm was used for examining the samples. A 30 second collection time was used per EDS collection point.

4.5 Results

4.5.1 Macrostability of Paste Cubes During Dehydration-Rehydration Cycling

Two main parameters were varied in this work to assess the macrostability of the paste cubes: (I) the cement type; and, (2) the dehydration temperature. Macrostability was determined by measuring the number of cycles a specimen could persist without failing while being cycled through the dehydration/rehydration process needed to charge and

discharge the thermochemical energy stored in the cement paste cubes. The mass of the cubes was measured, and the relative mass expressed as a percentage of the mass after the initial 28 days of hydration in the high RH humidity curing room was calculated. The initial mass was measured after dehydration at 40°C for two hours to remove the free and zeolitic water. The change is mass is caused by the loss of water during dehydration or intake of water during dehydration. The results for the average mass during dehydration and rehydration cycles for the C$A cement paste cubes are presented in Figure 4.1.

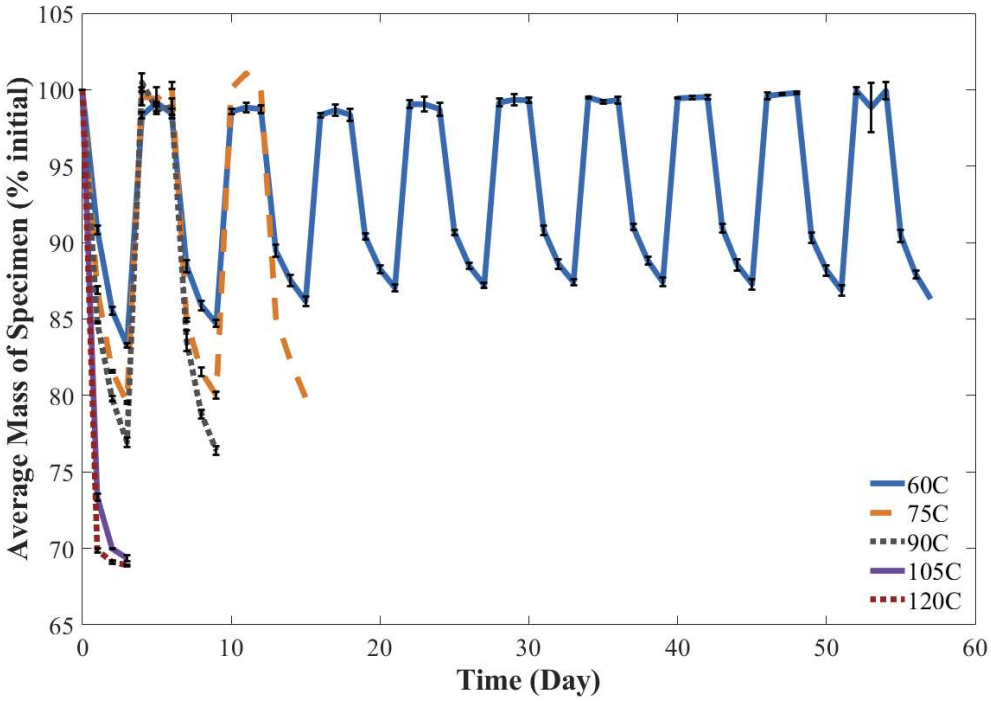

Figure 4.1 Relative mass change of C$A paste cube specimens exposed to cyclic dehydrated and rehydration.

An average mass of 100% represents the initial mass of the three specimens. This represented the baseline for a fully hydrated specimen used for energy storage. An increase in the dehydration temperature of the specimens resulted in a decrease in the length of time until macrostructure failure. At the lowest tested dehydration temperature of 60°C, the

specimens were able to be cycled nine times before failure during rehydration during the 10th cycle. With an increase of dehydration temperature to 75ºC, the stability was reduced to one and a half cycles for all three specimens. At a dehydration temperature of 90ºC, the specimens were able to maintain their stability through one and a half cycles, failing upon rehydration during the second cycle. For both dehydration temperatures of 105 and 120ºC, the specimens were able to maintain their stability for the dehydration part of the first cycle but failed when placed in water for rehydration.

Higher dehydration temperatures resulted in more mass loss during the dehydration cycling. At all tested dehydration temperatures, the greatest change in mass occurred by 24 hours after starting the dehydration process. For dehydration temperatures of 105ºC and 120ºC, a decrease in the average mass to less than 70% of the initial was observed. At 105ºC, this was reached by 48 hours after starting dehydration and by 24 hours for dehydration at 120ºC. After three days of dehydration, average masses of 83.28%, 79.55%, and 76.94% were observed for dehydration temperatures of 60ºC, 75ºC, and 90ºC, respectfully. For dehydration at 60ºC, as the number of cycles increased, the average mass after dehydration increased from 83.28% during cycle one to 87.03% by cycle four. For the remaining cycles, the average mass on dehydration remained between 86% and 88%. When rehydrated, the specimens regained their initial mass within 24 hours of the addition of water.

The number of C$A specimens measured each day during the cycles where failures occurred are presented in Table 4.2 where the shaded values represent a rehydration measurement. In the table it can be seen that dehydration at 60ºC resulted one specimen failure during rehydration in cycle nine, one during dehydration in cycle ten, and the last

during rehydration in cycle ten. Dehydration at 75ºC resulted in failure of two specimens during cycle two rehydration and the third during rehydration in cycle three. Dehydration at 90ºC resulted in failure of all three specimens during rehydration in cycle two. Dehydration at 105ºC and 120ºC resulted in the failure of all the specimens during rehydration during cycle one.

Table 4.2 Number of C$A Specimens Measured Each Day During Cycling Where Shaded Cells are Days Measuring Rehydration

Dehydration Temperature (°C)	Cycle 1						Cycle 2						Cycle 3						Cycle 9						Cycle 10					
60	3	3	3	3	3	3	3	3	3	3	3	3	3	3	3	3	3	3	3	3	3	3	2	2	2	2	1	0	0	0
75	3	3	3	3	3	3	3	3	3	1	1	1	1	1	1	0	0	0												
90	3	3	3	3	3	3	3	3	3	0	0	0																		
105	3	3	3	0	0	0																								
120	3	3	3	0	0	0																								

Presented in Figure 4.2 are the initial (A) and failed (B) states of a C$A specimen that underwent dehydration/rehydration cycling at a dehydration temperature of 60ºC. During progressive cycling, cracking developed within the specimen; though initially, the cracking was not significant enough to cause failure. Also observed was the failure of parts of the top surfaces of the specimen though this did not meet the failure criteria. Below the failed surface material, a larger network of cracks was observed. At failure, it can be seen that the specimen broke into multiple sections with each section heavily cracked. Presented in Figure 4.3 is the initial (A) and failure (B) states of the C$A specimen that underwent dehydration/rehydration cycling at a dehydration temperature of 120ºC. From both C$A failure image,s it is seen that at the higher dehydration temperature smaller sections are formed during failure compared to 60ºC, this trend was consistent for samples ranging from 60ºC to 120ºC dehydration temperatures.

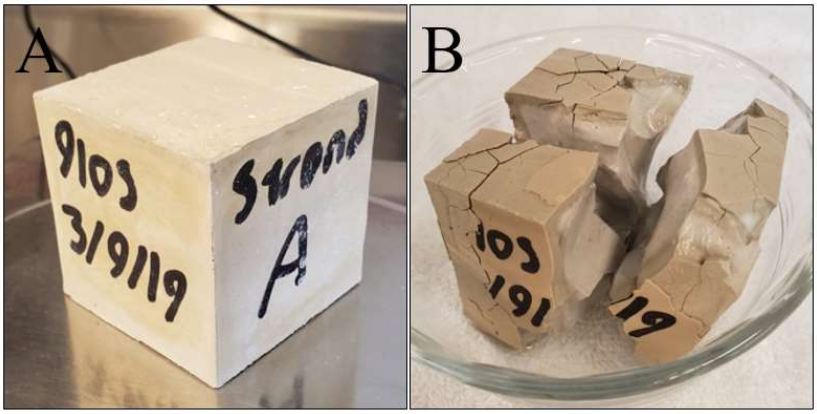

Figure 4.2 Condition of C$A specimen subjected to 60ºC dehydration-water rehydration cycle, (A) initial (B) failed.

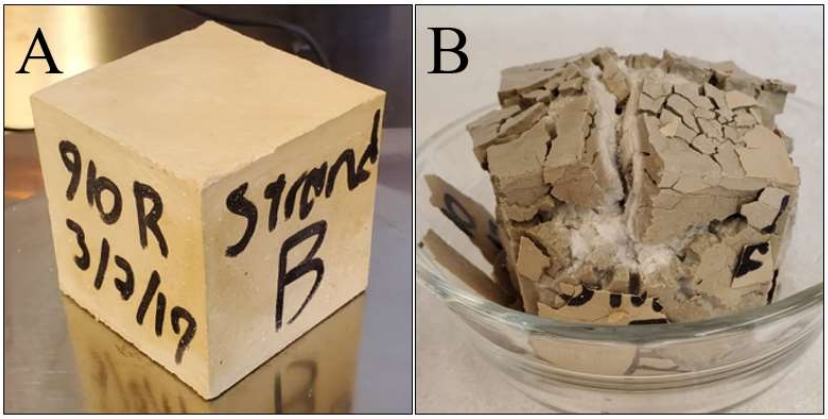

Figure 4.3 Condition of C$A specimen subjected to 120ºC dehydration-water rehydration cycle, (A) initial (B) failed.

In Figure 4.4 the average mass results during the dehydration and rehydration cycles for the CAC-C$ cement cubes is shown.

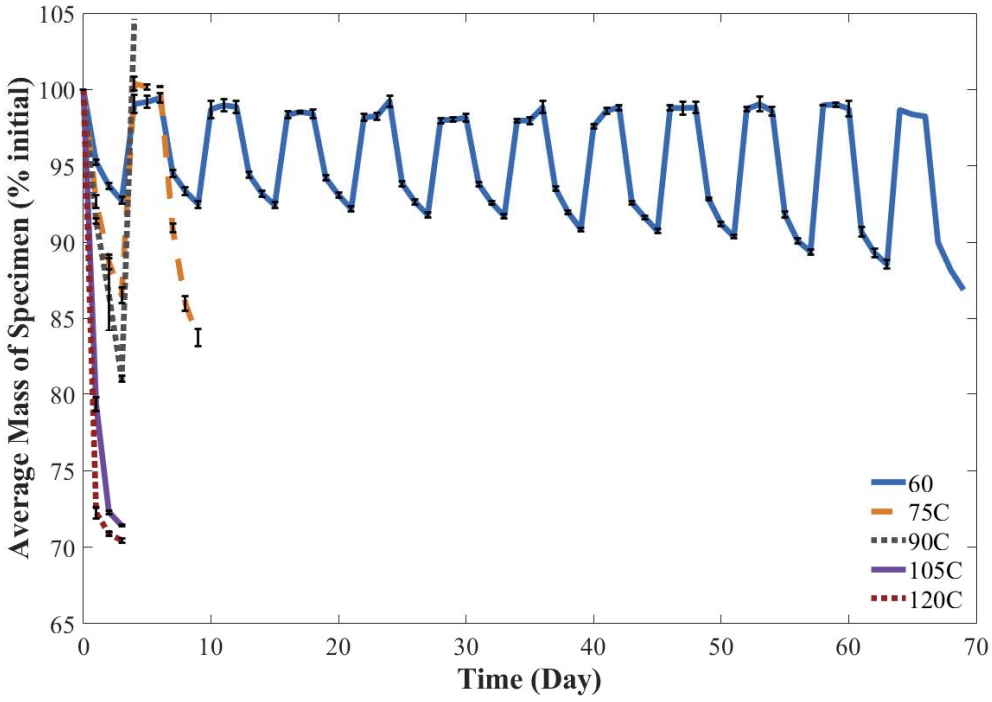

Figure 4.4 Stability of CAC-C$ cube specimens exposed to cyclic dehydrated and rehydration measuring water through mass of the specimens.

All CAC-C$ specimens dehydrated at 60ºC lasted for ten full cycles before failure. Two of the specimens failed upon rehydration during cycle 11 with the third failing during rehydration in cycle 12. At dehydration temperature of 75ºC, the amount of cycles before failure reduced with failure occurring during rehydration in cycle two. At 90ºC, 105ºC and 120ºC, all cubes failed during the first cycle of rehydration; one of the cubes dehydrated at 90ºC was able to survive until the second day of rehydration while the rest failed during the first 24 hours of rehydration.

The average mass of specimens dehydrated at temperatures of 105ºC and 120ºC reached similar values at 71.41% and 70.45%, respectfully, of the initial mass after three days of dehydration. There was minimal change in mass between the second and third days for both temperatures. At a dehydration temperature of 90ºC, the average mass of the

specimens reduced to 81.01% the initial mass after three days, only two-thirds of the change seen at two days for the highest two temperatures. Dehydration at 75ºC resulted in an average mass of 86.53% of the initial mass after the first cycle; and the mass loss during dehydration increased during the second cycle to 83.71% of the initial mass. The lowest mass loss at three days of dehydration was found in the specimens dehydrated at 60ºC. During the first dehydration cycle, an average mass of 92.73% compared to the initial condition was found. The mass loss was found to increase through progressive cycles reaching 86.88% during the last dehydration cycle. This is a similar mass value to that found during the first cycle at 75ºC.

The number of CAC-C$ specimens measured each day during the cycles where failures occurred are presented in Table 4.3 where the shaded values represent a rehydration measurement. In the table it can be seen that dehydration at 60ºC resulted one specimen failure during rehydration in cycle nine, one during rehydration in cycle ten, and the third during rehydration in cycle 11. Dehydration at 75ºC resulted in failure of all the specimens during cycle two. Dehydration at 90ºC resulted in failure of all three specimens during rehydration in cycle two, two on the first day with the third the second day. Dehydration at 105ºC and 120ºC resulted in the failure of all the specimens during rehydration during cycle one.

Table 4.3 Number of CAC-C$ Specimens Measured Each Day During Cycling Where Shaded Cells are Days Measuring Rehydration

Dehydration Temperature (°C)	Cycle 1						Cycle 2						Cycle 9						Cycle 10						Cycle 11					
60	3	3	3	3	3	3	3	3	3	3	3	3	3	3	3	3	2	2	2	2	2	1	1	1	1	1	1	0	0	0
75	2	2	2	2	2	2	2	2	2	0	0	0																		
90	3	3	3	1	0	0																								
105	2	2	2	0	0	0																								
120	2	2	2	0	0	0																								

Note: For dehydraion at 75°C, 105°C, and 120°C started with only two specimens

The initial and failure states of a CAC-C$ specimen subjected to dehydration at 120ºC are shown in Figure 4.5, initial is shown in (A) and failure in (B). Specimens lasting more than one cycle developed cracking on the surface and thin sections flaked off the surface during progressive cycles. The failure state of each specimen was observed to be similar. Multiple small sections comprised the failed specimen with the cracks within the interior observed to have progressed outwards from the center of specimen. The resulting sections were easily broken into smaller pieces.

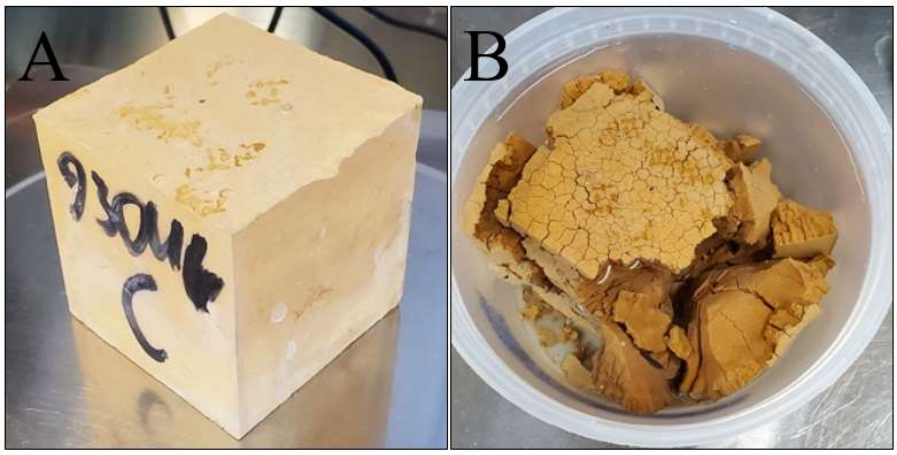

Figure 4.5 Condition of CAC-C$ specimen subjected to 120ºC dehydration-water rehydration cycle, (A) initial (B) failed.

In Figure 4.6, the average mass results during the dehydration and rehydration cycles for the OPC-CAC-C$ system are shown.

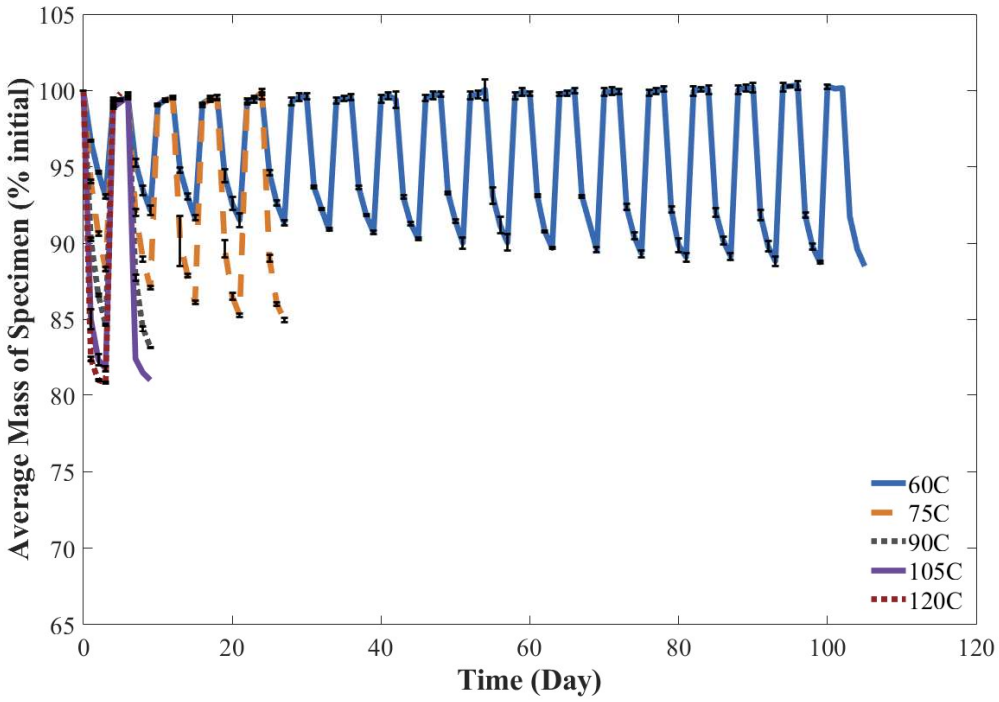

Figure 4.6 Stability of OPC-CAC-C$ cube specimens exposed to cyclic dehydrated and rehydration measuring water through mass of the specimens.

The OPC-CAC-C$ paste dehydrated for three days at 120ºC resulted in failure of the specimen upon rehydration. At a dehydration temperature of 90ºC and 105ºC, the ternary system maintained stability through the first cycle with failure of all specimens on rehydration during the second cycle. At a dehydration temperature of 75ºC, there was an increase in the amount of cycles to four full cycles where failure occurred during rehydration during cycle five. The ternary blend dehydrated at 60ºC resulted in the most amount of cycles before failure; 17 full dehydration/rehydration cycles of the specimens were completed before failure on rehydration during the 18th cycle.

The lowest measured average mass was found in the specimens dehydrated at 105ºC and 120ºC. The average mass of the two dehydration temperatures was found to be 81.71% and 80.82%, respectfully, after three days of dehydration. When dehydrated at

90ºC, the specimens were found to have an average mass percentage of 84.66% of the initial mass after three days, during the first cycle, and decreased during cycle two to 83.11% of the initial mass. For dehydration at 75ºC, the average mass percentage was 88.32% though decreased in subsequent cycles to 84.99% in cycle five. The highest average mass percentage after three days of dehydration was found for the specimens dehydrated at 60ºC. The average mass percentage for the specimens in cycle one was found to be 93.06%. Similar to the specimens dehydrated at 75ºC, the average mass in the specimens dehydrated at 60ºC decreased in each subsequent cycle and reached 88.50% of the initial mass during the cycle of failure.

The number of OPC-CAC-C$ specimens measured each day during the cycles where failures occurred are presented in Table 4.4 where the shaded values represent a rehydration measurement. In the table, it can be seen that dehydration at 60ºC resulted one specimen failure during rehydration in cycle 16, one during rehydration in cycle 17, and the third during rehydration in cycle 18. Dehydration at 75ºC resulted in failure of all the specimens during cycle five. Dehydration at 90ºC resulted in failure of all three specimens during rehydration in cycle two. Dehydration at 105ºC resulted in failure of two specimens during rehydration in cycle one and the third during rehydration cycle two. Dehydration at 120ºC resulted in the failure of all the specimens during rehydration during cycle one, two on the second day with the third on the third day.

Table 4.4 Number of OPC-CAC-C$ Specimens Measured Each Day During Cycling Where Shaded Cells are Days Measuring Rehydration

Dehydration Temperature (ºC)	Cycle 1						Cycle 2						Cycle 5						Cycle 16						Cycle 17						Cycle 18					
60	3	3	3	3	3	3	3	3	3	3	3	3	3	3	3	3	3	3	3	3	3	3	2	2	2	2	2	1	1	1	1	0	0	0
75	3	3	3	3	3	3	3	3	3	3	3	3	3	3	3	0	0	0																		
90	3	3	3	3	3	3	3	3	3	0	0	0																								
105	3	3	3	3	1	1	1	1	1	0	0	0																								
120	3	3	3	3	1	0																														

Presented in Figure 4.7 are the initial (A) and failure (B) states of the OPC-CAC-C$ specimen dehydrated at 60ºC. Similar failures were observed for specimens dehydrated at the other temperatures. For the specimens that lasted more than one cycle, cracks developed on all sides of the specimen. This cracking did not initially result in the failure of the specimen. Though when failure did occur during rehydration, the specimen separated into pieces defined by the larger of the cracks.

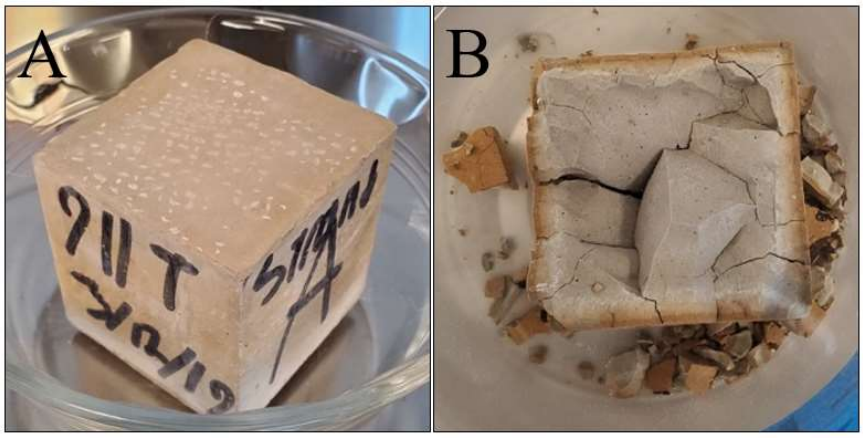

Figure 4.7 Condition of OPC-CAC-C$ specimen subjected to 120ºC dehydration-water rehydration cycle, (A) initial (B) failed.

From the data shown previous in Figure 4.1, Figure 4.4, and Figure 4.6 the results for average mass show that at all dehydration temperatures, the C$A paste system resulted in the lowest average mass percentage values of the three tested pastes. At dehydration of 60ºC, the CAC-C$ was found to have the highest average mass percentage. The average mass percentage of the OPC-CAC-C$ specimens was found to be similar to CAC-C$ when dehydrated at 60ºC This data is only applicable at three days' dehydration as at this point there is still noticeable mass loss between days two and three. At dehydration of 75ºC and above for three days, the OPC-CAC-C$ had the highest average mass percentage of the

three pastes with. The average mass of the CAC-C$ specimens was found to be similar to OPC-CAC-C$ when dehydrated at 75ºC and 90ºC and the C$A for dehydration temperatures of 105ºC and 120ºC. At 120ºC, the average mass values show minimal change after the first day of dehydration for the C$A and OPC-CAC-C$ systems.

A comparison of the macrostability of all three systems subjected to different dehydration temperatures is presented in Figure 4.8.

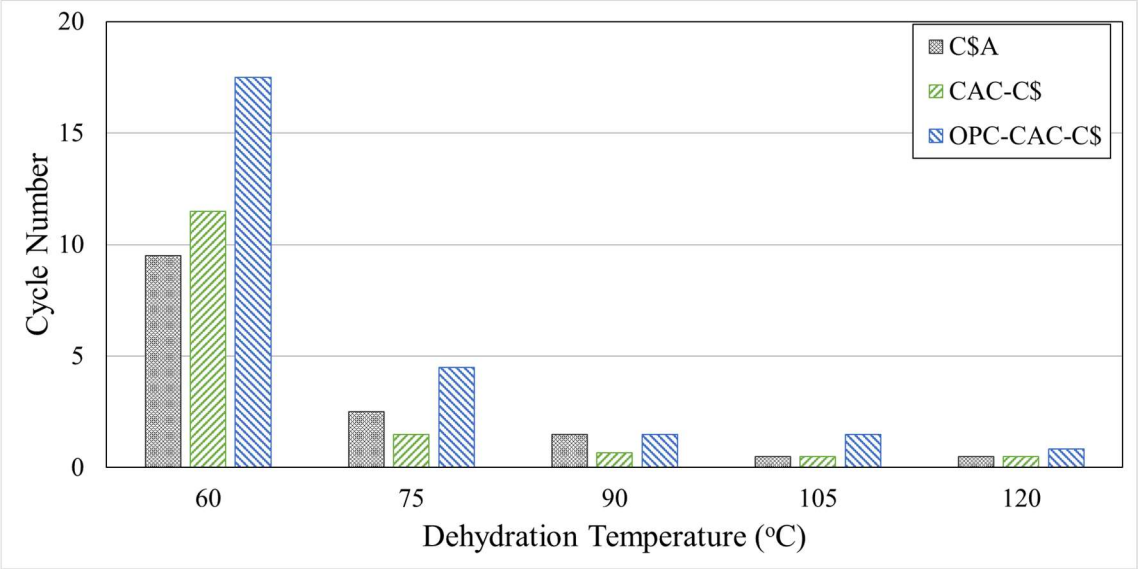

Figure 4.8 Stability comparison based on number of cycles until failure of the three cement paste systems for each of the five dehydration temperatures.

The specimens dehydrated at 60ºC failed during the rehydration portion of the cycle. The failure cycle counts for each cement for 60ºC dehydration were 9.5 cycles for C$A, 11.5 cycles for CAC-C$, and 17.5 cycles for OPC-CAC-C$. The specimens dehydrated at 75ºC failed during the rehydration portion of the cycle. The failure cycle counts for each cement for 75ºC dehydration were 2.5 cycles for C$A, 1.5 cycles for CAC-C$, and 4.5 cycles for OPC-CAC-C$. The specimens dehydrated at 90ºC failed during the rehydration portion of the cycle. The CAC-C$ specimens were not able to be

rehydrated without failure. The failure cycle counts for each cement for 90ºC dehydration were 1.5 cycles for C$A, 0.67 cycles for CAC-C$, and 1.5 cycles for OPC-CAC-C$. The specimens dehydrated at 105ºC failed during the rehydration portion of the cycle. The C$A and CAC-C$ specimens were not able to be rehydrated without failure. The failure cycle counts for each cement for 105ºC dehydration were 0.5 cycles for C$A, 0.5 cycles for CAC-C$, and 1.5 cycles for OPC-CAC-C$. The specimens dehydrated at 120ºC failed during the rehydration portion of the cycle. All specimens were not able to be rehydrated and last to the next dehydration without failure. The failure cycle counts for each cement for 120ºC dehydration were 0.5 cycles for C$A, 0.5 cycles for CAC-C$, and 0.83 cycles for OPC-CAC-C$.

4.5.2 Long-term Rehydration in Different Relative Humidity Conditions

In order for the cement system to retain the stored energy as efficiently as possible over long time periods (months to years), the system must maintain a dehydrated state. To study the impact of the RH of the specimen storage conditions on rehydration, dehydrated specimens were stored at varying RH and the change in mass over time was measured to determine ideal storage conditions. The calculated mass percentage gained back based on the change in mass was determined for each of the five different humidity percentages studied and are presented in Figure 4.9 Negative values represent an increase in the storage capacity of the specimens due to further dehydration. A value of 100% would represent the specimen had regained the initial found mass while 50% would represent a gain of half of the lost mass back. The humidity was controlled within a sealed bucket though the buckets were subjected to ambient temperature of the room in which they were stored. The minimum and maximum observed temperatures were 15.5 and 28.5ºC, respectfully.

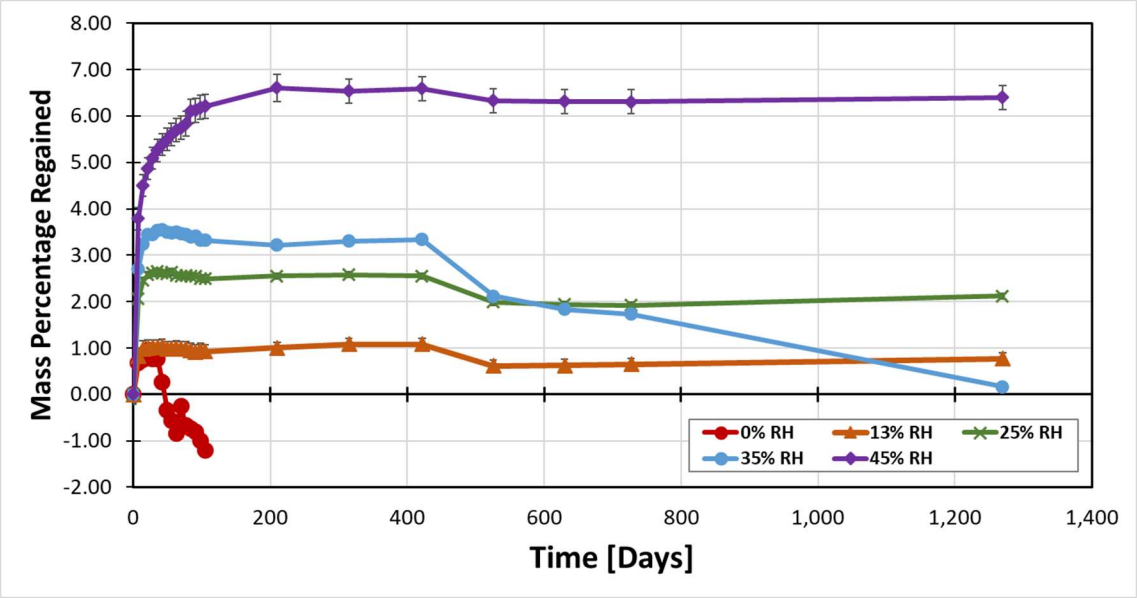

Figure 4.9 Percentage of mass lost gained back due to storage at relative humidity percentages below 45%.

For the tested relative humidity conditions, the greatest gain in mass for all RH storage conditions occurred in the early weeks after storage. The largest observed change in mass occurred in the first week with the rate of mass change in subsequent weeks reducing. The decrease in mass gain between 400 and 500 days was likely due to a recalibration of the scale used to measure the specimens. The specimens stored at 35% relative humidity continued to have decreased mass gain after this period, though. Mass gain was observed, in general, to be higher at higher relative humidity storage conditions; with a maximum mass gain of 6.5% observed for the specimens stored in the 45% RH condition. The specimens stored in a vacuum chamber to provide 0% relative humidity had a decrease in mass gain after storage for five weeks, due to mechanical problems with the vacuum pump system, testing on these specimens had to be halted after five weeks. For the 60 week measurements, the specimens stored at 45% RH were found to have the largest gain in mass at 6.59% back. For the other RH% of 13%, 25%, and 35%, the stored

specimens were found to have gained 1.09%, 2.55%, and 3.31% mass back. At the end of testing, the mass percentage gained back was observed to be 0.77% for 13%RH, 2.21% for 25% RH, 0.16% for 35% RH and 6.40% for 45% RH.

4.5.3 Compressive Strength

The compressive strength properties of the three cement paste systems were measured at three different times in the dehydration-rehydration cycle; initial, dehydrated, and rehydrated. The average compressive strengths for the three cements in the different states are presented in Figure 4.10.

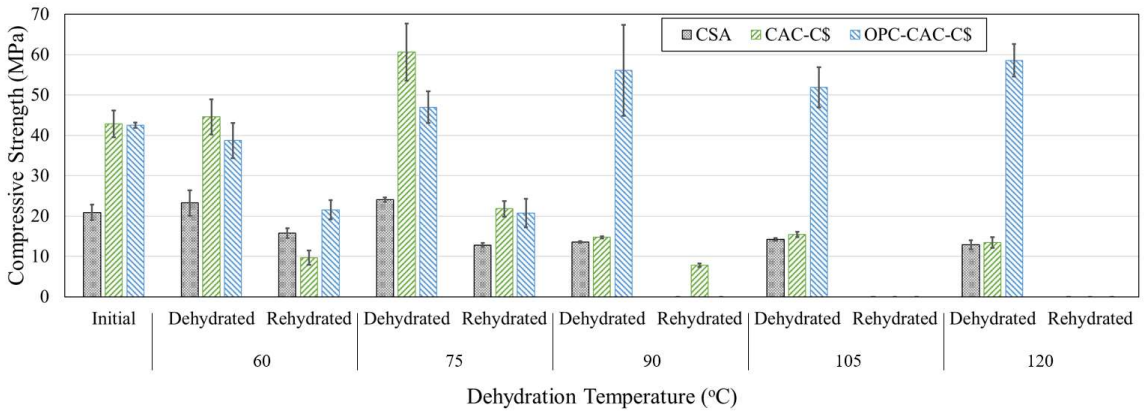

Figure 4.10 Compressive strength in MPa for the initial condition and dehydrated and rehydrated conditions when dehydrated at 60°C, 75°C, 90°C, 105°C, or 120°C.

In the initial state, the C$A cement system had a compressive strength of 20.9 MPa, the lowest initial compressive strength of the three systems. The compressive strength of the CAC-C$ in the initial condition was found to be 42.9 MPa and the OPC-CAC-C$ in the initial condition was found to be 42.5 MPa. The compressive strength of the C$A in the dehydrated state was found to increase from the initial condition to 23.2 MPa when dehydrated at 60°C and 24.0 MPa when dehydrated at 75°C. A loss in the dehydrated C$A

strength was observed in the dehydrated state at the higher dehydration temperature. For the CAC-C$, a compressive strength of 44.5 MPA was observed in the dehydrated condition at 60ºC, an increase to 60.6 MPa was observed when dehydrated at 75ºC. The compressive strengths of the CAC-C$ specimens in the dehydrated state when dehydrated at 90ºC, 105ºC, and 120ºC were found to be less than initial compressive strength for CAC-C$. For the OPC-CAC-C$ system, the compressive strength was reduced at 60ºC compared to the initial condition, and increased for each of the other tested dehydration temperatures. Failure of the specimens during rehydration resulted in compressive strengths in the rehydrated condition only being able to be determined for specimens first dehydrated at 60ºC, 75ºC, and 90ºC for the CAC-C$ system, and only specimens first dehydrated at 60ºC and 75ºC for the C$A and OPC-CAC-C$ systems. The compressive strengths for the rehydrated systems were found the be less than that of the initial condition for all systems, regardless of the temperature at which they were dehydrated. The C$A rehydrated specimens resulted in compressive strengths 24.9%% less than the initial condition when first dehydrated at 60ºC and 38.8% when first dehydrated at 75ºC. For the CAC-C$ systems, the compressive strength in the rehydrated systems from the initial condition was found to be reduced by 77.4% when dehydrate at 60ºC, 29.2% when dehydrated at 75ºC, and 81.8% when dehydrated at 90ºC. The rehydrated compressive strength of the OPC-CAC-C$ in the rehydrated systems was found to be reduced by 42.4% when dehydrated at 60ºC and 51.1% when dehydrated at 75ºC.

Table 4.5 presents the average loading area of the specimens used for compression testing. A change in the area represents instability in the specimen due to the change volume. In the C$A specimens at dehydration temperatures of 90ºC and above, there was

a decrease in the measured loading area of the specimens. A similar decrease was also observed in the CAC-C$ specimens at the same dehydration temperatures. In the rehydrated conditions, an increase in loading area was observed in the CAC-C$ specimens when compared to both the dehydrated and initial conditions of the specimens. Minimal change in area was observed in OPC-CAC-C$ specimens.

Table 4.5 Area of Compressive Strength Specimens

Dehydration Temperature (^{o}C)	None	60		75		90		105		120	
Specimen State/ Compressive Area Units	Initial (in^2)	Dehydrated (in^2)	Rehydrated (in^2)	Dehydrated (in^2)	Rehydrated (in^2)	Dehydrated (in^2)	Rehydrated (in^2)	Dehydrated (in^2)	Rehydrated (in^2)	Dehydrated (in^2)	Rehydrated (in^2)
CSA	3.98	4.02	4.00	3.98	4.03	3.85	-	3.83	-	3.81	-
CAC-C$	4.05	4.04	4.24	4.03	4.08	3.89	4.29	3.90	-	3.87	-
OPC-CAC-C$	4.06	4.04	4.10	4.05	4.09	4.02	-	4.03	-	3.99	-

4.5.4 Microstructural Analysis

4.5.4.1 XRD Analysis. Sample analysis using XRD to determine the crystalline structures present was conducted on each paste system at various points within the dehydration/rehydration cycle. An initial sample was taken before any specimens were subjected to dehydration. One sample was taken from a dehydrated specimen from each of the dehydration temperature conditions; and one sample was taken from a rehydrated specimen from each of the dehydration temperature conditions.

Presented in Figure 4.11 are the XRD scans of the C$A paste, (A) after three days of dehydration at each dehydration temperature and (B) after dehydration for three days and rehydration for three days, the scan for the initial state is included for reference.

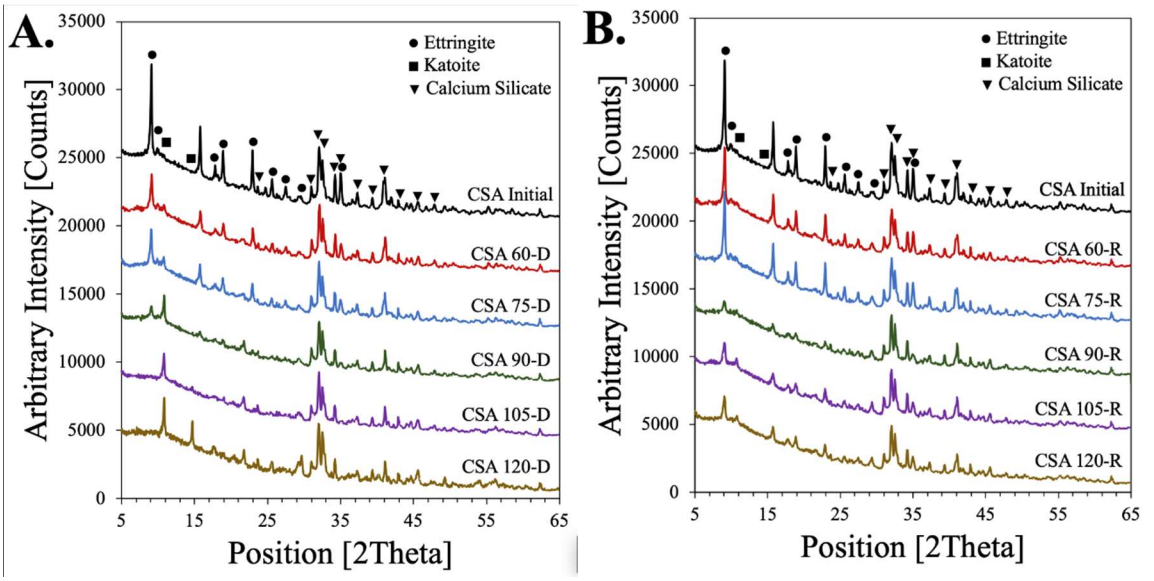

Figure 4.11 XRD scans of C$A paste (A) after dehydration in oven for three days and (B) after dehydration for three days and rehydration for three days, initial scan is included on both graphs.

In Figure 4.11 (A), it is seen that at ettringite is observed in the scans of dehydrated C$A paste for dehydration temperatures of 60ºC, 75ºC, and 90ºC. Ettringite was not observed in the scans of dehydrated C$A paste for dehydration temperatures of 105ºC and 120ºC. Katoite and calcium silicate are observed at the initial and all dehydrated states. In Figure 4.11 (B), it can be seen that ettringite was observed in the scans of rehydrated C$A paste for all dehydration temperatures. Calcium silicate was observed in all the tested rehydrated states.

Presented in Figure 4.12 are the XRD scans of the CAC-C$ paste, (A) after three days of dehydration at each dehydration temperature and (B) after dehydration for three days and rehydration for three days, the scan for the initial state is included for reference.

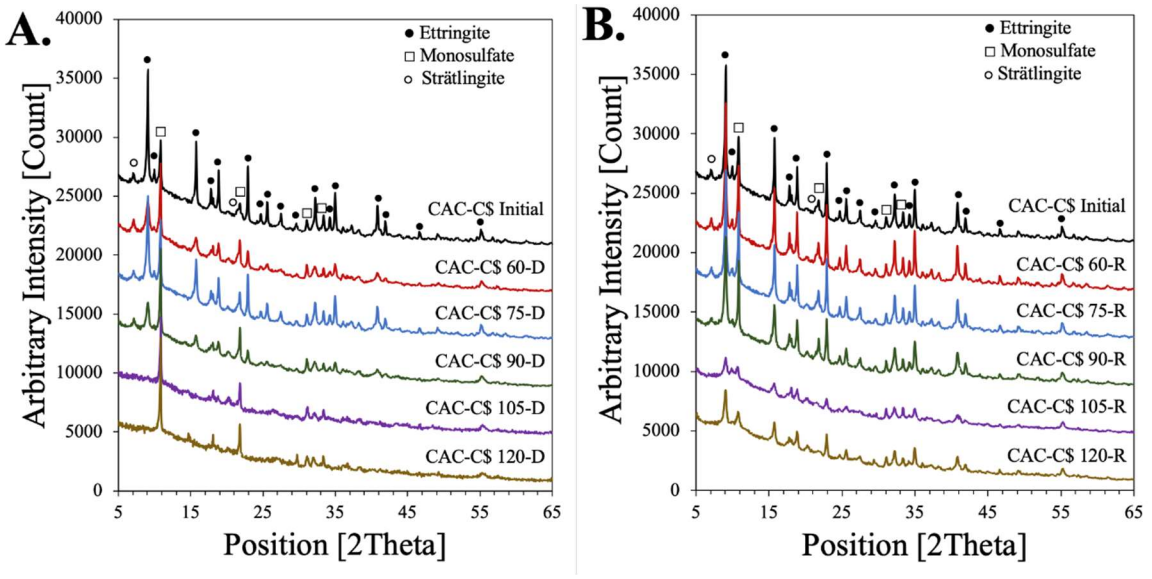

Figure 4.12 XRD scans of CAC-C$ paste (A) after dehydration in oven for three days and (B) after dehydration for three days and rehydration for three days, initial scan is included on both graphs.

In Figure 4.12 (A), it is seen that at ettringite is observed in the scans of dehydrated CAC-C$ paste for dehydration temperatures of 60ºC, 75ºC, and 90ºC. At dehydration temperatures of 105ºC and 120ºC, there is no observable peak for ettringite in the XRD data. Strätlingite was observed in the initial and dehydrated conditions for 60ºC, 75ºC, and 90ºC. Monosulfoaluminate was observed in the initial and all dehydrated scans. In Figure 4.12 (B), it can be seen that ettringite was observed in all the scans in the rehydrated state. Strätlingite was observed in the initial and rehydrated conditions for pastes dehydrated at 60ºC, 75ºC, and 90ºC.

Presented in Figure 4.13 are the XRD scans of the OPC-CAC-C$ paste (A) after three days of dehydration at each dehydration temperature and (B) after dehydration for three days and rehydration for three days, the scan for the initial state is included for reference.

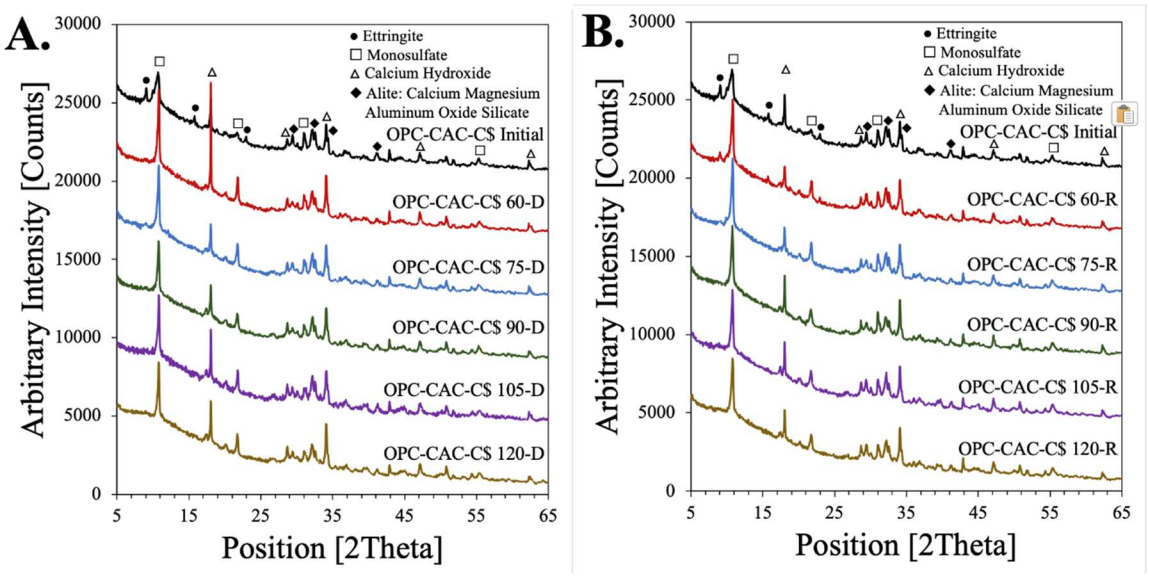

Figure 4.13 XRD scans of OPC-CAC-C$ paste (A) after dehydration in oven for three days and (B) after dehydration for three days and rehydration for three days, initial scan is included on both graphs.

In Figure 4.13 (A), it is seen that at ettringite is observed in the scans of dehydrated OPC-CAC-C$ pastes only in the initial condition after 28 days of curing and before dehydration. Monosulfoaluminate, calcium hydroxide, and calcium magnesium aluminum oxide silicate (alite) were observed in the initial and all dehydrate pastes. In Figure 4.13 (B), it can be seen that ettringite was observed in only the initial paste and the rehydrated paste dehydrated at 60°C.

4.5.4.2 SEM-EDS Analysis. Elemental analysis of samples through SEM-EDS analysis was also completed. This technique is used to supplement the XRD data as through EDS the meta-ettringite, which is X-ray amorphous, would still be detectable. Point analysis was completed at selected locations within each paste sample. Figure 4.14 presents an example of point analysis locations taken on a CAC-C$ paste sample. As an example, the EDS point analysis output of Site 028 from Figure 4.14 is presented in Table 4.6. For each point,

the content of calcium, aluminum, and sulfur are found and these are used to calculate the ratio of calcium to aluminum and sulfur to aluminum of all points analyzed.

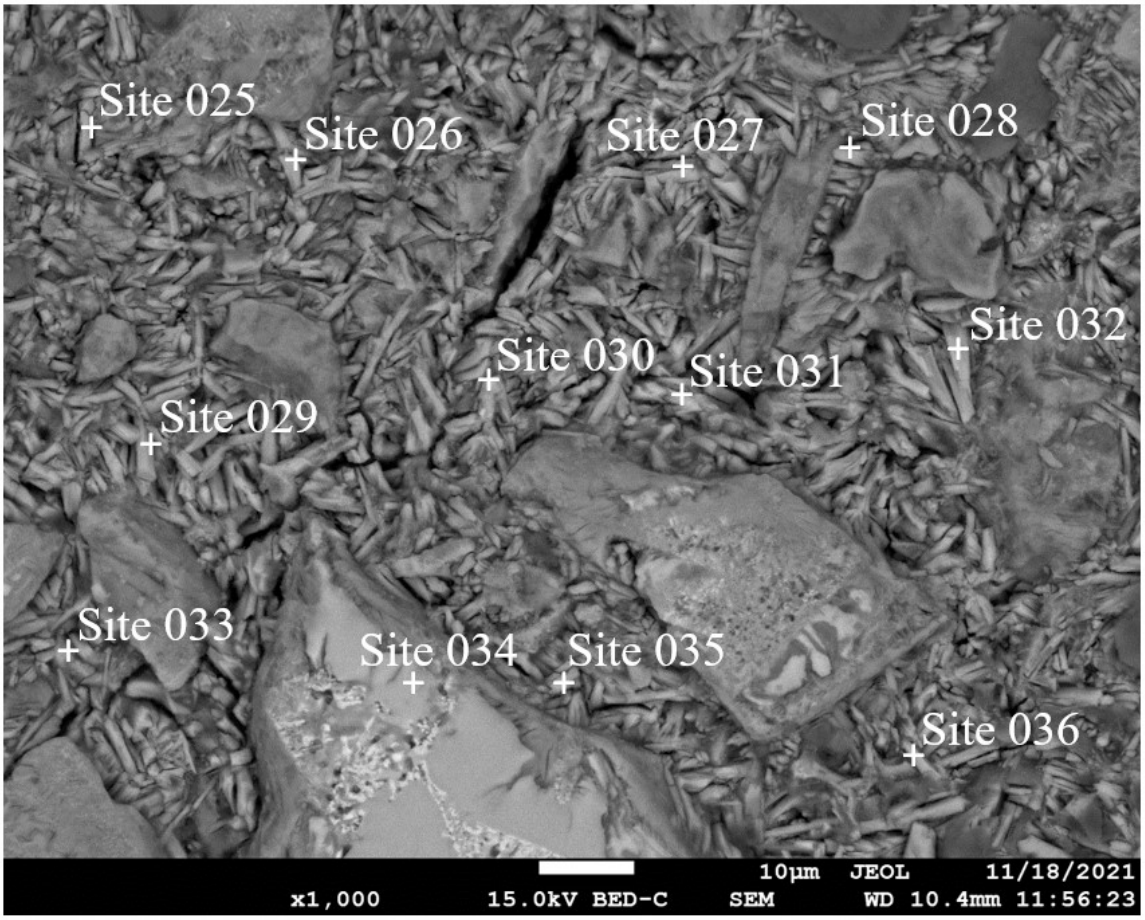

Figure 4.14 SEM image with EDS data point locations of rehydrated CAC-C$ paste where 60ºC was used for dehydration.

Table 4.6 EDS element analysis Site 028 of rehydrated CAC-C$ paste dehydrated at 60ºC

Element	O	C	Ca	S	Al	Si	Cu	Fe	Ni	Zn
Weight %	54.9	24.2	10.9	5.3	3.5	0.6	0.3	0.2	0.1	0.1

The EDS point analysis for the pastes in the initial, dehydrated at 60ºC, and rehydrated after 60ºC dehydration states are shown in Figure 4.15. Also shown in this figure are lines which represent the ratios for ettringite (AFt) and monosulfoaluminate

(AFm). The points for the sample were found to lie between the ettringite and monosulfoaluminate lines though on average closer to the ettringite.

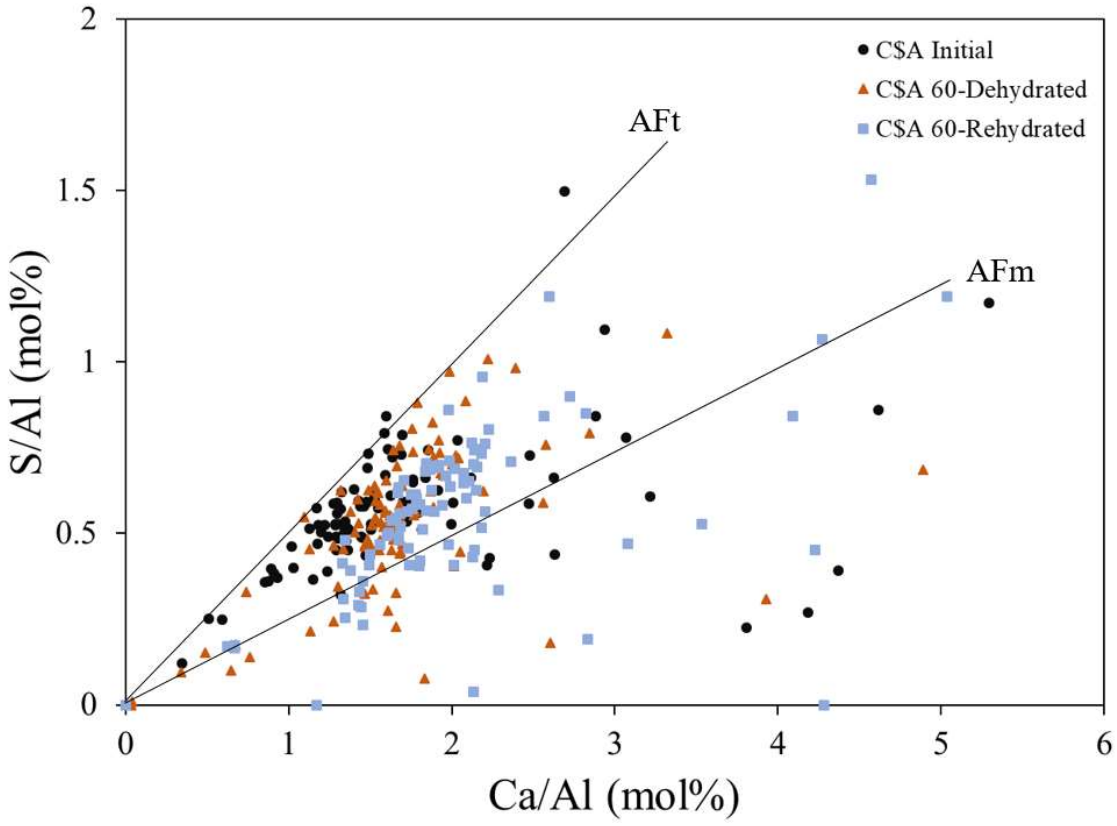

Figure 4.15 SEM-EDS point analysis for C$A paste in the initial, dehydrated at 60°C, and rehydrated after 60°C dehydration conditions.

The EDS point analysis for CAC-C$ in the initial and 60°C dehydrated conditions are presented in Figure 4.16. There are two major groupings of points observed for both conditions. One grouping representing ettringite has a Ca/Al ratio of between two and three and a S/Al ratio between one and 1.75. The other group representing monosulfoaluminate has a Ca/Al ratio of between one and two and a S/Al ratio between zero and 0.5.

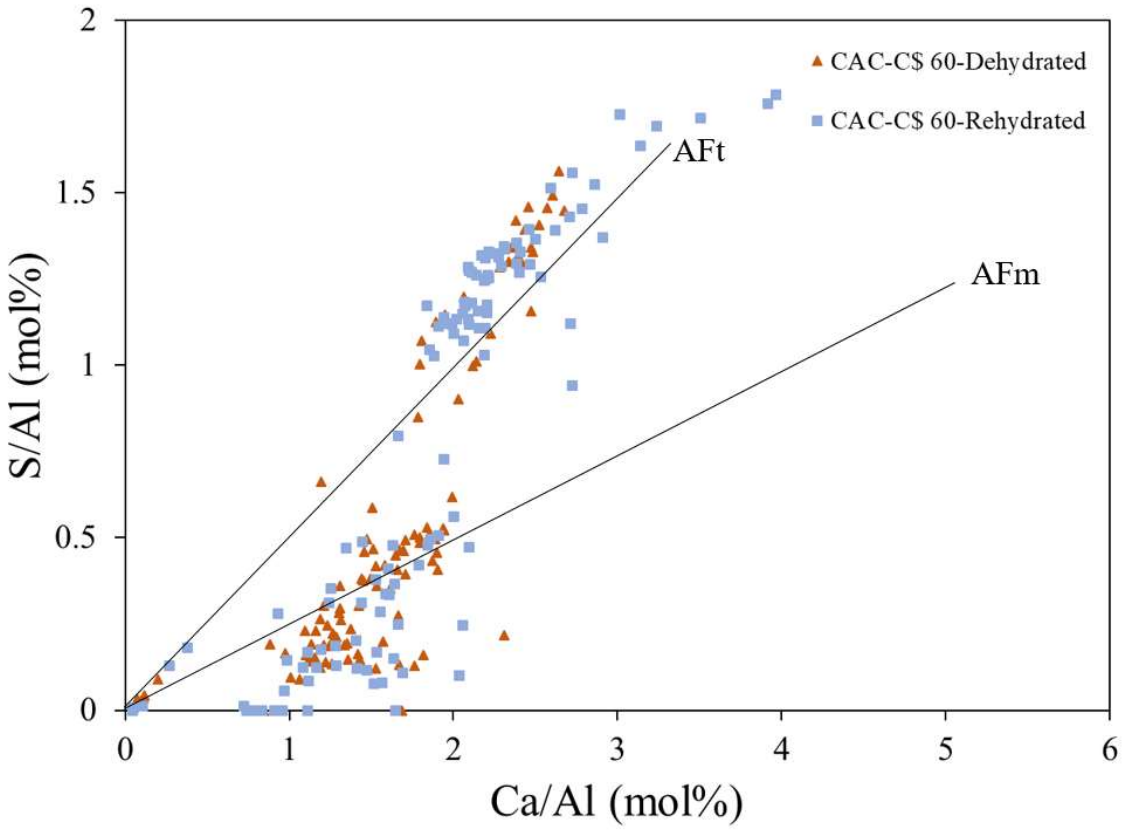

Figure 4.16 SEM-EDS point analysis of CAC-C$ pastes in the 60ºC dehydrated and rehydrated conditions.

The EDS point analysis for OPC-CAC-C$ in the initial and 60ºC dehydrated conditions are presented in Figure 4.17. All data points lie below the monosulfoaluminate line with no data point in alignment with the line indicating ettringite nor in the region between the ettringite and monosulfoaluminate. The primary cluster of points near the line for monosulfoaluminate is around a Ca/Al ratio of 2.25 and an S/Al ratio of 0.45.

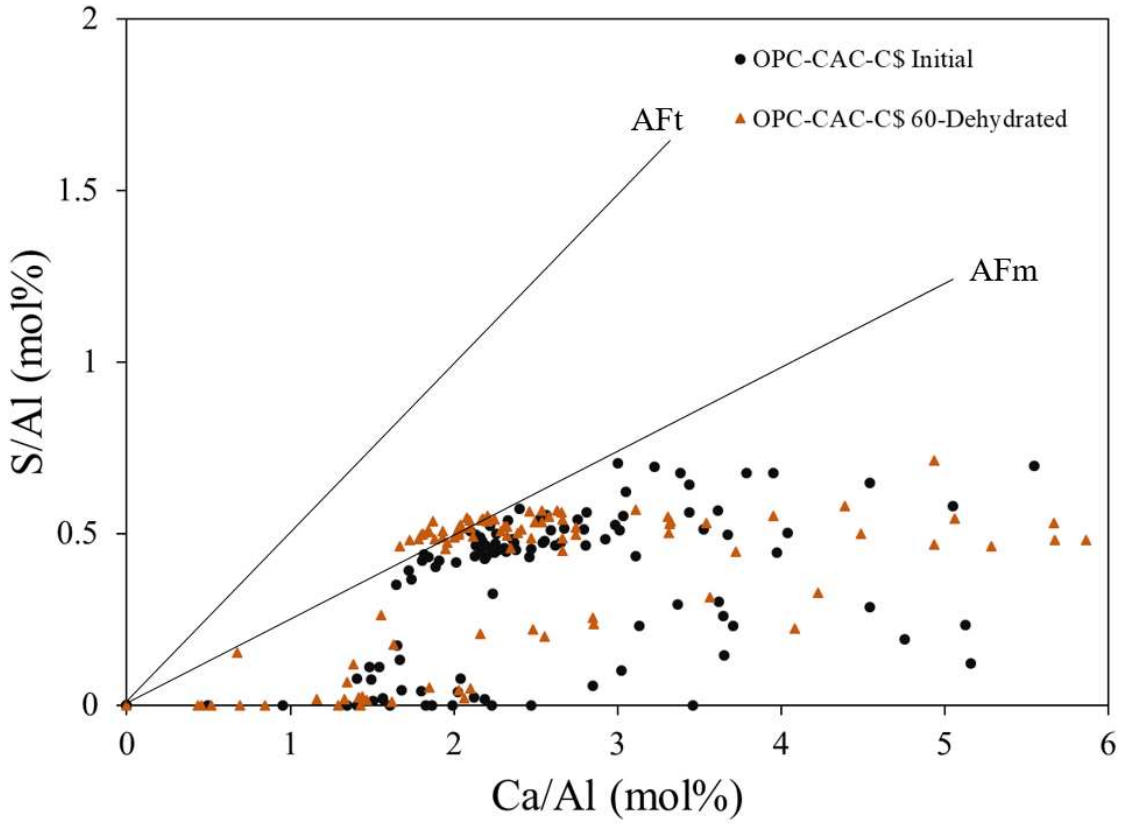

Figure 4.17 SEM-EDS point analysis for the OPC-CAC-C$ paste in the initial and 60ºC dehydrated states.

4.5.5 Calorimetry Cumulative Heat

In conjunction with the stability of the systems, heat is expected on the rehydration of the dehydrated pastes. The cumulative heat output after 24 hours of rehydration is presented in Figure 4.19 for the three cements at each dehydration temperature tested. The baseline cumulative heat is included as a reference from running a fully hydrated paste to determine the environmental heat level.

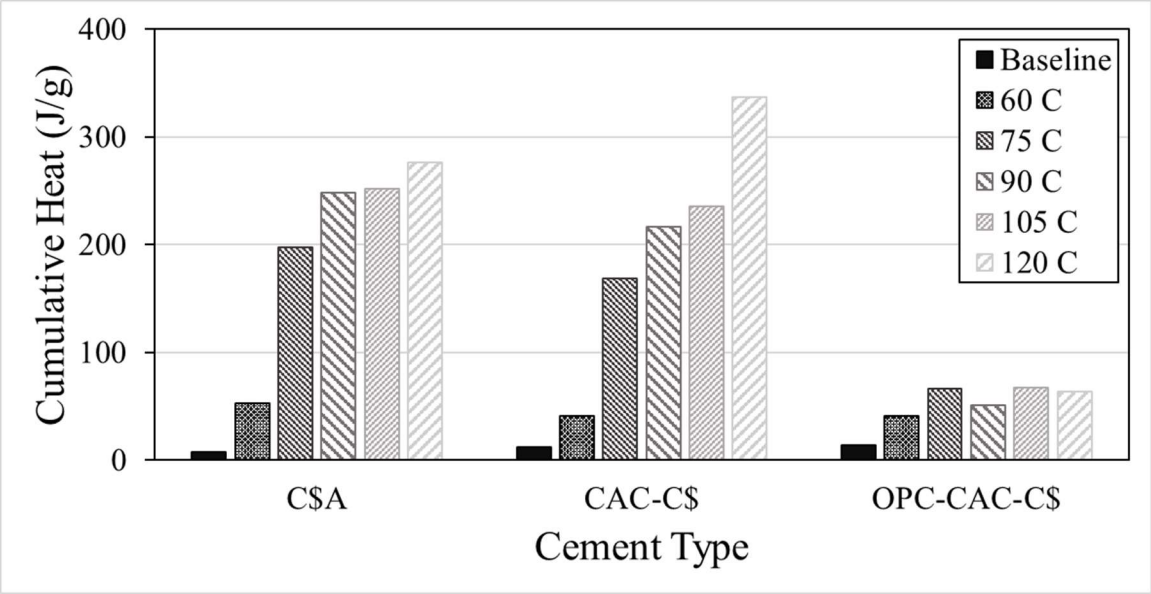

Figure 4.18 Cumulative heat output after 24-hour rehydration of dehydrated pastes for each cement and dehydration temperature

In Figure 4.19, it is shown that for both the C$A and CAC-C$ pastes that the cumulative heat output increased as the dehydration temperature was increased. The largest cumulative heat was observed for the pastes dehydrated at 120ºC where 276 J/g was observed for the C$A paste and 336 J/g was observed for the CAC-C$ paste. For both pastes, the largest increase in heat was observed between the pastes dehydrated at 60ºC and 75ºC. In the C$A paste between dehydration at 60ºC and 75ºC, an increase of 145 J/gram was observed and for the CAC-C$ paste a 127 J/g increase was observed. The cumulative heat in the OPC-CAC-C$ paste was observed to not significantly increase with the maximum output of 67 J/g observed in the paste dehydrated at 105ºC.

4.6 Discussion

For use as a storage medium, the understanding the stability that the cement will be used is needed for the design of the system. A more stable system will result in a broader pool of application uses such as in infrastructure or building. For infrastructure and building consideration, the systems used need to be stable in the dehydrated and hydrated states. The stability is needed to be maintained during cycling of the systems with sufficient compressive strength to ensure safety of the structure. Though, the stability needs to not be at the cost of the amount of energy that can be stored and released during the reaction. The use of the paste systems in architectural elements would provide a method to incorporate the systems into existing and new structures and allow for these elements to serve dual purposes.

Unstable macrostructure systems will need special considerations and setups for use such as a self-contained reactor. The two primary reactor systems are open and closed loop systems. For ease of construction and use, an open system reactor is preferred as the reaction is performed at atmospheric temperature and is in contact with the surrounding environment [12]. In a closed-system, the reactor is isolated from the environment with the water or water vapor used cycled in is closed loop, typically under negative pressure [12]. Additional systems to evaporate/condense the water as well as extra water reservoir space is necessary in a closed-system. Due to this, the design of an open system is simpler and requires a lower technical effort to use. The stability of the ettringite cement systems for their use as TCES mediums was studied in this work through the analysis of the cement type, dehydration temperature, time to failure, compressive strength, storage mass change, and microstructural changes.

The stability of the cement systems was greatly impacted by the dehydration temperature used with a decreasing stability found as the temperature was increased. This is seen in Figure 4.9 where there was a significant loss in the amount of cycles completed before failure of the specimens when the dehydration temperature was increased from 60°C to 75°C for all the cement systems tested. The cycle counts until failure continued to decrease as the dehydration temperature was increased and were not able to be rehydrated successfully at 120°C. This is in line with previous research showing that the decomposition of ettringite is found in the range of 100 to 125°C [13–15, 57–59, 67].

Analysis of the macrostructure provided insight to the chemical changes that were occurring during the cycling process. The hydration products expected to form from in the C$A systems were primarily ettringite with AH_3 from the hydration of ye'elimite [22]. Monosuloaluminate would be expected to be found if the content of the calcium sulfate decreased [22]. The presence of belite in the C$A cement is expected to result in strätlingite being found as a secondary hydrate product [22]. Similar to C$A, the primary hydrates expected to form in the CAC-C$ systems are ettringite and AH_3. When the sulfate content is insufficient, monosulfoaluminate and strätlingite may also be present with previous literature finding a 70-30 CAC to C$ ratio, similar to the 2.2:1 ratio of our blend, to form these hydrates after seven days [129]. In the OPC-CAC-C$, the addition of the CAC-C$ to the OPC is expected to result in the formation of ettringite and AH_3. The presence of AH_3 and CH would be expected to result in the formation of ettringite as they cannot co-exist thermodynamically [25]. The AH_3 can also react with alite from the OPC the form strätlingite and CH may be present from the reaction of alite and AH_3.

For use in energy storage, the ettringite crystal is needed to be found in the hardened paste system. For this determination, XRD and EDS microstructural analysis was used on cured cement paste samples taken from specimens cured for 28 days, the initial state before dehydration. The XRD and EDS analysis results of the C$A paste in the initial state indicate that the expected ettringite hydrate was formed during the hydration. Peaks for ettringite were found in XRD analysis and from SEM-EDS analysis, ettringite was likely observed in the C$A as the main grouping of points for the Ca/Al and S/Al ratios fell between the lines indicating the ratios for ettringite and monosulfoaluminate, and were clustered closer to the ettringite ratio line. The presence of ettringite as hydration product indicates that the C$A can be used to generate ettringite for thermochemical energy storage. This is in line with other studies which have also used C$A the generate ettringite for the study of TCES [14, 123, 130]. Though, the other expected hydrates of AH_3, monosulfoaluminate, and strätlingite were not present. From the XRD analysis of the initial C$A paste calcium silicate, belite, was observed. The presence of this anhydrous phase indicates that even with the high w/c ratio not all of the system hydrated. No AH_3 was observed in the paste though this may be due to the amorphous nature of the crystal formed in C$A not being able to be detected through XRD. The lack of AH_3 in hydrated C$A systems in XRD analysis was also seen in work by Kaufmann et al. though the AH_3 was observable through TGA analysis [67]. While not observed in this work, previous research has also found gypsum which when rehydrated would cause expansion within the system [123].

The XRD analysis of the hardened CAC-C$ paste in the initial state indicates that ettringite was formed as a hydration product as expected. The presence of monosulfoaluminate and strätlingite indicates that insufficient sulfate content was present

in the system. This result is in line with the results of Martin et al. as the CAC-C$ blend used was of the same blend and similar blend ratio [129].

The XRD analysis of the OPC-CAC-C$ paste in the initial condition indicates that ettringite was present in the system, though while not conclusive to the amount, the ettringite peaks were found to be just above background levels. In the OPC-CA-C$ system, the EDS data indicates that no ettringite is present as no data points were found along the line indicating a ratio for ettringite. For the initial OPC-CAC-C$ paste, the primary cluster of EDS points was found near the line for monosulfoaluminate. The EDS results showing that no ettringite present in the initial state suggest that if ettringite is present in the OPC-CAC-C$ system it is likely in small quantities. The lack of ettringite present in the OPC-CAC-C$ system suggests that while ettringite may form during the early ages of the reaction to promote setting, at later hydration stages the ettringite has converted. This indicates that this cement system is likely not suitable for energy storage as the thermochemical reaction relies on the presence of ettringite. This conversion of the ettringite in similar ternary systems was observed in previous work by Xu et al. [131]. Xu et al. found that the reduction in temperature during hydration to near freezing limited the conversion of ettringite at later stages of hydration [131]. Though in work by Moffat, the same cement blend was found to produce ettringite in the hardened paste [25]. Thus, from this work this OPC-CAC-C$ paste system cannot be termed a high ettringite cement for use in thermochemical energy storage due to the lack of ettringite as a final hydration produce.

The dehydration temperature used was found to influence the presence of ettringite in the C$A and CAC-C$ paste systems. In the dehydrated systems for both the C$A and

CAC-C$ systems, the ettringite peaks were not present in the XRD scans at the two highest tested dehydration temperatures of 105ºC and 120ºC. These temperatures are in the range that previous studies have found the decomposition of ettringite in XRD scans [67]. The lack of peaks for ettringite at 105ºC and 120ºC indicates that the crystalline ettringite has decomposed. The presence of ettringite peaks in the XRD scans of the C$A and CAC-C$ pastes in dehydrated specimens dehydrated at temperatures of 60ºC, 75ºC, and 90ºC suggest that not all ettringite was converted to the amorphous metaettringite state or a decomposition product for these temperatures and that the conversion of ettringite to the metaettringite state was not able to be completed within the three days for the pastes in these conditions. This is in agreement with the mass changes observed in the dehydration and rehydration cycling of the pastes as at these three temperatures changes in mass were still observed between days two and three. The mass of the 60ºC, 75ºC, and 90ºC after three days also had not reached the same values as the specimens dehydrated at 105ºC and 120ºC. The presence of ettringite was also confirmed in the EDS samples for dehydration temperature of 60ºC as points indicating ettringite were found for both C$A and CAC-C$ pastes. In previous work by Ndiaye et al., full decomposition of ettringite in C$A pastes dehydrated at 60ºC was observed with three days of dehydration [14, 15]. The difference is attributed to the solid paste samples tested for this work while aerated specimens were used in the work by Ndiaye et al. [14]. The larger surface area allowed for quicker removal of the water from the paste. Thus, an increase in the dehydration time of the solid pastes at these temperatures or an aerated paste would be needed to ensure complete decomposition of the ettringite. For OPC-CAC-C$, no ettringite was present in the dehydrated state and no change was observed in the hydrates found through XRD analysis between the

dehydration temperatures. For dehydrated OPC-CAC-C$ at 60ºC, EDS results also found that no ettringite was present in the paste. This indicates that for the OPC-CAC-C$ the dehydration temperature had no effect on the microstructure of the system.

For the other hydrates found in in the C$A paste, the dehydration temperature used did have an impact on the microstructure while no significant change was observed in the microstructure for the CAC-C$ and OPC-CAC-C$ specimens. In the C$A paste, katoite peaks were observed in both the dehydrated and rehydrated pastes with the higher dehydration temperatures. Katoite was also observed by Kaufman et al. in the C$A paste though this was the result of seven days of steam curing before cycling and not an impact of the cycle [67]. The presence of monosulfoaluminate in the systems for the CAC-C$ and OPC-CAC-C$ is liked with the expansion and deterioration of the paste [67]. Though from the presented work, while instability does exist, the presence of monosulfoaluminate in the OPC-CAC-C$ did not result in any noticeable decease in the deterioration time of the pastes between the different dehydration temperatures as it was present in all conditions.

The re-emergence of ettringite peaks in the rehydrated scans of the C$A and CAC-C$ pastes dehydrated at 105ºC and 120ºC indicates that at least some of the present decomposed ettringite was metaettringite and can successfully undergo the ettringite-metaettringite conversion. The results for ettringite present in dehydrated samples below 90ºC and not at 105ºC is in line with the cycle data results where a steady state mass was not reached after three days of dehydration. In the rehydrated C$A, a change in microstructure was observed as katoite was present. No new hydrates were observed in the rehydrated CAC-C$ and OPC-CAC-C$ pastes at any of the tested dehydration compared to the initial or dehydrated pastes.

The damage mechanisms observed were different based on the dehydration temperature and cement type. The degradation of the three cement specimens at 60ºC occurred over multiple cycles and was observed through the progressive cracking in the specimens. Also, during rehydration, significant amounts of air bubble released from the systems cause stress damage within and weaken the paste. The rehydration part of the cycle is where the most instability of the systems is as all but one of the cube specimens tested, C$A paste dehydrated at 60ºC cycle ten, failed during rehydration. The observed change in the area of the C$A and CAC-$ compression specimens indicates that the volume of these specimens were not stable and did contract and expand during dehydration and rehydration. As the dehydration temperature was increased, the change was more significant. The dehydration and rehydration are changing the crystal shape resulting in stresses in the paste from the contraction and expansion. These stresses would result in the cracking observed in the systems. At dehydration of 120ºC, the rapid volume expansion observed in the C$A indicates that expansive hydrates such as gypsum may have formed in the systems. Though from XRD analysis of the pastes these hydrates were not observed.

The dehydration temperature was shown to have a significant impact on the macro-stability of all three types of cement pastes. As seen for each of the three tested cement pastes, the higher the dehydration temperature the less the amount of cycles the systems could withstand. At the highest tested temperatures above 100ºC, the macrostructure of the system failed during the first cycle rehydration with only one of the OPC-CAC-C$ specimens lasting onto the second cycle. This failure upon the first rehydration indicate that any system to using these cements should not be used for structural systems. The failure of the specimens during rehydration when dehydration at 100ºC was used was also

observed by Kaufmann et al. [67]. At dehydration temperatures of 75ºC and 90ºC, only marginal gains in cycle count were achieved over dehydration at 105ºC and 120ºC. At dehydration of 90ºC, both the C$A and OPC-CAC-C$ systems were able to survive one complete cycle while the CAC-C$ failed on the first cycle similar to the higher dehydration temperatures. Modest gains were seen when dehydrated at 75ºC, with an increase of similar cycle counts of between one and four before failure. The best performing dehydration temperature was at 60ºC, where all three cements saw the most amount of cycles before failure. The amount of cycles significantly increased from the other dehydration temperatures with the C$A and CAC-C$ seeing similar cycle increases to nine and 11, respectfully, and the OPC-CAC-C$ seeing an increase to 16 cycles. These results indicate that the lower the temperature used for dehydration the longer the system can be cycled for while maintaining the integrity of the macrostructure. However, it is important to note that these macrostructure integrity results are based on dehydration of a solid paste system when a prescribed time and not dehydration level was used for dehydration.

At the lower dehydration temperatures, a steady state of the system was not observed to have been reached. This is shown at a dehydration of 120ºC where minimal mass change was observed on days two and three of heating while still occurring at the lower tested temperatures. Reaching this steady state may be alleviated if a porous system is used as seen in work done by Ndiaye et al. or the time of dehydration is increased [14]. These results indicate that for the dehydration and rehydration for the ettringite-metaettringite reaction lower dehydration temperatures are preferred to maintain the integrity of the system macrostructure. In systems where the macrostructure integrity is not paramount, higher temperatures may be able to be used.

The change in area, and thus change in volume, measured in the dehydrated C$A and CAC-C$ specimens when dehydrated at a temperature above 90°C and in the rehydrated CAC-C$ specimens shows instabilities exist for these conditions. This indicates that the removal and addition of water from the ettringite crystal can result in changes to the structural shape and manifest as macroscale volume changes. These changes were not observed in the OPC-CAC-C$ specimens which were found to contain minimal quantities of ettringite.

The type of cement used impacted the stability of the paste system. Of the three cement paste type systems tested, the ternary blend of OPC-CAC-C$ resulted in the most stable system. The 16 cycles for the OPC-CAC-C$ system at 60°C resulted in the specimens surviving almost double the amount of nine cycles found from the C$A paste specimens. When compared to the 11 cycles found in for the binary CAC-C$ paste, the 16 cycles for the OPC-CAC-C$ system represented an approximately 50% increase in stability. A C$A paste dehydrated at 60°C was found by Ndiaye et al. to last for seven cycles, though testing appears to have been stopped at this point instead of failure as no macroscopic cracks were observed [14]. At 105 and 120°C, the OPC-CAC-C$ paste was the only one of the three to result in a cube specimen surviving more than one day of rehydration during the first cycle. Though, similar to the other paste types, did not survive the entire cycle. In the comparison of mass change, the loss of 10% of the specimen mass for both the CAC based systems at 60°C was the least observed for all the conditions. The loss observed in the C$A was similar at 15%. At dehydration temperatures of 105 and 120°C, the mass percentage after dehydration compared to the initial state was 70% for C$A and CAC-C$ while in the OPC-CAC-C$ the mass percentage was at 80%. This

represents 1/3 the amount of water being removed in the OPC-CAC-C$ system compared to the other two cement systems. This indicates that the loss of water other than from ettringite may be present. An ultimate mass loss of 30% in the C$A specimens due to removal of water is similar to the results found by Ndiaye et al. [14]. Further work is needed to determine the impact of specimen size and specimen surface area to the mass change of the specimen as aerated C$A pastes in work by Ndiaye et al. showed a stabilization in mass at dehydration of 60^{o}C within three days, a result that was not observed in this work testing solid paste cubes [14].

The presence of ettringite in the C$A and CAC-C$ in the initial systems as well as in the rehydrated systems for all dehydration temperatures indicates that these cements pastes have the ability to be used for TCES. While ettringite is present in the OPC-CAC-C$ in the initial and rehydrated state when dehydrated at 60^{o}C, the lack of ettringite present in the EDS and in the XRD scans of the rehydrated paste specimens dehydrated at 75^{o}C or above indicates that this system will not be suitable for use to store energy. These observations of the microstructure relate to the cumulative heat where the OPC-CAC-C$ system was found to perform the worst of the three cement systems in terms of energy release when rehydrated. The C$A and CAC-C$ pastes were found to release significantly more energy than the OPC-CAC-C$. This difference is attributed to the observed ettringite contents found through the XRD and EDS microstructural analysis in the C$A and CAC-C$ pastes and not in the OPC-CAC-C$. For the three cement paste systems, the OPC-CAC-C$ system provided the best stability in terms of longevity in cycle count before failure. The least stability was found in the CAC-C$ system. The OPC-CAC-C$ system while found to perform the best in terms of stability was found

have minimal amounts of ettringite in the hardened systems. This low amount of ettringite resulted in a low amount of heat returned on rehydration seen from the cumulative heat observed being the lowest of the three cement for each of the tested dehydration temperatures. Thus, while the OPC-CAC-C$ system may be the best fit for stability, it has low ability to store energy.

For dehydration temperature, as the lower dehydration temperatures were found to be more stable, dehydration at 60ºC would be recommended from the stability results. Though from the cumulative heat results, higher dehydration temperatures resulted in more energy release on rehydration. The combination of the stability and cumulative heat results suggest that they are inversely related to each other based on dehydration temperature. Thus, the reactor systems would need to be optimized for this relationship. An open reactor needing a more stable dehydration temperature while if the integrity of the system is not needed in the closed reactor then a higher dehydration temperature may be able to be used. Of the tested systems the C$A paste dehydrated at 75ºC performed the best for both stability and energy as at dehydration of 75ºC the paste resulted in the most released energy of the three cements when rehydrated and was second best in terms of number of cycles that were performed before macrostability.

In terms of energy, the stability data indicates that the C$A system dehydrated at 120ºC is likely the best in performance in terms of energy released during rehydration. This is due to this system resulting in the largest mass change of all the tested systems. If this is all from the loss of water and no decomposition has occurred in the ettringite then this system will result in the most energy during rehydration. This is shown in the cumulative heat results as the paste specimens dehydrated at 120ºC performed the best for energy

released on rehydration though the energy released from the CAC-C$ was observed to be higher than the C$A at 120ºC, at all other dehydration temperatures the C$A performed the best of the three cements in terms of energy released on rehydration. Energy is expected to be able to be recovered from a second dehydration and rehydration of the C$A and CAC-C$ paste systems as from chemical analysis ettringite is present in the rehydrated system. The presence of ettringite will allow the cycle to be able to be repeated.

The presence of relative humidity below 45% did not result in gain in mass of stored C$A specimens. The largest observed gain of mass for the specimens stored at 45% RH with a 6.40% recovery of the mass lost during dehydration. Unlike more traditional systems where discharge in the stored state occurs progressively over a period of time, the majority of the mass of the systems was regained early time period after the system was stored charged. At later ages, the mass gained remained consistent for most of the conditions tested. At 0% RH, a further dehydration of the systems was observed. This was due to the vacuum environment causing a further removal of water from the system over the amount removed from oven dehydration. This removal of water from ettringite in a vacuum is used as a hydration arresting technique [132]. At 35% RH, the loss in capacity initially follows a similar trend to the other RH percentage conditions, though starts to lose mass after 410 days. No identifiable reason for this increase was identified as no observable trends were noticed in the RH of the storage container or with the temperature effecting any of the other storage conditions.

An increase in the storage RH was found to increase the gain of mass of the specimens during the storage period. While not directly verified as a part of this work, an increase in the mass should correspond to a decrease in the charge of the system. Though

the gain in the worst performing storage condition of 45% RH did not represent a significant gain in the mass lost from the initial dehydration and stabilized over subsequent observations. The results indicated that at lower RH percentages, storage of the systems in the dehydrated state over an extended period of time is possible. While an increase in mass is observed at high storage RH percentages, the large range and stabilization in the mass gain after an initial period show that the storage in the dehydrated state is not extremely sensitive to the presence of moisture when stored in RH below 45%. Though this stabilization may be the result of the hydration of the surface preventing further ingress of moisture into the specimen. In terms of energy storage efficiency, this means that if the presented storage RH conditions are used then minimal energy would be needed to keep the system in the dehydrated state.

For use in a load bearing capacity, the impact that the dehydration and rehydration of the ettringite cement is needed. From the tested systems lower dehydration temperatures may result in a slight increase in compressive strength when compared to the strength at 28 days. Though any strength gain is lost when rehydrated as there was found to be at minimum a 50% decrease in the strength in the rehydrated systems compared to the initial strength before cycling. These results indicate that such cement systems are not suitable for load bearing application. Further work on the impact of the dehydration and rehydration on the compression strength of these ettringite pastes needs to be done to understand the impact of the cycle on the properties of the systems, especially when cycled through multiple cycles.

The degradation of the stability from cycling the pastes indicate that these systems should not be used in architectural concrete capacity. These systems should be used in

systems where the degradation of the paste can be contained. A closed system reactor where the dehydration and rehydration can be conducted in an isolated environment will allow the specimen to continue to function even if the stability is compromised. These systems may also be suitable to start with slid samples the degrade over cycles or hold granulated pastes. Storage of the systems at ambient conditions is possible if the relative humidity is not expected to exceed 45%, though further testing is needed to determine the upper boundary of this condition. Though as architectural pieces these results do indicate that the systems would be unsuitable as these sub 45% RH conditions are not able to be maintained when exposed to weather.

An energy analysis of the system is needed to understand the amount of energy that is needed to dehydrate the systems and the amount that can be recovered from the system after storage over multiple cycles. The size and shape of the specimens needs to be further investigated to determine the impact that this has on the rate of the reaction and the stability of the system.

The long term storage of other high ettringite cements such as the CAC-C$ system at the full range of RH percentages is needed to see if these other systems perform similar to the C$A system. To verify the observed stabilization and mass gained in storage of the solid specimens, future work should also examine aerated and crushed systems where the surface area is greater.

This work presented results examining the stability of three ettringite based cement systems under various conditions. Further work related to the stability of these systems is suggested to develop and enhance the understanding of both the dehydration and rehydration cycle and storage of the dehydrated system. This work focused on the macro-

stability of the system and not on the stability of the system once failure had initiated. Failure of the macro-stability of the system does not result in an unusable system in self-contained systems. Thus, future work is needed to analyze the impact of the dehydration-rehydration loop on the system after loss of the macrostructure integrity, specifically on the energy needed and released during the reaction. This will help understand the cycle limits of these cement based systems. Additional work is needed to assess OPC-CAC-C$ systems when cast at near freezing temperatures to determine the stability of the system when ettringite is found as a main hydration product as that was not the case in this work. For use as an energy storage medium, the time and conditions that result in loss of stored energy are important. Future work is needed to study the impact of capacity lost when specimens are stored at above 50% RH. If the storage environment is expected to exceed 45% then from the results of this work this the minimal mass change observed in this work may not hold true and at high RH would be expected to rehydrate the systems. The CAC-C$ paste should be examined for the impact of storage on capacity lost due to environmental humidity. Monitoring of the carbonation is also needed as while not in the scope of this dissertation has been found to be a concern for ettringite [73, 75, 133]. The chemical analysis of the systems is needed to determine if the salt used to control the RH resulted in changes. The microstructural analysis is also needed to determine the composition and phase of ettringite present and the degree that carbonation and salt may have impacted the paste.

4.7 Conclusions

The work studied the stability of high ettringite cement paste systems for their use as an energy storage medium. A stable system would allow these systems greater flexibility in their use as they could be implemented as structural or architectural elements. Differences in the stability were noticed as the dehydration temperature was changed with higher dehydration temperatures resulting in a more unstable system. At 105ºC and 120ºC, none of the tested systems were able to successfully last one complete dehydration and rehydration cycle. Though at the higher dehydration temperatures more energy was found to be able to release on rehydration. This inverse relationship between stability and energy is important for design of the system. A closed reactor setup would be able to make use of the unstable macrostructure of the paste as long as the ettringite does not decompose over multiple cycles limiting the reaction. Differences in the cement type were also noticed as the OPC-CAC-C$ paste resulted in the most stable system of the three cement types though as this system was found to have limited ettringite is not recommended for use in energy storage. This was confirmed as this system was found to release the least energy on rehydration of the three pastes. The compressive strength was found to vary and decreased in the C$A and CAC-C$ systems when dehydrated at the higher temperatures. While an increase of strength was noted for the OPC-CAC-C$ system in the dehydrated state, the strength was found to be reduced in the rehydrated state and not able to be determined for rehydrated specimens dehydrated at 105ºC and 120ºC. The C$A paste was found to be able to maintain the dehydrated state when stored at RH values below 45%. This showed that stable storage of the systems over an extended period of time is possible. Thus, from the presented work the C$A and CAC-C$ systems can work for energy storage though due to

the macrostability issues a closed reactor system will be needed as the systems will not be able to function for structural or architectural purposes.

Further work will be needed to examine the CAC-C$ for long term storage and higher RH percentages are needed to determine the upper boundary for storage. The microstructure of the systems when subjected to multiple cycles is needed to determine how this changes through subsequent cycles and monitor any changes in hydrates. Further study of the systems for carbonation is needed if the systems are not to be used in a self-contained reactor setup. The energy release from these systems over multiple cycles is needed to determine the impact that cycling has on the energy released from the systems during rehydration. This should then be compared to the energy needed to dehydrated the systems.

CHAPTER 5

CONCLUSIONS AND RECOMENDATIONS

Energy storage will play a role to satisfy the energy demand fluctuations that occur on a daily and yearly basis while easing strain on the current system. Thermochemical energy storage (TCES) systems using ettringite based cement systems are poised to offer a possible storage method that can be effective over short and long-term storage periods. While the conversion of ettringite to the low water metaettringite state has been shown to be reversible, the limits of the stability, potential applications, and energy efficiency of the systems are not well understood. Related to the stability and application, the work presented in this dissertation provided new understanding on the macrostability ettringite based cement pastes for use in TCES using three different cement systems which were dehydrated at different temperatures, the time that the systems can be stored in the dehydrated state, the microstructure of the systems, the compressive strength at each step during a dehydration cycle, and if the systems were suitable for open reactor based systems. In regards to energy storage and energy efficiency, this dissertation provided new understanding of the energy that can be recovered from the systems from rehydration using three different cement systems and five dehydration temperatures. Additionally, the energy recovered from multiple rehydration cycles was also quantified.

5.1 Key Findings

Key findings from this work are summarized below:

- The stability of the cement paste systems during dehydration-rehydration cycling was significantly impacted by the dehydration temperature:
  - An increase in dehydration temperature was found to significantly reduce the time to failure of the cement paste systems. A reduction in the number of cycles before failure was observed to be inversely proportional to an increase the dehydration temperature to 75ºC from 60ºC;
  - Dehydration at 60ºC was found to result in a longer cycle performance of the systems for all three cements; and,
  - Dehydration at 105ºC and 120ºC resulted in very unstable systems that failed during the first rehydration cycle.

- The type of cement system used was found to impact the amount of cycles the cement paste systems could withstand the dehydration-rehydration cycling before failure:
  - The impact was more pronounced at lower temperatures where the systems lasted more than one cycle the OPC-CAC-C$ system was found to last the longest of the three; and,
  - At higher dehydration temperatures, the cement type was found to not to be as impactful in terms of the number of cycles before failure.

- Ettringite was found in all three systems in the initial state, prior to dehydration, through XRD analysis of the three pastes; though EDS results indicate that if ettringite is present in the OPC-CAC-C$ system the quantity is likely to be low.

- Three days of dehydration of the solid systems is not enough the convert all the ettringite to metaettringite at lower dehydration temperatures:
  - Ettringite was still observed in the crystalline state for C$A and CAC-C$ cement paste systems after three days when dehydration temperatures up to 90ºC were used.

- The chemistry of the three cements systems was found to not be significantly be altered over multiple dehydration and rehydration cycles

- The OPC-CAC-C$ cement paste, which was found to have minimal amounts of ettringite, performed the best of the three cements in terms of time to failure:
  - Other than the changes in ettringite no significant change in system chemistry was observed.

- The compressive strength was found to vary depending on the state of the specimens:
    - In the dehydrated state, the compressive strength was found to increase for the OPC-CA-C$ pastes when dehydration of 75ºC or greater was used;
    - Noticeable strength gain was found in the C$A and CAC-C$ after the systems were dehydrated at 75ºC; and,
    - A loss in strength from the initial state was observed after rehydration for all cement paste systems at all dehydration temperature levels.

- The storage of the C$A paste at relative humidity of 45% or lower was not found to result in system rehydration.

- Increasing the dehydration temperature was found to increase the energy release on rehydration.

- The cement type was found to impact the amount of heat released upon rehydration:
    - The OPC-CAC-C$ cement paste system was observed to have low levels of energy recovery at higher dehydration temperatures compared to the CSA and CAC-C$ cement paste systems.

- The C$A cement paste system was found to be able to release heat on rehydration over multiple cycles, even if macrostability failure had occurred.

- There is a tradeoff between energy release and stability as the more stable systems were found to release less energy upon rehydration. This was observed for all dehydration temperatures and cement types.

- The failure of the cement paste systems within 20 dehydration-rehydration cycles, and the compressive strength changes between the initial, dehydrated, and rehydrated states, indicated that these systems should not be used in structural or architectural applications:
    - A self-contained closed reactor setup is needed for these materials; and,
    - Recovery of energy after macrostability failures of the systems was possible.

5.2 Future Work

The following is a list of recommendations for additional work to build on the work presented in this dissertation:

- The OPC-CAC-C$ system should be examined when cast at lower temperatures and at different blend ratios to determine if ettringite can be found in the hydrated paste system, as indicated by other researchers.

- Further examination of the ability to store the systems for a long period of time for the CAC-C$ paste and for RH above 50%. This should be done to determine if other paste systems exhibit the same behavior as the C$A at RH below 45%. Storage at RH between 50% and 100% will also help researchers understand the impact of RH on the storage of the systems and the rate that they will rehydrate.

- The microstructure of the systems when subjected to multiple cycles is needed to determine how this changes through subsequent cycles and monitor any changes in hydrates.

- Further work is needed to understand the efficiency of the dehydration and rehydration cycling of these systems. The amount of energy needed to dehydrate the ettringite in the sample and the amount of energy used during the process should be determined

- The energy returned from cycle testing of these pastes should be further expanded in the scope of cements, temperatures, and cycle count to develop a comprehensive understanding of the performance of prolonged cycling of the systems.

- Further work is needed to determine the impact of the physical shape properties of the paste on the stability, mass change, and energy transfer of the systems.

REFERENCES

[1] United States Department of Energy. (2013). *Grid Energy Storage*, Washington, D.C., United States Depertment of Energy.

[2] Dincer, I., Erdemir, D. (2021). Chapter 1 - Fundamentals and Concepts, I. Dincer; D. Erdemir (Eds.), *Heat Storage Systems for Buildings*, Elsevier, Cambridge, MA, 1–35. doi:https://doi.org/10.1016/B978-0-12-823572-0.00007-2.

[3] Obringer, R., Nateghi, R., Maia-Silva, D., Mukherjee, S., CR, V., McRoberts, D. B., Kumar, R. (2022). Implications of increasing household air conditioning use across the United States under a warming climate, *Earth's Future*, Vol. 10, No. 1. doi:10.1029/2021EF002434.

[4] Penn, I. (2020, August 17). California expresses frustration as blackouts enter 4th day, *The New York Times*, New York.

[5] Sabihuddin, S., Kiprakis, A., Mueller, M. (2015). A numerical and graphical review of energy storage technologies, *Energies*, Vol. 8, No. 1, 172–216.

[6] Center for Sustainable Systems. (2018). University of Michigan, U.S. grid energy storage factsheet, No. CSS15-17.

[7] Sandia National Laboratories. (2018). Global energy storage database projects, U.S. DOE, from https://sandia.gov/ess-ssl/gesdb/public/index.html, accessed 18-6-2018.

[8] U.S. Energy Information Administration. (2018). *'Technical Report', Electric power monthly with data for march 2018*, Washington DC, U.S. Department of Energy.

[9] U.S. Energy Information Administration. (2018). Frequently asked questions: how much electricity does an American home use?, U.S. Energy Information Administration.

[10] Ding, Y., Riffat, S. B. (2013). Thermochemical energy storage technologies for building applications: a state-of-the-art review, *International Journal of Low-Carbon Technologies*, Vol. 8, No. 2, 106–116. doi:10.1093/ijlct/cts004.

[11] Dincer, I., Erdemir, D. (2021). Chapter 2 - Heat Storage Methods, I. Dincer; D. Erdemir (Eds.), *Heat Storage Systems for Buildings*, Elsevier, Cambridge, MA, 37–90. doi:https://doi.org/10.1016/B978-0-12-823572-0.00010-2.

[12] Letcher, T. (2016). *Storing Energy*, Elsevier, Oxford, UK. doi:https://doi.org/10.1016/B978-0-12-803440-8.00017-8.

[13] Zhou, Q., Lachowski, E. E., Glasser, F. P. (2004). Metaettringite, a decomposition product of ettringite, *Cement and Concrete Research*, Vol. 34, No. 4, 703–710. doi:https://doi.org/10.1016/j.cemconres.2003.10.027.

[14] Ndiaye, K., Cyr, M., Ginestet, S. (2017). Durability and stability of an ettringite-based material for thermal energy storage at low temperature, *Cement and Concrete Research*, Vol. 99, 106–115. doi:http://dx.doi.org/10.1016/j.cemconres.2017.05.001.

[15] Ndiaye, K., Ginestet, S., Cyr, M. (2018). Experimental evaluation of two low temperature energy storage prototypes based on innovative cementitious material, *Applied Energy*, Vol. 217, 47–55.

[16] Mehta, P. K., Monteiro, P. J. M. (2014). *Concrete : Microstructure, Properties, and Materials* (4th ed.), McGraw-Hill Education, New York.

[17] Odler, I. (2000). *Special Inorganic Cements*, Taylor and Francis, London, UK.

[18] Alvarez-Pinazo, G., Cuesta, A., García Maté, M., Santacruz, I., Losilla, E. R., De la Torre, A., Leon-Reina, L., Aranda, M. (2012). Rietveld quantative phase analysis of yeelimite-containing cements, *Cement and Concrete Research*, Vol. 42, No. 7, 960–971. doi:10.1016/j.cemconres.2012.03.018.

[19] Matschei, T., Lothenbach, B., Glasser, F. P. (2007). The AFm phase in portland cement, *Cement and Concrete Research*, Vol. 37, No. 2, 118–130. doi:https://doi.org/10.1016/j.cemconres.2006.10.010.

[20] Taylor, H. F. W. (1997). *Cement Chemistry* (2nd ed.), Thomas Telford Publishing, London, UK.

[21] Hargis, C. W., Kirchheim, A. P., Monteiro, P. J. M., Gartner, E. M. (2013). Early age hydration of calcium sulfoaluminate (synthetic ye'elimite, C4A3S) in the presence of gypsum and varying amounts of calcium hydroxide, *Cement and Concrete Research*, Vol. 48, 105–115.

[22] Winnefeld, F., Lothenbach, B. (2010). Hydration of calcium sulfoaluminate cements — experimental findings and thermodynamic modelling, *Cement and Concrete Research*, Vol. 40, No. 8, 1239–1247.

[23] Bizzozero, J., Gosselin, C., Scrivener, K. L. (2014). Expansion mechanisms in calcium aluminate and sulfoaluminate systems with calcium sulfate, *Cement and Concrete Research*, Vol. 56, 190–202.

[24] Christensen, A. N., Jensen, T. R., Hanson, J. C. (2004). Formation of ettringite, Ca6Al2(SO4)3(OH)12·26H2O, AFt, and monosulfate, Ca4Al2O6(SO4)·14H2O, AFm-14, in hydrothermal hydration of portland cement and of calcium aluminum oxide—calcium sulfate dihydrate mixtures studied by in situ synchrotron X-ray powder, *Journal of Solid State Chemistry*, Vol. 177, No. 6, 1944–1951.

[25] Moffatt, E. G. (2016). *Durability of rapid-set (ettrinigte-based) concrete*, University of New Brunswick, Fredericton, New Brunswick, Canada.

[26] Gastaldi, D., Canonico, F., Boccaleri, E. (2009). Ettringite and calcium sulfoaluminate cement: Investigation of water content by near-infrared spectroscopy, *Journal of Materials Science*, Vol. 44, 5788–5794. doi:10.1007/s10853-009-3812-1.

[27] Telesca, A., Marroccoli, M., Pace, M. L., Tomasulo, M., Valenti, G. L., Naik, T. R. (2013). Expansive and non-expansive calcium sulfoaluminate-based cements, *Third International Conference on Sustainable Construction Materials and Technologies*, Kyoto.

[28] CTS. (2013, October). The use of calcium sulfoaluminate rapid setting cement for underground construction, *TBM: Tunnel Business Magazine*\.

[29] Glasser, F. P., Zhang, L. (2001). High-performance cement matrices based on calcium sulfoaluminate–belite compositions, *Cement and Concrete Research*, Vol. 31, No. 12, 1881–1886. doi:https://doi.org/10.1016/S0008-8846(01)00649-4.

[30] Juenger, M. C. G., Winnefeld, F., Provis, J. L., Ideker, J. H. (2011). Advances in alternative cementitious binders, *Cement and Concrete Research*, Vol. 41, No. 12, 1232–1243. doi:https://doi.org/10.1016/j.cemconres.2010.11.012.

[31] Biello, D. (2008, August). Cement from co2: a concrete cure for global warming, *Scientific American*, Vol. 7, 61.

[32] Sharp, J. H., Lawrence, C. D., Yang, R. (1999). Calcium sulfoaluminate cements—low-energy cements, special cements or what?, *Advances in Cement Research*, Vol. 11, No. 1, 3–13, article. doi:10.1680/adcr.1999.11.1.3.

[33] Zhang, L., Su, M., Wang, Y. (1999). Development of the use of sulfo- and ferroaluminate cements in China, *Advances in Cement Research*, Vol. 11, No. 1, 15–21, article. doi:10.1680/adcr.1999.11.1.15.

[34] Chen, I. A., Hargis, C. W., Juenger, M. C. G. (2012). Understanding expansion in calcium sulfoaluminate–belite cements, *Cement and Concrete Research*, Vol. 42, No. 1, 51–60. doi:https://doi.org/10.1016/j.cemconres.2011.07.010.

[35] Ogawa, K., Roy, D. M. (1982). C4A3S̄ hydration, ettringite formation, and its expansion mechanism: III. Effect of CaO, NaOH and NaCl; conclusions, *Cement and Concrete Research*, Vol. 12, No. 2, 247–256. doi:https://doi.org/10.1016/0008-8846(82)90011-4.

[36] Ogawa, K., Roy, D. M. (1981). C4A3S hydration ettringite formation, and its expansion mechanism: I. expansion; Ettringite stability, *Cement and Concrete Research*, Vol. 11, Nos. 5–6, 741–750.

[37] Hargis, C. W., Telesca, A., Monteiro, P. J. M. (2014). Calcium sulfoaluminate (Ye'elimite) hydration in the presence of gypsum, calcite, and vaterite, *Cement and Concrete Research*, Vol. 65, 15–20.

[38] Winnefeld, F., Barlag, S. (2009). Influence of calcium sulfate and calcium hydroxide on the hydration of calcium sulfoaluminate clinker, *ZKG International*, Vol. 62, No. 12, 42–53.

[39] Wang, Y., Su, M., Yang, R., Baoyuan, L. (1992). A quantative study of paste mircostructures and hydration characters of sulphoaluminate cement, *9th International Congress on the Chemistry of Cement Volume 4*, New Delhi, 454–460.

[40] Janotka, I., Krajci, L., Mojumdar, S. C. (2007). Performance of sulphoaluminate-belite cement with high C4A3S contents, *Ceramics Silikaty*, Vol. 51, 74–81.

[41] Scrivener, K. L., Capmas, A. (2003). Calcium Aluminate Cements, P. Hewlett (Ed.), *Lea's Chemistry of Cement and Concrete* (4th ed.), Butterworth-Heinemann, Oxford, UK, 713–782. doi:https://doi.org/10.1016/B978-075066256-7/50025-4.

[42] Scrivener, K. L. (2008). 100 years of calcium aluminate cements, *Calcium Aluminates Cements Century Conference*, Avignon, France.

[43] Scrivener, K. L. (2001). Historical and present day applications of calcium aluminate cements, *Proceedings of the International Conference on Calcium Aluminate Cements*, Heriot Watt University Edinburgh, Scotland, UK, 3–23.

[44] Martin, I., Patapy, C., Cyr, M. (2014). Parametric study of binary and ternary ettringite-based systems, *International Congress on Calcium Aluminates*, Avignon, France.

[45] Lamberet, S. (2005). *Durability of ternary binders based on portland cement, calcium aluminate cement and calcium sulfate*, École polytechnique fédérale de Lausanne, Lausanne, Switzerland.

[46] Mehta, P. K. (1973). Effect of Lime on Hydration of Pastes Containing Gypsum and Calcium Aluminates or Calcium Sulfoaluminate, *Journal of the American Ceramic Society*, Vol. 56, No. 6, 315–319, article. doi:10.1111/j.1151-2916.1973.tb12503.x.

[47] Fernández-Carrasco, L., Vázquez, E. (2009). Reactions of fly ash with calcium aluminate cement and calcium sulphate, *Fuel*, Vol. 88, No. 9, 1533–1538. doi:10.1016/J.FUEL.2009.02.018.

[48] Le Saout, G., Lothenbach, B., Taquet, P., Fryda, H., Winnefeld, F. (2014). Hydration study of a calcium aluminate cement blended with anhydrite, *Calcium Aluminates International Conference: Proceedings of the Fourth Conference*, Avignon, France.

[49] Evju, C., Hansen, S. (2001). Expansive properties of ettringite in a mixture of calcium aluminate cement, Portland cement and β-calcium sulfate hemihydrate, *Cement and Concrete Research*, Vol. 31, No. 2, 257–261. doi:10.1016/S0008-8846(00)00495-6.

[50] Fryda, H., Lamberet, S., Dunster, A. (2008). Calcium aluminate cement concrete in old marine structures, C. Fentiman; R. Mangabhai; K. Scrivener (Eds.), *Calcium Aluminate Cements, Proceedings of the Centenary Conference*, Avignon, France, 209–220.

[51] Berger, S., Fryda, D., Niepmann, D., Tourlakis, D. (2014). Impact of calcium sulfate type on hydration and properties of ettringite systems, C. Fentiman; R. Mangabhai; K. Scrivener (Eds.), *Calcium Aluminate Cements, Proceedings of the Centenary Conference*, Avignon, France.

[52] Moffatt, E., Thomas, M. (2018). Durability of rapid-strength concrete produced with ettringite-based binders, *ACI Materials Journal*, Vol. 115. doi:10.14359/51701006.

[53] Scrivener, K. L. (1984). *The development of microstructure during the hydration of Portland cement* (dissertation), École polytechnique fédérale de Lausanne, Lausanne, Switzerland.

[54] Renaudin, G., Filinchuk, Y., Neubauer, J., Goetz-Neunhoeffer, F. (2010). A comparative structural study of wet and dried ettringite, *Cement and Concrete Research*, Vol. 40, No. 3, 370–375.

[55] Scholtzová, E., Kucková, L., Kožíšek, J., Tunega, D. (2015). Structural and spectroscopic characterization of ettringite mineral –combined DFT and experimental study, *Journal of Molecular Structure*, Vol. 1100, No. Supplement C, 215–224. doi:https://doi.org/10.1016/j.molstruc.2015.06.075.

[56] Scholtzová, E., Tunega, D., Speziale, S. (2015). Mechanical properties of ettringite and thaumasite—DFT and experimental study, *Cement and Concrete Research*, Vol. 77, No. Supplement C, 9–15.

[57] Baquerizo, L. G., Matschei, T., Scrivener, K. L. (2016). Impact of water activity on the stability of ettringite, *Cement and Concrete Research*, Vol. 79, No. Supplement C, 31–44. doi:https://doi.org/10.1016/j.cemconres.2015.07.008.

[58] Zhou, Q., Glasser, F. P. (2001). Thermal stability and decomposition mechanisms of ettringite at <120°C, *Cement and Concrete Research*, Vol. 31, No. 9, 1333–1339. doi:http://dx.doi.org/10.1016/S0008-8846(01)00558-0.

[59] Pourchez, J., Valdivieso, F., Grosseau, P., Guyonnet, R., Guilhot, B. (2006). Kinetic modelling of the thermal decomposition of ettringite into metaettringite, *Cement and Concrete Research*, Vol. 36, No. 11, 2054–2060.

[60] Skoblinskaya, N. N., Krasilnikov, K. G. (1975). Changes in crystal structure of ettringite on dehydration. 1, *Cement and Concrete Research*, Vol. 5, No. 4, 381–393.

[61] Hartman, M. R., Brady, S. K., Berliner, R., Conradi, M. S. (2006). The evolution of structural changes in ettringite during thermal decomposition, *Journal of Solid State Chemistry*, Vol. 179, No. 4, 1259–1272.

[62] Moore, A. E., Taylor, H. F. W. (1970). Crystal structure of ettringite, *Acta Crystallographica Section B*, Vol. 26, No. 4, 386–393.

[63] Speziale, S., Jiang, F., Mao, Z., Monteiro, P. J. M., Wenk, H.-R., Duffy, T. S., Schilling, F. R. (2008). Single-crystal elastic constants of natural ettringite, *Cement and Concrete Research*, Vol. 38, No. 7, 885–889.

[64] Skoblinskaya, N. N., Krasilnikov, K. G., Nikitina, L. V, Varlamov, V. P. (1975). Changes in crystal structure of ettringite on dehydration. 2, *Cement and Concrete Research*, Vol. 5, No. 5, 419–431.

[65] Shimada, Y., Young, J. F. (2001). Structural changes during thermal dehydration of ettringite, *Advances in Cement Research*, Vol. 13, No. 2, 77–81. doi:10.1680/adcr.2001.13.2.77.

[66] Bannister, F. A. (1936). Ettringite from Scawt Hill, Co. Antrim, *Mineralogical Magazine Mineralogical Magazine*, Vol. 24, No. 153, 324–329.

[67] Kaufmann, J., Winnefeld, F., Lothenbach, B. (2016). Stability of ettringite in CSA cement at elevated temperatures, *Advances in Cement Research*, Vol. 28, No. 4, 251–261. doi:10.1680/jadcr.15.00029.

[68] Jiménez, A., Prieto, M. (2015). Thermal stability of ettringite exposed to atmosphere: implications for the uptake of harmful ions by cement, *Environmental Science & Technology*, Vol. 49, No. 13, 7957–7964.

[69] Shi, C., Zhang, G., He, T., Li, Y. (2016). Effects of superplasticizers on the stability and morphology of ettringite, *Construction and Building Materials*, Vol. 112, No. Supplement C, 261–266. doi:https://doi.org/10.1016/j.conbuildmat.2016.02.198.

[70] Prince, W., Edwards-Lajnef, M., Aïtcin, P. C. (2002). Interaction between ettringite and a polynaphthalene sulfonate superplasticizer in a cementitious paste, *Cement and Concrete Research*, Vol. 32, No. 1, 79–85. doi:https://doi.org/10.1016/S0008-8846(01)00632-9.

[71] Cody, A. M., Lee, H., Cody, R. D., Spry, P. G. (2004). The effects of chemical environment on the nucleation, growth, and stability of ettringite [Ca3Al(OH)6]2(SO4)3·26H2O, *Cement and Concrete Research*, Vol. 34, No. 5, 869–881. doi:https://doi.org/10.1016/j.cemconres.2003.10.023.

[72] Komatsu, R., Mizukoshi, N., Makida, K., Tsukamoto, K. (2009). In-situ observation of ettringite crystals, *Journal of Crystal Growth*, Vol. 311, No. 3, 1005–1008. doi:https://doi.org/10.1016/j.jcrysgro.2008.09.124.

[73] Nishikawa, T., Suzuki, K., Ito, S., Sato, K., Takebe, T. (1992). Decomposition of synthesized ettringite by carbonation, *Cement and Concrete Research*, Vol. 22, No. 1, 6–14.

[74] Strohbauch, G., Kuzel, H. J. (1988). *Carbonation Reactions as Cause of Damage to Heat-Treated Precast Concrete Units* (Vol. 41).

[75] Xiantuo, C., Ruizhen, Z., Xiaorong, C. (1994). Kinetic study of ettringite carbonation reaction, *Cement and Concrete Research*, Vol. 24, No. 7, 1383–1389. doi:10.1016/0008-8846(94)90123-6.

[76] ASTM C305-14. (2014). Standard Practice for Mechanical Mixing of Hydraulic Cement Pastes and Mortars of Plastic Consistency, *Annual Book of ASTM Standards*, Vol. 04.01.

[77] International, A. (2016). ASTM C109 / C109M-16a, Standard Test Method for Compressive Strength of Hydraulic Cement Mortars (Using 2-in. or [50-mm] Cube Specimens), ASTM International, West Conshohocken, PA.

[78] Zhang, J., Scherer, G. W. (2011). Comparison of methods for arresting hydration of cement, *Cement and Concrete Research*, Vol. 41, No. 10, 1024–1036. doi:10.1016/J.CEMCONRES.2011.06.003.

[79] Schäfer, B., Beck, C., Aihara, K., Witthaut, D., Timme, M. (2018). Non-Gaussian power grid frequency fluctuations characterized by Lévy-stable laws and superstatistics, *Nature Energy*, Vol. 3, No. 2, 119–126. doi:10.1038/s41560-017-0058-z.

[80] Mehta, P. K. (1976). Scanning electron micrographic studies of ettringite formation, *Cement and Concrete Research Cement and Concrete Research*, Vol. 6, No. 2, 169–182.

[81] Bayoux, J. P., Bonin, A., Marcdargent, S., Verschaeve, M. (1990). Study of the hydration properties of aluminous cement and calcium sulphate mixes, R.J. Mangabhai (Ed.), *Calcium Alumiante Cements*, 320–334.

[82] Deschner, F., Winnefeld, F., Lothenbach, B., Seufert, S., Schwesig, P., Dittrich, S., Goetz-Neunhoeffer, F., Neubauer, J. (2012). Hydration of portland cement with high replacement by siliceous fly ash, *Cement and Concrete Research*, Vol. 42, No. 10, 1389–1400. doi:https://doi.org/10.1016/j.cemconres.2012.06.009.

[83] Thomas, M., Folliard, K., Drimalas, T., Ramlochan, T. (2008). Diagnosing delayed ettringite formation in concrete structures, *Cement and Concrete Research*, Vol. 38, No. 6, 841–847. doi:https://doi.org/10.1016/j.cemconres.2008.01.003.

[84] Burris, L., Ley, J., Moser, R., Kurtis, K. (2015). Novel alternative cementitious materials for development of the next generation of sustainable transportation infrastructure, *FHWA Techbrief*.

[85] Burris, L. E., Alapati, P., Moser, R. D., Ley, M. T., Berke, N., Kurtis, K. E. (2015). Alternative cementitious materials: challenges and opportunities, *ACI SP 305-15*, 1–10.

[86] Ramseyer, C., Perez, V. (2009). *Highway panel replacement - CSA concrete in california*.

[87] Brown, P. W., Bothe Jr, J. V. (1993). The stability of ettringite, *Advances in Cement Research*, Vol. 5, No. 18, 47–63.

[88] Myneni, S. C. B., Traina, S. J., Logan, T. J. (1998). Ettringite solubility and geochemistry of the Ca (OH) 2–Al2 (SO4) 3–H2O system at 1 atm pressure and 298 K, *Chemical Geology*, Vol. 148, Nos. 1–2, 1–19.

[89] Perkins, R. B., Palmer, C. D. (2000). Solubility of Ca6[Al(OH)6]2(CrO4)3·26H2O, the chromate analog of ettringite; 5–75°C, *Applied Geochemistry*, Vol. 15, No. 8, 1203–1218. doi:https://doi.org/10.1016/S0883-2927(99)00109-2.

[90] Perkins, R. B., Palmer, C. D. (1999). Solubility of ettringite (Ca6[Al(OH)6]2(SO4)3 · 26H2O) at 575°C, *Geochimica et Cosmochimica Acta Geochimica et Cosmochimica Acta*, Vol. 63, Nos. 13–14, 1969–1980.

[91] Warren, C. J., Reardon, E. J. (1994). The solubility of ettringite at 25 deg C, *Cement and Concrete Research*, Vol. 24, No. 8, 1515–1524.

[92] Struble, L. J., Brown, P. W. (1986). Heats of dehydration and specific heats of compounds found in concrete and their potential for thermal energy storage, *Solar Energy Materials*, Vol. 14, No. 1, 1–12. doi:http://dx.doi.org/10.1016/0165-1633(86)90008-0.

[93] Ndiaye, K., Ginestet, S., Cyr, M. (2018). Thermal energy storage based on cementitious materials: A review, *AIMS Energy*, Vol. 6, No. 1, 97–120.

[94] Bosphetty, S., Nayak, J., Sukhatme, S. (1992). Performance analysis of a solar concrete collector, *Energy Conversion and Management*, Vol. 33, 1007–1016.

[95] Hazami, M., Kooli, S., Lazãar, M., Farhat, A., Belghith, A. (2010). Energetic and exergetic performances of an economical and available integrated solar storage collector based on concrete matrix, *Energy Conversion and Management2*, Vol. 51, 1210–1218.

[96] Wu, M., Li, M., Xu, C., He, Y., Tao, W. (2014). The impact of concrete structure on the thermal performance of the dual-media thermocline thermal storage tank using concrete as the solid medium, *Applied Energy2*, Vol. 113, 1363–1371.

[97] Martins, M., Villalobos, U., Delclos, T., Armstrong, P., Bergan, P. G., Calvet, N. (2015). New concentrating solar power facility for testing high temperature concrete thermal energy storage, *Energy Procedia*, Vol. 75, 2144–2149.

[98] Shui, Z., Xuan, D., Chen, W., Yu, R., Zhang, R. (2009). Cementitious characteristics of hydrated cement paste subjected to various dehydration temperatures, *Construction and Building Materials*, Vol. 23, No. 1, 531–537.

[99] Girardi, F., Giannuzzi, G. M., Mazzei, D., Salomoni, V., Majorana, C., Di Maggio, R. (2017). Recycled additions for improving the thermal conductivity of concrete in preparing energy storage systems, *Construction and Building Materials*, Vol. 135, 565–579. doi:https://doi.org/10.1016/j.conbuildmat.2016.12.179.

[100] Salomoni, V. A., Majorana, C. E., Giannuzzi, G. M., Miliozzi, A., Di Maggio, R., Girardi, F., Mele, D., Lucentini, M. (2014). Thermal storage of sensible heat using concrete modules in solar power plants, *Solar Energy*, Vol. 103, 303–315. doi:https://doi.org/10.1016/j.solener.2014.02.022.

[101] Özrahat, E., Ünalan, S. (2017). Thermal performance of a concrete column as a sensible thermal energy storage medium and a heater, *Renewable Energy*, Vol. 111, 561–579. doi:https://doi.org/10.1016/j.renene.2017.04.046.

[102] Ings, J. B. (1982). *An Evaluation of Hydrated Calcium Aluminate Compounds as Energy Storage Media*, (P. W. Brown, Ed.), book, U.S. Dept. of Commerce, National Institute of Standards and Technology, Gaithersburg, MD.

[103] Struble, L., Brown, P. (1984). *Evaluation of ettringite and related compouds for use in solar energy storage*, *Program Report of the National Bureau of Standards*.

[104] Chen, B., Kuznik, F., Horgnies, M., Johannes, K., Morin, V., Gengembre, E. (2019). Physicochemical properties of ettringite/meta-ettringite for thermal energy storage: Review, *Solar Energy Materials and Solar Cells*. doi:10.1016/j.solmat.2018.12.013.

[105] Chen, B., Johannes, K., Horgnies, M., Morin, V., Kuznik, F. (2021). Characterization of an ettringite-based thermochemical energy storage material in an open-mode reactor, *Journal of Energy Storage*, Vol. 33, 102159. doi:10.1016/J.EST.2020.102159.

[106] International, A. (2018). ASTM C150/C150M-18 Standard Specification for Portland Cement, ASTM International, West Conshohocken, PA.

[107] Scrivener, K., Snellings, R., Lothenbach, B. (2015). *A Practical Guide to Microstructural Analysis of Cementitious Materials*, CRC Press, Boca Raton, Florida.

[108] Bizzozero, J. (2014). *Hydration and dimensional stability of calcium aluminate cement based systems*, École polytechnique fédérale de Lausanne, Lausanne, Switzerland.

[109] Gosselin, C. (2009). *Microstructural development of calcium aluminate cement based systems with and without supplementary cementitious materials*, École polytechnique fédérale de Lausanne, Lausanne, Switzerland.

[110] Scrivener, K., Bazzoni, A., Mota, B., Rossen, J. E. (2016). Electron microscopy, K. Scrivener; R. Snellings; B. Lothenbach (Eds.), *A Practical Guide to Microstructural Analysis of Cementitious Materials* (1st ed.), CRC Press, Boca Raton, Fl, 351–419.

[111] Monroe, R. (2022, February 9). Why Texas's Power Grid Still Hasn't Been Fixed, *The New Yorker*.

[112] Akhil, A. A., Huff, G., Currier, A. B., Kaun, B. C., Rastler, D. M., Chen, S. B., Cotter, A. L., Bradshaw, D. T., Gauntlett, W. D. (2013). *DOE/EPRI 2013 Electricity Storage Handbook in Collaboration with NRECA* (Vol. 1), Sandia National Laboratories Albuquerque, NM, USA.

[113] Rommel, M., Hauer, A., Van Helden, W. (2016). IEA SHC Task 42 / ECES Annex 29 compact thermal energy storage, *Energy Procedia*, Vol. 91, 226–230. doi:10.1016/J.EGYPRO.2016.06.208.

[114] Ali, S., Deshmukh, S. P. (2020). An overview: Applications of thermal energy storage using phase change materials, *Materials Today: Proceedings*, Vol. 26, 1231–1237. doi:10.1016/J.MATPR.2020.02.247.

[115] Chen, B., Horgnies, M., Huet, B., Morin, V., Johannes, K., Kuznik, F. (2020). Comparative kinetics study on carbonation of ettringite and meta-ettringite based materials, *Cement and Concrete Research*, Vol. 137, 106209. doi:10.1016/J.CEMCONRES.2020.106209.

[116] Fridrichová, M., Dvořák, K., Gazdič, D., Mokrá, J., Kulísek, K. (2016). Thermodynamic stability of ettringite formed by hydration of ye'elimite clinker, *Advances in Materials Science and Engineering*, Vol. 2016.

[117] Honorio, T., Maaroufi, M., Al Dandachli, S., Bourdot, A. (2021). Ettringite hysteresis under sorption from molecular simulations, *Cement and Concrete Research*, Vol. 150, 106587. doi:10.1016/J.CEMCONRES.2021.106587.

[118] Guimarães, D., Oliveira, V. de A., Leão, V. A. (2016). Kinetic and thermal decomposition of ettringite synthesized from aqueous solutions, *Journal of Thermal Analysis and Calorimetry*, Vol. 124, No. 3, 1679–1689.

[119] Hall, C., Barnes, P., Billimore, A. D., Jupe, A. C., Turrillas, X. (1996). Thermal decomposition of ettringite Ca6[Al(OH)6]2(SO4)3·26H2O, *Journal of the Chemical Society, Faraday Transactions*, Vol. 92, No. 12, 2125–2129. doi:10.1039/FT9969202125.

[120] Portland Cement Association. (2001). *Ettringite Formation and the Performance of Concrete*, Portland Cement Association, Skokie, IL.

[121] Huang, G., Pudasainee, D., Gupta, R., Victor Liu, W. (2019). Hydration reaction and strength development of calcium sulfoaluminate cement-based mortar cured at cold temperatures, *Construction and Building Materials*, Vol. 224, 493–503. doi:https://doi.org/10.1016/j.conbuildmat.2019.07.085.

[122] Chen, B., Johannes, K., Ratel, L., Horgnies, M., Morin, V., Kuznik, F. (2021). Investigation on ettringite as a low-cost high-density thermochemical heat storage material: Thermodynamics and kinetics, *Solar Energy Materials and Solar Cells*, Vol. 221, 110877. doi:10.1016/J.SOLMAT.2020.110877.

[123] Kaufmann, J., Winnefeld, F. (2019). Seasonal heat storage in calcium sulfoaluminate based hardened cement pastes – experiences with different prototypes, *Journal of Energy Storage*, Vol. 25, 100850. doi:10.1016/J.EST.2019.100850.

[124] ŠATAVA, V., VEPŘEK, O. (1975). Thermal decomposition of ettringite under hydrothermal conditions, *Journal of the American Ceramic Society*, Vol. 58, Nos. 7–8, 357–359. doi:https://doi.org/10.1111/j.1151-2916.1975.tb11513.x.

[125] Rockland, L. B. (1960). Saturated salt solutions for static control of relative humidity between 5° and 40° C., *Analytical Chemistry*, Vol. 32, No. 10, 1375–1376.

[126] Winnefeld, F., Schöler, A., Lothenbach, B. (2016). Sample preparation, K. Scrivener; R. Snellings; B. Lothenbach (Eds.), *A Practical Guide to Microstructural Analysis of Cementitious Materials* (1st ed.), CRC Press, Boca Raton, Fl, 1–37.

[127] Liu, M., Luo, S., Yang, L., Ren, J. (2020). Influence of water removal techniques on the composition and microstructure of hardened calcium sulfoaluminate cement pastes, *Materials and Structures*, Vol. 53, No. 4, 89. doi:10.1617/s11527-020-01527-3.

[128] Liu, M., Luo, S., Yang, L., Ren, J. (2020). Influence of water removal techniques on the composition and microstructure of hardened calcium sulfoaluminate cement pastes, *Materials and Structures*, Vol. 53, No. 4, 89. doi:10.1617/s11527-020-01527-3.

[129] Martin, I., Patapy, C., Cyr, M. (2015). Impact of calcium sulfate type and additions on hydration and properties of ettringite-based systems, *ICCC 2015 BEIJING the 14th International Congress on the Chemistry of Cement, Beijing*.

[130] Winnefeld, F., Kaufmann, J. (2011). Concrete produced with calcium sulfoaluminate cement—A potential system for energy and heat storage, *First Middle East Conference on Smart Monitoring, Assessment and Rehabilitation of Civil Structures (SMAR 2011), Dubai, United Arab Emirates*.

[131] Xu, L., Wang, P., Zhang, G. (2012). Formation of ettringite in portland cement/calcium aluminate cement/calcium sulfate ternary system hydrates at lower temperatures, *Construction and Building Materials*, Vol. 31, 347–352. doi:10.1016/J.CONBUILDMAT.2011.12.078.

[132] Luo, S., Liu, M., Yang, L., Chang, J. (2019). Effects of drying techniques on the crystal structure and morphology of ettringite, *Construction and Building Materials*, Vol. 195, 305–311. doi:10.1016/J.CONBUILDMAT.2018.11.078.

[133] Grounds, T., G Midgley, H., V Novell, D. (1988). Carbonation of ettringite by atmospheric carbon dioxide, *Thermochimica Acta*, Vol. 135, 347–352. doi:https://doi.org/10.1016/0040-6031(88)87407-0.